CANADIAN THESES

THÈSES CANADIENNES

NOTICE

The quality of this microfiche is heavily dependent upon the quality of the original thesis submitted for microfilming. Every effort has been made to ensure the highest quality of reproduction possible.

If pages are missing, contact the university which granted the degree.

Some pages may have indistinct print especially if the original pages were typed with a poor typewriter ribbon or if the university sent us an inferior photocopy.

Previously copyrighted materials (journal articles, published tests, etc.) are not filmed.

Reproduction in full or in part of this film is governed by the Canadian Copyright Act, R.S.C. 1970, c. C-30. Please read the authorization forms which accompany this thesis.

AVIS

La qualité de cette microfiche dépend grandement de la qualité de la thèse soumise au microfilmage. Nous avons tout fait pour assurer une qualité supérieure de reproduction.

S'il manque des pages, veuillez communiquer avec l'université qui a conféré le grade.

La qualité d'impression de certaines pages peut laisser à désirer, surtout si les pages originales ont été dactylographiées à l'aide d'un ruban usé ou si l'université nous a fait parvenir une photocopie de qualité inférieure.

Les documents qui font déjà l'objet d'un droit d'auteur (articles de revue, examens publiés, etc.) ne sont pas microfilmés.

La reproduction, même partielle, de ce microfilm est soumise à la Loi canadienne sur le droit d'auteur, SRC 1970, c. C-30. Veuillez prendre connaissance des formules d'autorisation qui accompagnent cette thèse.

THIS DISSERTATION
HAS BEEN MICROFILMED
EXACTLY AS RECEIVED

LA THÈSE A ÉTÉ
MICROFILMÉE TELLE QUE
NOUS L'AVONS REÇUE

NL 339 (r 86/01)

Canada

SLOPE STABILITY ANALYSIS BY OPTIMISATION TECHNIQUES

by

A . Verma

A thesis
presented to the School of Graduate Studies and Research
at the University of Ottawa
in partial fulfillment of the
requirements for the degree of
Master of Applied Sciences
in
Civil Engineering

OTTAWA, Ontario, 1984

UNIVERSITÉ D'OTTAWA
UNIVERSITY OF OTTAWA

SUMMARY

At present, most of the techniques available to find the location of the critical slip surface rely on search techniques that are random, or arbitrary to some degree. Since a large number of slip surfaces has to be generated, the search techniques are generally incorporated in less sophisticated but faster methods of slope stability analysis. These methods, i.e. Simplified Bishop method for circular slip surfaces and Janbu Simplified method for noncircular, concave slip surfaces, do not satisfy all the equations of static equilibrium.

This study deals with the development of a search procedure to locate the critical slip surface which is mathematically rigorous, systematic, and overcoming the shortcomings of the existing methods.

The formulation of the problem is based on the Generalised Limit Equilibrium Method (GLEM), which assumes the existence of an unstable area composed of a number of elements. The three equations of equilibrium for each element and the failure criteria along the interfaces are satisfied. It has been shown that the general mathematical formulation of this problem leads directly to an optimisation problem and specifically, to a linear program.

This is a fortunate result, since powerful, reliable and fast procedures exist to solve this problem. An additional important feature of the formulation is that one can use the sensitivity analysis technique in order to locate the critical slip surface in a systematic way. The proposed search procedure is based on this feature, and a number of assumptions, concepts, and techniques derived from the theories of limit equilibrium, linear programming, and sensitivity analysis are incorporated.

From the case studies analysed, it was observed that the most critical slip surface (in fact the most critical geometric configuration) could be obtained after five to ten iterations. It was also noticed that the convergence to the final, most critical slip surface by starting from two different initial slip surfaces was remarkably good for all the cases studied. The number of elements and the topology (different configurations for the same number of elements) of which the slope is composed of were found to affect the critical slip surface.

A natural slope failure at Rosemere, Quebec, was analysed by the proposed method. The analysis indicated that the failure could be progressive and a critical surface which closely approximated the one actually measured in the field was obtained.

The main advantages of the proposed method are that no restrictions have to be imposed on the shape of the slip surface and that any failure mechanism can be simulated.

ACKNOWLEDGEMENTS

The author wishes to express his sincere gratitude to his supervisor Dr. C. Papantonopoulos for stimulating discussions and helpful advise throughout the duration of this research.

The author also thanks Mr. A. Fusco and K. Ramakrishan for the advise and help given to him.

Finally financial support provided by EMR (grant SKN-IPO-LCD) and by the University of Ottawa is gratefully acknowledged.

CONTENTS

LIST OF FIGURES

LIST OF TABLES

NOTATIONS

a : Symbol for the side of the triangular element.

a'_{ij} : Coefficient of the unknown variables corresponding to the equality restrictions in the LP.

a_{ij} : Coefficient of the unknown variables corresponding to the inequality restrictions in the LP.

b, c : Symbol for the sides of the triangular element.

c'_i : Constant terms in the equality equations of the LP.

c_i : Constant terms in the inequality equations of the LP.

d_j : Coefficient of the unknown objective functions in the LP.

e : Non dimensional parameter defining the position of a point on the sides of the element (general symbol).

e_0 : Parameter defining the point of application of the concentrated force P.

e_k : Parameter defining the point of application of the forces U_a, U_b and U_c ($k=1,2,3$ respectively)

i,j,k: Indices of the nodes of the triangular element.

i_x, i_z: Hydraulic gradient in the direction of the axes X and Z.

m : a) Symbol for the element. b) total number of restrictions in the LP.

n : a) Symbol for the element. b) total number of unknowns in the LP.

p : a) Point of application of the force P. b) number of restrictions in the equations of the LP.

q : Number of positive variables in the LP.

r : General symbol for the indices of the element.

s : General symbol for the sides of the element.

t(i) : Displacement of the node i,j or k.

{t} : Vector of the constraints σ_{rs} and τ_s applied to the sides of the triangle.

u_i : Dual variables in the LP.

w_i : Dual variables in the LP.

x_j : a) Unknown variable in the LP, i.e. σ_{rs} , τ_s . b) primal value.

x'_j : Unknown positive variables.

x''_j : Unknown positive variables.

z : general symbol for the objective function.

[A] : Restriction matrix composing of the matrices $[A_1]$ and $[A_2]$.

$[A_1]$: Equilibrium matrix (contains coefficients a'_{ij}).

[A2] : Inequality matrix (contains coefficients a_{ij}).

{B} : Constant vector composed of vector {B1} and {B2}.

{B1} : Vector of external forces (contains coefficients of c'_i)

{B2} : Cohesion vector (contains coefficients c_i)

C_s : Cohesion at the interface of the side s.

{D} : Vector of the coefficients d_j.

E : Double area of the triangular element.

FS : Global factor of safety.

FS : Local factor of safety corresponding to the side s.

F_x, F_z : Seepage force in the direction of the axes X and Z.

G : Centroid of the triangular element.

[I] : Unit matrix.

K : Seismic coefficient.

LP : Linear Programme.

{M} : Vector of the external moments.

M_i : Moment constraints applied to the sides a, b, c, (i.e. i=1, 2, 3) about the centroid G.

M_0 : External moment applied at the Centroid of the element.

M_p : Moment due to the force P about the centroid G.

M_s : Function of the element coordinates (s=a, b, c)

M_{ua} : Moment at the centroid G due to the pore water pressure acting on the side a.

MCR : Most Critical slip surface

MS : Global margin of safety.

MS : Local margin of safety corresponding to the side s.

NDMAX : Maximum displacement of the nodes.

[0] : Null matrix.

P : Applied external force acting on the side b.

P_1 : Component of P normal to the side b.

P_2 : Component of P parallel to the side b.

P_x, P_z : Components of the force P in the direction of the axes X and Z.

$\{Q_1\}, \{Q_2\}$: Vector of the forces P_1 and P_2.

{R} : Vector of the coefficients R_1, R_2, R_3.

R_1, R_2 : Horizontal and vertical component of the force due to the application of pore water pressures on the sides of the triangular element.

R_3 : Moment applied at the centroid due to pore water pressure.

S_i, S_i' : Resultant normal forces (general symbol).

S_{xa}, S_{za} : Resultant normal forces due to the stresses applied on side a.

$[S]$: Coefficient matrix of the resultant normal forces.

T_i, T_i' : Resultant tangential forces (general symbol).

T_s : Tangential force applied at the side s.

$[T]$: Coefficient matrix of the tangential constraints.

u_i : Dual value.

U_{xa}, U_{za} : Resultant forces due to the pore water pressure applied at the side a.

W : Weight of the element.

$\{W\}$: Vector of the constant terms due to the weight of the element and the seismic force.

X : X coordinates of the indices r=i, j, k.

X_{ij}, X_{jk} : Function of the coordinates X .

$\{X\}$: Vector of the unknown variables in the LP.

X_G, Z_G : Coordinates of the centroid of the element.

X_m', Z_m' : Coordinates of the point m with reference to X and Z axes.

Z : Z coordinates of the indices r = i, j, k.

Z_{ij}, Z_{jk} : Functions of the coordinates Z .

γ : Unit weight of the material.

n_1 n_2 : Paramater defining M_p.

θ_s : a) angle defining the orientation of the sides of the element. b) displacement given to the nodes, s = i, j, k.

μ_s : Tangent of the angle of friction.

σ_i : Normal stresses (general symbol)

σ_{rs} Stresses at the indices r normal to the sides s.

$\{\sigma\}$: Vector of normal stresses applied on the sides of the triangular element.

τ_s : Tangential stresses (general symbol).

τ_s : Tangential stresses along the side s.

τ_{rs} Tangential stresses acting at the indices r, parallel to the side s.

$\{\tau\}$: Vector of tangential stresses applied on the sides of the triangular element.

ϕ_s : Angle of friction on the side s.

ω : Angle between the resultant force P and the normal component P_r.

Δf : Change in the objective function.

Σ : Summation.

ΣT_a : Summation of the tangential forces along the slip surface lines.

ΣT_r : Summation of the tangential forces mobilised along the slip surface lines.

$[\ ]$: Matrice.

$[\ ]^T$: Transpose of a matrix.

$\{\ \}$: Vector.

$\{\ \}^T$: Transpose of a vector.

Chapter I

INTRODUCTION

1.1 GENERAL DISCUSSION

Ensuring the stability of both man-made and natural slopes affected by the works of man has proven to be one of the least successful endeavours of civil engineers. Failures of natural slopes, man-made fills and cuts in earth probably occur more frequently than all other failures of civil engineering structures combined.

The methods commonly used for the analysis of slope stability can be divided in two groups :

1. Those that take into account the deformability of the soil medium, and
2. The limit equilibrium methods.

The former are based essentially on some continuum mechanics theory and, in principle, they can provide a unique answer assuming the constitutive equation of the media are known. These are complex boundary problems, and they have to be treated numerically. The most popular and the most versatile numerical technique is that of the Finite element method.

However, in spite of more than a decade of active research, this method has not yet become a convenient tool for everyday problems. Some basic problems that limit the usefulness of the method are as follows :

1. Reliable and widely acceptable constitutive equations have not yet been established even for few "simple" materials.
2. Advanced numerical models of this kind are highly iterative and even today are expensive to run.
3. They fail to answer directly the stability problem, and instability is detected indirectly by failure of the procedure to converge, by excessive deformations and unconfined "plastified" areas, or by coming back to an almost conventional analysis where the state of stress along a more or less arbitrary slip line is estimated on the basis of the calculated stress field.

The conventional limit equilibrium methods on the other hand have been developed as semi-empirical or "engineering" methods. These methods neglect the stress-strain and the compatibility equations. They are inspired by the kinematics of failure, but formulate and solve the problem strictly in terms of statics and they strive to satisfy all the equations of force and moment equilibrium and the strength criteria (Mohr-Coulomb) along certain lines.

Since the methods neglect the stress-strain relationships, they cannot answer the problem of deformability. However, since deformations are of little concern for most slope stability problems, the limit equilibrium methods have been considered appropriate and they are extensively used for slope stability problems.

The conventional limit equilibrium methods suffer from two inherent uncertainities. The first is that the problem formulated in terms of statics is indeterminate, i.e., an infinite number of force (stress) fields satisfy the equations of equilibrium. Few conventional methods try to solve this problem, i.e. Frohlich (1955) and Biarez (1961). The majority render the problem determinate by additional "reasonable" assumptions. This means that the factor of safety as determined in the methods of Bishop, Janbu, Morgenstern-Price, etc. is not unique for a given sliding surface. This fact is deliberately overlooked.

The second uncertainty is that the actual slip surface is not known. One has to assume that this will be the one which gives to an associated stability criterion its minimum value. This is usually the factor of safety as defined by the method of slices.

Neither the first nor the second uncertainty is answered satisfactorily by the conventional limit equilibrium methods which assume an arbitrary stress distribution and concentrate to find the most critical surface by various trial procedures. These procedures have severe limitations that will be discussed in Chapter 2.

The generalised limit equilibrium method, as proposed by Papantonopoulos and Ladanyi (1973), has removed most of the uncertainties of the first kind by providing rigorous upper and lower bounds that bracket the true solution for a given

slip surface. The method has been extended subsequently by Papantonopoulos (1984), who proposed a procedure to treat the uncertainities of the second kind, i.e. the slip surface is not known. According to this procedure a piece-wise linear slip surface is moved vertically untill a critical position is obtained. The procedure is iterative and subject to geometrical limitations.

1.2 OBJECTIVE OF THE STUDY

The objective of this study is to develop a search procedure which improves the one proposed by Papantonopoulos (1984) :

1. By removing the geometrical restrictions, and
2. By minimising the number of iterations.

By removing the geometrical restrictions, one can eliminate a) any a priori assumptions about the shape of the slip surface, and b) the possibility to miss the critical one.

By minimising the number of iterations, one can obtain an efficient and economical search procedure.

1.3 OUTLINE OF THE THESIS

Chapter two presents the review of literature concerning the existing limit equilibrium methods, and the various search techniques available to determine the critical slip surface. The assumptions made in each of the methods to make the system determinate are discussed in Appendix A.

In Chapter three, the formulation of the slope stability as an optimisation problem is presented. A brief introduction is made of the "quasi-static", method and its incorporation in the optimisation procedures is discussed.

Chapter four presents the procedure for determining the critical slip surfaces using sensitivity analysis. A brief survey of the theory relevant to the problem is presented and a flow-chart is included to explain the step-by-step procedures of the search algorithm.

In Chapter five, numerical experiments are conducted in order to: a) establish the convergence and termination criteria for the critical slip surfaces, and b) to examine the effect of a number of factors on these surfaces. These factors are :

1. The variation of the nodal displacement increment.
2. The number of elements of which the unstable soil mass is composed of.
3. The topology of the elements (triangles).
4. The degrees of freedom of the system of nodes.
5. Discontinuous normal stresses along the slip surface.
6. The convergence to the same final slip surface when one starts from two different initial slip surfaces.

A discussion of the results obtained is presented.

In Chapter six, a case study of a failed slope at Rosemere, Quebec is presented. The proposed method is used to predict the failure and locate the critical slip surface.

Comparison is made between the proposed,the Simplified Bishop, and the Janbu methods.

Chapter II

LITERATURE REVIEW

2.1 INTRODUCTION

Since the proposed search procedure is an outgrowth of the limit equilibrium methods, the literature review is limited to the methods of this type.

For a more comprehensive presentation, it is considered appropriate to present a general classification of the limit equilibrium methods, as well as their common theoretical basis and other interrelationships.

2.2 BASIC ASSUMPTIONS OF THE LIMIT EQUILIBRIUM METHODS

The following assumptions are common to all limit equilibrium methods of analysis :

1. A potentially unstable area is separated from the stable part by a fictitious slip line.
2. The area is decomposed to one or more elements (slices, wedges etc.)
3. The equations of force and/or moment equilibrium are formulated as functions of the unknown forces (stresses).
4. The failure criteria on the interfaces of the elements have to be satisfied (as equalities or

inequalities). Usually, one assumes a linear Mohr-Coulomb criterion.

The above are the basic assumptions of these methods. However, because the number of equations is less than the number of unknowns, the problem is indeterminate.

Two approaches to the solution are possible. The first is to introduce additional assumptions such as a constant factor of safety along the slip surface (an almost universal assumption) and various others concerning the interslice forces. This is the approach followed by all the widely used limit equilibrium methods, and this is what confers to them most of their semi-empirical character. Here, these methods are referred to as the conventional limit equilibrium methods.

The second approach is to remove the indeterminacy by seeking to optimise (maximise or minimise) a particular function (factor of safety) subject to the constraints derived from assumptions 3 and 4. These methods can be classified as the Variational methods proposed by Kopacsy (1961), Baker and Garber (1978), Castillo and Revilla (1977), Goldstein (1969) and Narayan et al. (1976 and 1977) and the mathematical programming method proposed by Papantonopoulos and Ladanyi (1973) and Papantonopoulos (1979 and 1984).

In the following sections, these three classes of limit equilibrium methods are discussed with emphasis on the existing search procedure.

2.3 CONVENTIONAL LIMIT EQUILIBRIUM METHODS

2.3.1 Introduction

The conventional limit equilibrium methods provide a means for calculating the factor of safety for a given slip surface. They cannot locate the critical slip surface with the minimum factor of safety directly. This important aspect of the analysis is accomplished by repeated trials. Following this approach, the factor of safety (FS) of a number of possible slip surfaces is calculated, and the one with the least FS is considered as the most critical. The repeated trials can be done for slip surfaces having regular or irregular shapes. By regular shape is meant surfaces whose shape is mathematically defined (circles, logarithmic spirals, cycloids, etc). The particular assumptions for a number of commonly used conventional methods can be seen in Appendix A.

2.3.2 Search for regular shapes

2.3.2.1 Types of search techniques

In the case of homogenous soil, the shape of the critical failure surface is often assumed to be circular or that of a logarithmic spiral. For both of these shapes, a search for the most critical location of the failure surface may be performed by using either of the two following techniques.

1. Grid search
2. Random search

1. Grid search :

The principle of this technique (widely used in practice) is shown in Fig.2.1 for a failure surface of circular shape. In order to locate the most critical surface, the centre of the circle or the pole of the logarithmic spiral is varied according to a chosen grid pattern and the radius R (initial radius for a log. spiral) is varied between Rmax and Rmin. The use of the grid search is based on the observation that the centres or poles of different surfaces will form contour lines of equal factors of safety with the centre or pole of the most critical surface (the one having the least factor of safety) located at the lowest contour.

2. Random search

This was developed at Purdue University by Siegel (1975). Trial failure surfaces of circular shapes are generated from a number of initiation points with equal horizontal spacing along the ground surface at the base of the slope.

The direction θ , of the first line segment defining a slip surface is chosen randomly between two direction limits, as shown in Fig. 2.2. θ is defined as shown below :

$$\theta = \alpha_2 + (\alpha_1 - \alpha_2) R^2 \qquad 2.1$$

where α_1 and α_2 are counterclockwise and clockwise direction limits, and R represents the random function Ranf(x). Ranf(x) is a pseudorandom number function which generates

real numbers in the range from 0 to 1. Using R squared introduces a bias in the random selection of θ so that angles closer to the clockwise direction limit are more likely. The primary reason for introducing the bias is to obtain a good distribution of completed surfaces.

For a circular shaped surface, each succeeding line segment is generated by changing the direction by some constant angle $\Delta\theta$ chosen randomly between limits defined by the termination limits for the surfaces at the top of the slope, as illustrated in Fig.2.3. The constant change in the angle is given by :

$$\Delta\theta = (\Delta\theta_{max} - \Delta\theta_{min}) R^2 \qquad 2.2$$

The new angle of inclination is given by :

$$\theta_{i+1} = \theta_i + \Delta\theta \qquad 2.3$$

where θ_i is the inclination of the ith line segment of the circulr failure surface.This search technique can be used only for regular shapes.

2.3.3 Search for irregular shapes

2.3.3.1 Types of search techniques

To enable a search technique for irregular shapes, the following techniques have been proposed:

1. Carters search.
2. Random search
3. Simplified search

1. Carter's search

Carter (1971) developed a first approach to a search for critical slip surfaces of irregular shapes. Slip surfaces vary between limits defined by Xo, Ymin, Xmin, Xmax and Ymax, see Fig.2.4. The irregular surface is composed of straight line segments connecting coordinate points (Xk, Yk), where Yk is defined by a cosine function, and Xk is determined in such a way that the slope of each succeeding line segment is in Fibonacci multiples of the slope of the initial line segment. The Fibonacci series is defined as follows:

$$T_1 = T_0 = 1$$
$$T_i = T_{i-1} + T_{i-2} \qquad 2.4$$

The surface terminates at the top of the slope between Xmin and Xmax.

If the (Xo, Ymin) point is defined below the ground surface, the surface is completed by an additional line segment directed back to the ground surface at angles of 30°, 45°, and 60° to the horizontal. The surfaces so generated have a smooth shape.

2. Random search

The random search for irregular shapes was developed by Siegel (1975).

For an irregular surface, the direction of each succeeding line segment is chosen randomly within limits determined by the direction of the preceding line segment, as shown in Fig.2.5.

The counterclockwise limit for the direction of a line segment, $\Delta\theta_1$ is normally deflected 45° counterclockwise from the projection of the preceding line segment. If for a particular line segment the orientation of the counterclockwise direction limit, θ_1, is greater than 90° (measured with respect to the horizontal), the inclination of θ_1 is adjusted to 90°.

The clockwise deflection limit for the direction of a line segment, $\Delta\theta_2$, is randomly selected for each shear surface generated, and is given as follows :

$$\Delta\theta_2 = R^2.45° \qquad (2.5)$$

In the above equation, R is as defined before. If for a particular line segment the inclination of the clockwise direction limit, θ_2, is less than -45°, it is set at this value. The inclination of a line segment is then established by :

$$\vartheta = \theta_2 + (\theta_1 - \vartheta_2) R^{(1+R)} \qquad 2.6$$

where the angular extent of permissible directions, $\alpha_1 - \alpha_2$, is multiplied by a random number raised to a random power between 1 and 2 and added to the inclination of the clockwise direction limit, θ_2.

The above procedure, although somewhat arbitrary, does produce reasonable irregular surfaces of random shape and position.

3. Simplified search

This method was proposed by Celestino and Duncan (1981). This approach has a theoretical basis for the search of non-circular slip surfaces.

Each trial begins by shifting each of the points defining the slip surface to two new positions, and calculating the factor of safety. As this is done, all of the other points are kept in their original positions as shown in Fig.2.6. The first and second shifts are always equal and in the same direction.

After each point has been shifted, its optimum position is estimated using the following equations:

$$x_i^* = x_i^\circ + \Delta x/2 + \Delta x(F0 - F1)/(F0 - 2F1 + F2) \qquad (2.7(a))$$

$$y_i^* = y_i^\circ + y/2 + y(F0 - F1)/(F0 - 2F1 + F2) \qquad (2.7(b))$$

where x_i^*, y_i^* are the estimated optimum coordinates of the point i; x_i, y_i are the original co-ordinates of the point i; Δx, Δy are the shift increments; Fo is the factor of safety (F) before shifting; F = F after the first shift of point i; F2 = F after the second shift of point i. The equations are derived according to the minimizing scheme. The assumptions for each iteration are: (1) the optimum position for a point can be estimated based on the change in F caused by the movement of this point only. (2) The partial minimum of F with respect to a single variable x_i or y_i can be estimated using a local approximation of the function F versus x_i or y_i by a second degree curve.

The values of x_i^* and y_i^* are estimated using equations 2.7(a) and 2.7(b), the factor of safety of the slope is calculated with point moved to x_i^* and y_i^*, all other points being in their original position. If this value of F (called F*) is smaller than Fo, the coordinates of value x_i^*, y_i^* are retained for use in the next step of the iterative process. If not, then the point is returned to the position which corresponds to the lowest value among Fo, F1, and F2.

This process is repeated for each point in turn for a number of iterations. To check whether or not a minimum was reached after an iteration has been completed, the partial derivatives of F with respect to all x_i and y_i are calculated. If all are smaller than a specified value, the search is terminated. If not, it is continued.

2.3.3.2 Criticism of the search technique

The search procedures proposed by Carter (1971), Siegel (1975) ,and Celestino and Duncan (1981), suffer the following limitations when incorporated in the conventional limit equilibrium methods:

1. the factor of safety is not unique and
2. a uniform factor of safety is assumed along the slip surface.

The a priori assumption that the slip surface is regular in shape will result in an error of unknown magnitude : the smallest value of the factor of safety found by studying circular arcs can be higher than the minimum value corresponding to other surfaces. Consequently the results might overestimate the actual stability of the slope.

The search procedures for irregular shapes of tha slip sutface are random by nature. Hence, judgement and repeated trials have to be carried out adding considerably to the time and cost of analysis. Such a search often fails to locate the most critical surface.

Although the search technique proposed by Celestino and Duncan (1981), utilises the optimisation concepts, it is rather simplistic in nature and minimises any factor of safety which is not unique.

2.3.4 Variational approach

This approach uses an "apparently" rigorous mathematical technique to analyse the slope stability problems. The stability problem is treated as a minimization problem of the calculus of variations, wherein the shape of the slip surface and the distribution of interslice forces are unknown functions of X and Z coordinates that are to be determined. Simultaneously, the critical slip surface and the associated interslice force distribution functions (whenever they are taken into account) are obtained by satisfying the necessary and sufficient conditions for the minimality of a given functional i.e. total weight of the unstable mass or the factor of safety. The procedure has been introduced by Kopacscy (1961), and later by Goldstein (1969). It gained a new interest lately with the work done by Narayan et al.(1976, 1977), Baker and Garber (1978) and Castillo and Revilla (1977). No a priori assumptions regarding a definite shape of the slip surface or the line of thrust, i.e. direction of the resultant interslice forces, have to be made. Instead some minimality conditions of the calculus of variations have to be satisfied. The analysis is solely based on limiting equilibrium and respects all equilibrium conditions..

2.3.4.1 Criticism of the variational approach

It has been shown by De Josselin De Jong (1981) that at least some variational methods for determining the critical slip surface suffer from a serious mathematical fallacy; a functional describing the stability of the slope is considered which has a degenerate character and possesses no minimum. Thus, the critical slip surface obtained by these methods can have no mathematical or physical meaning.

In addition to and irrespective of the possible hidden mathematical defects, these methods stay always with the basic limitation of the conventional methods, i.e. assumption of a constant factor of safety along the slip surface. They also neglect the effect of the interslice forces and the internal equilibrium considerations. In practice, they appear difficult - if possible - to apply to actual problems with complex material and water pressure distribution.

2.3.5 The Mathematical optimisation approach

The conventional limit equilibrium method has been generalised by Papantonopoulos and Ladanyi (1973) and Papantonopoulos (1979) who developed the Generalised limit equilibrium method (GLEM).

It has been proven that a slope stability problem can be formulated as a problem of mathematical optimisation in general, and, with an appropriate choice of an objective function, as a linear program.

Initially, the method was intended to determine the most critical stress (force) field that minimises or maximises the margin of safety (MS) for a given failure surface.

The method has been extended later by Papantonopoulos (1984) who developed a simplified procedure in order to determine the most critical slip surface.

A brief description of this approach is given below, while more detailed information is given in Chapter 3 and Appendix B.

The problem can be formulated in the following form (Papantonopoulos and Ladanyi 1973, and Papantonopoulos 1979).

$$\text{(maximise or minimise)} \quad Z = \{d\}\{X\}$$

subject to the constraints

$$[A]\{X\} \leq \{b\}$$

$$\{X\} \geq 0$$

[A] is the coefficient matrix of the three equilibrium equations of each element and the failure criteria constraints along each interface.

{X} is the vector of the unknown stresses, i.e. (σ_{rs}, τ_s).

{Z} is the margin of safety to be optimised.

{d} is the coefficient vector of the margin of safety.

{b} is the vector of external forces and the cohesive force along each interface of the elements.

For further details of the [A] matrix and the {B} vector refer to Chapter 3 and Appendix B.

For determining the minimum MS, a reasonable trial piecewise linear slip surface is chosen and the unstable soil mass is discretized into a number of triangular elements. The problem is solved for this position of the failure surface. By solution is meant the determination of the system of forces that satisfy all three equations of equilibrium of each element and the corresponding failure criteria (as inequalities) along the interfaces such that the objective function is either maximised or minimised. Each trial begins by shifting each of the nodes defining the slip surface to new positions in the vertical direction so as to obtain decreasing values of the MS. For this purpose the equation proposed by Saaty (1966) is used.

$$\Delta f = \left(-\sum_{i,j=1}^{m,n} \left(u_i * x_j * \frac{da_{ij}}{dt}\right) + \sum_{j=1}^{n} \left(x_j * \frac{dd_j}{dt}\right) + \sum_{i=1}^{m} \left(u_i * \frac{db_i}{dt}\right)\right) \Delta t \qquad (2.8)$$

where {u} and {x} are the vector of the dual and primal variables. Δf is the change in the objective function, a_{ij} are the coefficients of the [A] matrix and b_i are the coefficients of the {b} vector.

The formula provides the sensitivity of the objective function with regard to an implicit parameter t in the neighbourhood of the optimal solution. For a small increment Δt, the effect on the objective function can be evaluated, i.e., an increase or decrease.

To use the Saaty equation, the coefficients a_{ij} and b_i must be expressed in terms of the implicit parameter t. To achieve this, each node on the slip surface is given a displacement of t units in the vertical direction, all the other nodes remaining fixed. The new coordinates of this node are

$$X' = X \quad \text{and} \quad Z' = Z + t \qquad (2.9)$$

where X and Z are the original coordinates.
From this new position, a small perturbation Δt is given in the vertical direction to evaluate the change in the objective function using Saaty's equation. The derivative of a_{ij} and b_i are easily evaluated and suitable values given to t and Δt. If the change in the objective function is negative, i.e. decrease in the MS, the node is moved in the vertical direction by an amount equal to t units. If it is positive, it is moved in the opposite direction following the same procedure. By moving the nodes a new slip surface is obtained having a reduced value for the MS. The procedure is repeated until no further decrease is possible. This identifies the critical slip surface.

2.3.5.1 Comments on the optimisation approach

The optimisation approach as applied to slope stability problems does not suffer from the problems of the variational approach. The extreme values exist. The

restriction of displacements in the vertical direction is rather rigid but the approach has a great potential especially for complex problems encountered in practice. In the present study it is this approach that has been been generalised to remove the restrictions on the displacements.

Chapter III

GENERALISED LIMIT EQUILIBRIUM METHOD

3.1 INTRODUCTION

Since the proposed algorithm is based on the Generalised limit equilibrium method (GLEM), proposed by Papantonopoulos (1979) and since this work is mostly unpublished and not available in English, it becomes necessary to present in this Chapter and in the Appendix B, an extensive summary of the general methodology and of the mathematical formulations relevant to this work.

The GLEM theory can be divided into two different approaches

1. The quasi-static approach and
2. The energy approach.

The former is similar to the conventional limit equilibrium methods and to the static approach (lower bound) of the limit analysis theory of plasticity. The latter is similar to the kinematic approach (upper bound) of the theory of limit analysis. Both seek to determine a stress (force) field that minimises (or maximises) a given stability criterion. For the quasi-static approach, this criterion is the margin of safety along a given failure surface. For the energy approach, this criterion is the difference between

the energy provided to the system and the energy dissipated within the system for a given kinematically admissible mechanism of failure.

The first approach is called "quasi-static" because, although it is formulated in terms of statics only, it does have implicit kinematic constraints such as the sign of the shearing forces along the interfaces of sliding elements.

The search method developed in this thesis follows the quasi-static approach. The basic assumptions of this approach are outlined in the following section.

3.2 BASIC ASSUMPTIONS AND PROCEDURE

To formulate the quasi-static approach the following procedure has to be followed :

1. Separate the unstable region from the stable by assuming a slip line.
2. Divide the unstable area into elements, triangles or quadrilaterals.
3. Choose the failure criterion along the slip line and along the interfaces of each element. For soils a linear Mohr-Coulomb criterion is usually assumed.
4. Form the equilibrium equation of each element as a function of the internal and external forces acting on it (equality constraints).
5. Form the relations corresponding to the failure criteria along each interface and along the assumed slip line (inequality constraints).

6. Form the supplementary equations which restrict the sign and/or magnitude of certain unknown variables (equality constraints).

It has been mentioned already in Chapter two, and it will be further illustrated in Section 3.3.6, that the relation obtained in steps 4, 5 and 6 provide more unknowns than equations. In principle, therefore, the problem has no unique answer. But, if for some reasons one wants at the same time to find the maximum or minimum (extremum) of a linear or non-linear function of the unknowns, the problem becomes one of mathematical programming and it, possibly, admits a unique answer. Such a function can be the margin of safety or the factor of safety along the failure surface. The seventh step will then be :

7. Choose a function in terms of the unknown variables that must be minimised (or maximised) according to the specific design requirements. This function is called the objective function.

Thus the problem can be formulated as follows :
Given a potentially unstable area divided in elements find the stress (force) field that :

1. Keeps each element of the system in equilibrium.
2. Satisfies the failure criteria on the interfaces of the elements and on the slip surface.
3. Gives to the objective function its minimum (maximum) value.

It is important to note that, in the quasi-static approach, the stability criterion is simply the existence of a stress (force) field that satisfies the equations of equilibrium and the failure criteria. The objective function if it is the margin of safety or the factor safety is merely a side information giving a "distance from failure".

This constitutes at the same time a significant conceptual departure from the conventional limit equilibrium methods and a link between their intuitive "engineering" approach and the lower bound approach of limit analysis theory of plasticity.

In addition, by minimising and maximising the objective function for the same slip surface, one obtains the limits between which the actual values will lie.

3.3 FORMULATION OF THE QUASI-STATIC APPROACH

It is appropriate to mention now that the quasi-static approach can have a number of variants depending on the choice of the stress distribution along the elements and the choice of the objective function. Several variants have been suggested by Papantonopoulos (1979). In the present thesis, the "force field - margin of safety" variant is considered, which reduces the problem to a linear programming one. In the following sections, the governing equations are formulated.

3.3.1 Force field and element type

Type of elements: Triangular elements are chosen for simplicity but other geometric forms are possible.

The assumed stress field is as follows: the nodes of the triangle are denoted by i,j,k, and the length of the sides ij, jk and ki by a, b and c, respectively. Thus, σ_{rs} means the stress acting at nodes r = i,j,k and normal to the sides s = a,b,c. Shear stresses are denoted by τ_s, which are parallel to the sides s = a,b,c. Thus, there are three unknown stresses on each side of the element (see Fig. 3.1). This stress distribution corresponds to a force whose normal and tangential components are defined by the two normal stresses and by the shear stress τ_s. The requirement that each of the normal stresses has to be positive ensures that the resultant of the total force acts within the middle third of each side for each triangular element (see Fig. 3.2).

3.3.2 Equations of equilibrium for the element

Fig. 3.1 shows the element type. Letters a,b,c symbolise the length of the sides ij, jk and ki of the element. i,j,k denote the nodes of the element. The sign conventions for the stresses are shown in Fig. 3.3.

The forces acting on the element are shown in Fig. 3.3 and are explained as follows:

1. W: is the weight of the element. It is assumed that it acts at the centroid of each element.
2. KW: is the seismic force applied at the centroid of each element. K is the ratio of the horizontal acceleration due to the seismic forces to the acceleration due to gravity.
3. P: is the concentrated external force acting on the side b at a distance e*b from node j. ω is the angle as shown in Fig.3.3.
4. Mo: is the external moment acting on the triangle. This could be caused by the non-homogeneity of the mass as then the centroid of the triangular element does not coincide with the centre of mass, or because of the seismic force in a heterogeneous triangle.
5. U_a, U_b, U_c are the resultant forces due to the water pressure acting on sides a,b,c of the element. e_1, e_2, e_3 are the points of application.
6. σ_{rs}, τ_s : normal and tangential stresses acting on the side s and the node r. s takes the values a,b,c and r the values i,j,k, respectively.

For each element, the force equilibrium in the X and Z direction and the moment equilibrium around the centroid are to be satisfied.

The equilibrium equations can be expressed in the matrix form as shown:

$$[S'] \{t\} = \{W\} + P1\{Q1\} + P2\{Q2\} + \{R\} + \{M\} \quad (3.1)$$

The matrix [S'] and the vectors {t}, {W}, {Q1}, {Q2}, {R} and {M} are shown in Table 3.1 and the detailed calculations are shown in the appendix B. The coefficients Z_{ij} , X_{ij} , . . ., E, M_a, M_b, e_1 , e_2 , e_3, e_0 and R_1 , R_2, R_3, U_a, U_b, U_c are also shown in the Appendix B. γ is the average unit weight of the element (dry, saturated or partly saturated). The vector {t} is the stress vector, i.e.the vector that contains σ_{rs} and τ_s . The stresses are considered to be zero on the surface of the slope boundary.

The equilibrium equations in matrix form are shown in Table 3.1, and the detailed calculations are shown in Appendix B.

3.3.3 Equilibrium constraints at the interfaces

For the two adjacent elements as shown in Fig. 3.4, side 'a' is the common side. Then for equilibrium to be satisfied at this interface the additional constraints are:

$$\left| \begin{array}{l} {}^{m}\sigma_{ra} = {}^{n}\sigma_{ra} \\ \\ {}^{m}\tau_{a} = {}^{n}\tau_{a} \end{array} \right| \qquad r = i,j \qquad (3.2)$$

This is done automatically in the matrix assembly.

3.3.4 Failure criteria

For the element type considered here, the failure criteria are satisfied along each of the interfaces and along the slip surface, but not at every point within the element.

Linear Mohr-Coulomb criterion is considered and are given by:

$$T_s < S_s \mu_s + C_s L_s \qquad (3.3)$$

$$T_s = \tau_s L_s \ , \ \mu_s = \tan\phi_s \qquad (3.4)$$

$$S_s = \frac{1}{2} (\sigma_{is} + \sigma_{js}) L_s \qquad (3.5)$$

The normal stress σ_{rs} should be greater than or equal to zero, but this condition is automatically satisfied by the Simplex method used to solve the linear program, where the implicit condition is that all the unknown variables have to be greater than or equal to zero.

The condition in equation (3.3) corresponds to the following inequalities :

$$T_s < S_s \mu_s + C_s L_s$$

$$-T_s < S_s \mu_s + C_s L_s \qquad (3.6)$$

3.3.5 Additional constraints

In addition to the restrictions already mentioned, other restrictions have also to be imposed. These can be divided into three categories:

1. Restrictions on the signs of the variables;
2. Restrictions on the magnitudes of the variables;
3. Linear relations of the unknown variables.

To take into account the mechanism of failure, i.e. kinematics of failure, certain restrictions have to be imposed on the sign of the tangential stresses. Such restrictions have the form :

$\tau_s \leq 0$ and $\tau_s \geq 0$.

These are precisely the constraints that confer to the method its quasi-static character. The restriction on the magnitude could be that the stresses on the slope boundary should be zero:

σ_{rs} and $\tau_s = 0$ (example: tension crack)

At the node i, the condition could be imposed that the magnitude $\sigma_{in} = \sigma_{im}$ (see Fig.3.5). This gives a quasi-continuous distribution of normal stresses and also simplifies the calculation by reducing the number of unknowns.

3.3.6 Constraints and their nature

The relationships developed in the previous sections (equations and inequalities) form a set of constraints that an admissible solution (force system or force field) should satisfy. It is known that all these equations and inequalities are linear functions of the unknown (effective) normal and tangential stresses. So, the problem has linear constraints. It is also apparent that the number of unknowns is greater than the number of equations.

This is best illustrated by a simple example shown in Fig.3.6. The unstable region is divided into four triangles and the slip line consists of three lines. For each element, there are three unknowns on the interface and along the slip lines, i.e. two unknown normal stresses and one unknown tangential stress. The number of interfaces including the slip line is six, thus the total number of unknowns is 18.

No of elements	unknowns	equations
4	6x3 = 18	4x3 = 12

Thus, it can be seen that the number of unknowns exceeds the number of equations, and if the number of elements is increased, this further increases the ratio of the unknowns to the number of equations. Thus, it can be concluded that an infinite number of solutions (force field) exist which satisfy the static equations of equilibrium and the failure

criterion along the interfaces. Each force field gives a different value to the objective function (factor of safety or margin of safety).

3.3.7 Objective function

The indeterminacy is removed if an appropriate objective function is chosen. While any function of the unknown variable is admissible, a linear function reduces the problem to that of a linear program which can be solved reliably and efficiently with the well established Simplex method. The following functions are good candidates for an objective function.

a) The global margin of safety (MS)

This is defined in the following way:

$$MS = \Sigma T_r - \Sigma T_a \qquad 3.7$$

ΣT_a is the sum of all the tangential forces applied along the slip surface.

ΣT_r is the sum of the resistance force along the slip surface.

$$\Sigma T_r = \sum_{v} (S_s \mu + C_s L_s)$$

$$\Sigma T_a = \sum_{v} | T_s | \qquad 3.8$$

v = Number of interfaces along the slip surface.

$$|T_s| = \tau_s L_s \ , \ S_s = \frac{1}{2} (\sigma_{is} + \sigma_{js}) L_s \qquad (3.9)$$

Notice that the margin of safety is a linear function of the unknown variables, and also that the global margin of safety has to be greater or equal to zero, since the failure criteria (section 3.3.4) have to be satisfied.

b) Local margin of safety

This is the margin of safety along any interface or along a number of interfaces that form a segment of the entire slip surface. Minimising local margins of safety helps to simulate progressive failure processes. Note that the local margins of safety are calculated as byproducts even when the global margin of safety is optimised.

c) The factor of safety

The conventional definition of the factor of safety for slope stability problems is given by :

$$FS = \frac{\Sigma T_a}{\Sigma T_r} \qquad (3.10)$$

As it can be seen, the factor of safety is a non-linear function of the unknowns, and, in principle, cannot be used as the objective function unless one resorts to non-linear programming.

d) Relationships between margins of safety and factors of safety

The relationship between margins of safety and factor' of safety are the following :

$$FS = 1 + \frac{MS_s}{\Sigma T_a} \qquad (3.11)$$

$$FS = 1 + \frac{MS}{\Sigma T_a} \qquad (3.12)$$

To each global or local MS, a FS corresponds that is related non-linearly to MS. It is important to note that, in the GLEM, neither the local MS nor the corresponding local FS are equal for each segment. Thus, the requirement of constant FS of the conventional methods is completely relaxed. If the margin of safety tends to zero the factor of safety tends to one.

If one optimises the margin of safety for two or more different slip line configurations (1, 2, 3 . . N), one obtains :

$MS(1) \leq MS(2) \leq MS(3) \ldots\ldots \leq MS(N)$

This does not imply that,

$FS(1) \leq FS(2) \leq FS(3) \ldots\ldots \leq FS(N)$, because the relationship between the FS and MS is not linear.

3.3.8 The linear program formulation

The slope stability problem can be posed as an optimisation problem as shown below :

$$\text{maximise/minimise} \quad Z = \sum_{j=1}^{n} d_j X_j \qquad (3.13)$$

Subject to the constraints

$$\sum_{j=1}^{n} a_{ij} X_j = C_i \quad i=1,.....p \qquad (3.14)$$

$$\sum_{j=1}^{n} a_{ij} X_j \leq C_i \quad i=p+1,.....m \qquad (3.15)$$

$$\sum X_j \geq 0 \quad j=1,.....q \qquad (3.16)$$

$$\sum X_j \leq 0 \quad \text{(unknown)} \qquad (3.17)$$

where n is the number of unknowns, m is the number of equations and p is the number of equality equations.

Equation (3.13) is the objective function to be maximised or minimised which represents the margin of safety along the slip surface.

Equation (3.14) represents the forces and moment equilibrium equations of the elements.

Equation (3.15) represents the failure criteria along the interfaces of the elements, i.e. shear strength of the soil must be greater than or equal to the existing shear stress. These consist of (m-p) essential restrictions.

The inequalities of equations (3.16) and (3.17) impose the sign on the unknown variables.

In the above set of equations

$\{d_j\}$ is the coefficient vector of the objective function

$\{a'_{ij}\}$ is the coefficient matrix of the equilibrium equations of each element, i.e. [S'] matrix of Table 3.1.

$\{a_{ij}\}$ is the coefficient matrix of the failure criteria along each interface of the elements they correspond to the $\pm$ 1/2 u_s relations.

$\{C'_i\}$ is the vector of the external forces acting along each interface of the element, i.e. {B} vector of Table 3.1.

$\{C_i\}$ is the vector containing the values of the cohesive force along each interface of the element.

$\{X_j\}$ is the vector of the unknown stresses along each interface of the elements, i.e. (σ_{rs}, τ_s)

The equations can be seen as representing a mix of equality and inequality constraints. The inequality constraints can be converted to equality constraints by adding artificial slack variables of m-p numbers. Then the problem reduces to:

(maximise or minimise) $Z = [D]^T \{X\}$

subject to the constraints

$$[A]\ \{X\} = \{B\}$$

The matrix [A] is called the constraint matrix and is presented in Fig.3.7. The matrix is of dimension m x (m+n) and is composed of six sub-matrices. The matrix [A1] contains the terms of a'_{ij} of equation (3.14). The matrix [A2] contains the terms of a_{ij} of the inequality (3.15). The matrix [I] is the unit matrix of dimension pxp and (m-p) x (m-p) and [0] is the null matrix. The vector {X} contains (m+n) unknown variables, i.e. σ_{rs} , τ_s and the artificial variables. The vector {B} contains two subsets {B1} and {B2}. The vector {B1} contains the external forces and the vector {B2} contains the cohesion terms for the inequalities. $[D]^T$ symbolises the transpose of the vector of coefficients d_j of the objective function. The detailed assembly of the matrix for a particular slope configuration is shown in Appendix C.

The linear program utilises the simplex method. In this method, all the unknown variables have to be positive. Since the sign of the tangential stresses can be positive or negative, the substitution X = X' - X" where X' and X" are ≥ 0 allows to have positive or negative values of X depending upon the magnitude of X' and X" where both are positive numbers.

The Simplex algorithm then finds the unknown variables such that the objective function, i.e. MS, is maximised or

minimised by putting all the artificial variables to be equal to zero. If a solution exists, then, the magnitude of the objective function is calculated. There are four possible responses to the linear program:

1. The solution does not exist;
2. The solution exists and is optimal;
3. An infinite number of optimal solutions exist that give to the objective function the same optimum value.
4. The value of the optimal (min or max) objective function tends towards $\pm\infty$.

The response number 1 implies that the system is unstable globally or locally. The responses 2 and 3 have both a physical meaning and correspond to stable conditions, while the response 4 if ever arises should indicate in this context input and/or numerical errors.

Chapter IV

PROCEDURE TO DETERMINE THE CRITICAL SLIP SURFACE

4.1 DESCRIPTION OF THE SEARCH ALGORITHM

The limitations of the available search techniques based on the conventional limit equilibrium methods have been discussed in Chapter 2. In the same chapter, the potential of the generalized limit equilibrium to locate the most critical surface with the help of sensitivity analysis has been pointed out.

In this chapter, the previous work done in this direction by Papantonopoulos (1984) is extended in order to find a search algorithm which leads to the determination of the most critical slip surface in a converging procedure reliably and economically.

The main steps of the proposed method are similar to those proposed by Papantonopoulos (1984).

First, a reasonable piece-wise linear slip surface is chosen as a starting point. The problem is solved for this position of the failure surface. By solution is meant the determination of the system of forces that satisfy all three equations of equilibrium of each element and the corresponding falure criteria (as inequalities) along the interfaces of the elements. Next, the nodes defining the

slip surface are moved to new positions such that the margin of safety decreases. In contrast to the method of Papantonopoulos (1984), in the present procedure

1. the displacement increment t is not in the vertical direction but can be inclined in any direction θ,
2. both the magnitude t and the direction θ of the movement are determined by a sensitivity analysis of the linear program.

The procedure is repeated successively until no further decrease is possible, or until an infeasible solution is declared in which case the slope is unstable. This clearly indicates if and when the critical failure surface has been obtained. The sensitivity analysis is done adapting Saaty's procedure to the particular limit equilibrium problem. Following Saaty's procedure, it is possible to determine the angle θ that gives the maximum decrease to the objective function (margin of safety) for a given small displacement t. This can be obtained as a function of the values of the primal and dual solution of the linear program. Saaty's sensitivity analysis as well as a brief review of concepts of sensitivity analysis and the related primal and dual solutions are presented in the next section.

4.2 SENSITIVITY ANALYSIS

4.2.1 Purpose and types of sensitivity analysis

Sensitivity analysis is a post optimal problem. This means that one is interested to estimate the behaviour of the solution vector and the corresponding objective function when some or all of the parameters of the initial problem are subject to small variations. This can be done efficiently by exploiting the information already obtained by the solution of the linear program.

There are several different types of post optimality problems, but they can be grouped rather arbitrarily into three general categories:

1. Problems involving discrete parameter changes: These arise when the numerical values of a_{ij}, b_i, or d_j are altered and one wants to know their effect on the objective function while the solution vector remains optimal.
2. Problems involving continuous parameter changes: This category includes problems in which one or more of the parameters are perturbed or varied in some given direction and one wants to see their effect on the objective function while the solution vector remains optimal.
3. Problems involving structural changes. These arise when the linear program is reformulated by adding or deleting constraints or variables presumably in order

to reflect an alternate operating mode, or a fundamental change in the mathematical model.

The proposed search procedure is based on the sensitivity analysis of the second type owing to the nature of the problem.

4.2.2 Primal and dual problem

To understand the theory of sensitivity analysis one must understand the primal and dual problem concepts.

To every linear program formulated as:

$$\text{(maximise or minimise)} \quad Z = \{D\}^T \{X\}$$

subject to the constraints,

$$[A]\ \{X\} \leq \{B\}$$

corresponds another linear program:

$$\text{(maximise or minimise)} \quad Z = \{B\}^T \{u\}$$

subject to the constraints

$$[A]^T \{u\} \geq \{D\}$$

which is called the Dual of the original program.

$\{X\}$ is the vector of primal variables (θ_{rs}, τ_s in our case).

$\{u\}$ is the vector of dual variables.

In some problems, the dual variables have a physical meaning but not in our case.

Many interesting relations connect the Dual and Primal programs. Those more relevant to our problem are the following:

1. A feasible solution {X} to the primal problem is optimal if and only if there exists a feasible solution {u} to the dual problem such that,

$$Z(\text{optimal}) = \{D\}^T \{X\} = \{B\}^T \{u\}$$

2. The Simplex Algorithm gives as by-product of the analysis the dual solution {u}.

In practice, 1 and 2 are combined to give an easy check of the convergence of the numerical procedure, thus enhancing its reliability.

4.2.3 Application of Saaty's analysis to determine the critical slip surface

The analysis proposed by Saaty falls into the second category of the post optimal problems. Saaty develops an equation which can be solved explicitly to obtain the sensitivity of the objective function with regard to an implicit parameter in the neighbourhood of the optimal solution. Expressing the Primal and Dual problem in a different form as follows:

(maximise or minimise) $f = \sum_j d_j X_j$

subject to the constraints

$$\sum_i a_{ij} X_j \geq b_i \qquad i = 1,2,3 \ldots\ldots,m$$

$$x_j \geq 0 \qquad j = 1,2,3 \ldots ,n$$

and (maximise or minimise) $f = \sum_i b_i u_i$

subject to the constraints

$$\sum_j a_{ij} u_i \leq d_j \qquad j = 1,2,3 \ldots ,n$$

$$\sum u_i \geq 0 \qquad i = 1,2,3 \ldots ,m$$

When the function f is considered as a function of a_{ij}, b_i and d_j and these elements are considered as functions of an implicit parameter t, the total derivative of f with respect to t is given by

$$\frac{df}{dt} = \sum_{i,j=1}^{m,n} \left(\frac{\partial f}{\partial a_{ij}} * \frac{da_{ij}}{dt}\right) + \sum_{j=1}^{n} \left(\frac{\partial f}{\partial d_j} * \frac{dd_j}{dt}\right) + \sum_{i=1}^{m} \left(\frac{\partial f}{\partial b_i} * \frac{db_i}{dt}\right) \qquad (4.1)$$

This is strictly valid only if the new and the old solution have the same variables in the optimal vector. If the new basis is different, it is then possible to find an increased objective function in the next step. At this point, it has been reckoned that even if this happens after a local perturbation, the continuation of the procedure will lead again to lower values and eventually to the determination of the most critical slip surface.

This requires an optimization problem that behaves well and has a stable convergence by its nature. Fortunately,

the subsequent results of this study validated this point. In this case the total derivative can then be written in a computable form as :

$$\frac{df}{dt} = -\sum_{i,j=1}^{m,n} (u_i * x_j * \frac{da_{ij}}{dt}) + \sum_{j=1}^{n} (x_j * \frac{dd_j}{dt}) + \sum_{i=1}^{m} (u_i * \frac{db_i}{dt}) \qquad (4.2)$$

where u_i and x_j are the dual and primal variables obtained by utilising the Simplex method for the optimization problem. In equation (4.2), all the partials and derivatives can be solved explicitly. The formula provides the sensitivity of the objective function with regard to an implicit parameter in the neighbourhood of the optimal solution.

For a small increment of t, the change in the objective function is given by :

$$\Delta f = (-\sum_{i,j=1}^{m,n} (u_i * x_j * \frac{da_{ij}}{dt}) + \sum_{j=1}^{n} (x_j * \frac{dd_j}{dt}) + \sum_{i=1}^{m} (u_i * \frac{db_i}{dt})) \Delta t \qquad (4.3)$$

This change in the objective function can be evaluated by giving a small perturbation Δt to the implicit parameter. The parameter may be given any suitable value. The values of Δt must be small so as to ensure that the new and the old solution have the same optimal basis. The optimal basis is the vector which contains all the unknowns (σ_{rs} and τ_s) which are different than zero and optimizes the objective function.

In this study, it is assumed that in the Saaty's equation the coefficients of the objective function $\{d_j\}$ are constant. Consequently, the second term of equation (4.2) is neglected. This assumption has been done for simplicity and is absolutely true when the length of the segments on the failure surface are equal. The more these lengths become inequal, the more one should expect a deviation from the exact solution. The impact of this assumption is thought to be small, but this should be the subject of future investigations.

In order to use the Saaty's equation to find the change in the objective function, the coefficients a_{ij}, and b_i must be expressed in terms of an implicit parameter. To achieve this, each node on the slip surface is given a displacement of t units in the direction Θ; all the other nodes are kept fixed. The new co-ordinates of the node are given by

$$X' = X + t*\sin\Theta$$
$$Z' = Z + t*\cos\Theta \qquad (4.4)$$

where X' and Z' are the co-ordinates of the new positions and X and Z are those of the original position. This expresses the coefficients a_{ij} and b_i in terms of the implicit parameter t and Θ. From this new position, a small perturbation Δt is given in the same direction Θ to evaluate the change in the objective function, i.e. increase or decrease. This can be done by using equation (4.3). The

values u_i and x_j are those of the dual and primal values obtained from the Simplex method prior to giving the displacement to the nodes. The derivatives with respect to t of the a_{ij} and b_i elements are easily evaluated if the direction Θ is assumed for each node. If the change in the objective function Δf is positive, then the movement of the node in the direction Θ by a distance t increases the margin of safety of the slip surface. The direction of movement should then be $\Theta + 180°$. This is obvious as equation (4.3) is a function of Sin θ and Cos θ when expressed in terms of the implicit parameter and takes the form $\Delta f = a \{ \text{Sin } \theta + b \text{ Cos } \theta$. Thus, the two values of Θ which maximise or minimise the change in the objective function are Θ and $\Theta + 180°$.

The above procedure is followed for all the nodes on the slip surface and the corresponding Δf are evaluated, i.e. $\Delta f(1), \Delta f(2), \Delta f(3), \ldots \Delta f(n)$, where n is the number of nodes on the slip surface. The new position of the slip surface is located such that there is a decrease in the global margin of safety. The node whose movement induces the maximum decrease in the margin of safety is moved by an amount t and the others in a suitable fraction of t corresponding to their respective sensitivity values. For example let $\Delta f(3)$ be the maximum among $\Delta f(i)$. Then the distance moved by the nodes t(i) in the direction $\Theta(i)$ will be as shown below.

$$t(i) = \frac{\Delta f(i)}{\Delta f(3)} * t \qquad (4.5)$$

where i varies from i = 1, n

The new coordinates of the slip surface will be given by

$$X' = X + t(i)*\sin\theta(i)$$

$$Z' = Z + t(i)*\cos\theta(i) \qquad (4.6)$$

where i varies from i = 1, n

After obtaining the new slip surface, the whole problem is solved again and the procedure is repeated until the value of the global or local margin of safety either stabilizes or increases. This determines the critical slip surface.

The parameter t can be normalised with respect to the height of the slope. To obtain faster convergence, large values may be given to t but care must be exercized because for large values instability occurs. Tentative normalised values for optimum performance have been established in Chapter 5.

4.3 EVALUATION OF THE OPTIMUM ANGLE θ

The direction of the movement Θ for each of the nodes is unknown. It is possible to assume the direction of movement of each node on the slip surface, and this is useful when one wants the node to move along a given line (slope surface, material interfaces). This direction need not be the direction in which the margin of safety attains its fastest decrease. If this is not the case, it is more efficient to calculate the direction Θ corresponding to the fastest MS decrease. To evaluate this direction, equation (4.2) can be differentiated with respect to Θ instead of t and will be as shown below:

$$\frac{df}{d\theta} = -\sum_{i,j=1}^{m,n} (u_i * x_j * \frac{da_{ij}}{d\theta}) + \sum_{j=1}^{n} (x_j * \frac{dd_j}{d\theta}) + \sum_{i=1}^{m} (u_i * \frac{db_i}{d\theta}) \qquad (4.7)$$

The coefficients a_{ij} and b_i are differentiated with respect to Θ. By putting $\frac{df}{d\theta}$ equal to zero, one can evaluate the optimal direction Θ uniquely in such a way that the movement of the nodes along this direction decreases the margin of safety by an optimal amount. Since perturbation is given to one node at a time, the right hand side of equation 4.7 will be in terms of only one unknown, i.e. Θ which can be obtained uniquely.

4.3.1 Direct assembly of the differentiated matrix to evaluate the optimum angle θ

The direct assembly of the matrix has been developed in Chapter 3 and is shown in Fig. 3.7. In the Saaty's equation, the a_{ij} elements correspond to those of [A] matrix and b_i to those of the {B} vector.

Once the derivatives of the [A] matrix and {B} vector with respect to θ are known, the optimum angle of movement of the nodes can be obtained uniquely by utilising equation (4.7).

4.3.1.1 Derivative of [A] matrix and the {B} vector with respect to θ

The [A] matrix consists of six sub-matrices, i.e. [A1], [A2], [I] and [O]. The derivatives of the unit and null matrix with respect to θ are zero. The inequality matrix [A2] represents the Mohr-Coulomb failure criterion and is independent of the co-ordinates. Hence its derivative with respect to θ will also be zero. Thus the only matrix whose derivative exists with respect to θ is the [A1] matrix, i.e. the equality matrix whose elements are shown in Table 3.1.

The vector {B} consists of two sub-vectors {B1} and {B2}. The vector {B2} consists of the cohesive terms hence its derivatives with respect to θ will be zero. Thus the only vector whose derivative exists is {B1}.

For the triangular element having nodes i, j and k, three possible movements exist:

1. node i is moved, nodes j and k are fixed.
2. node j is moved, nodes k and i are fixed.
3. node k is moved, nodes i and j are fixed.

For each different nodal movement, the differentiated [A1] matrix and the {B1} vector take different forms. The detailed analysis is shown in the appendix D and, Tables 4.1, 4.2 and 4.3 show the differentiated matrix by moving nodes i, j and k, respectively. Table 4.4 shows the differentiated {B1} vector by moving the nodes i, j and k respectively. The assembly of the differentiated [A1] matrix and the {B1} vector for a particular slope configuration by giving a nodal displacement to any one of the nodes is shown in Appendix E.

4.4 EVALUATION OF THE SENSITIVITY COEFFICIENTS

Once the optimum angle is found for each node, the next step is to find the change in the objective function by moving the particular node a suitable distance t in the direction θ. A suitable perturbation Δt is given from this new position. The purpose of this procedure is to move the nodes in proportion to their sensitivities. It is only logical to do this to ascertain the shape of the critical slip surfaces.

Using Saaty's equation (4.3) one can find the sensitivity coefficient for each node. The assembly of the differentiated matrix with respect to t will be similar to

the procedure as explained before but the assembly will be done utilising Tables 4.5, 4.6 and 4.7, which correspond to the differentiation of the [A1] matrix with respect to t by moving nodes i, j and k, respectively. Since θ for each node is now known one can find the sensitivity coefficients.

For the assembly of the {B1} vector, the procedure is the same as before, but Table 4.8 is used, which corresponds to the diffrentiation of the {B1} vector with respect to t by moving nodes i, j and k, respectively. For further details on the differentiated [A1] matrix and {B1} vector with respect to t see Appendix D.

The flow chart for the search procedure can be seen in Fig.4.1.

Chapter V

NUMERICAL EXPERIMENTS AND DISCUSSIONS

5.1 INTRODUCTION

In the proposed method, the objective function (MS) could be either maximised or minimised resulting in two kinds of slip surfaces. One corresponding to a force field that minimises the margin of safety, and one corresponding to a force field that maximises the margin of safety. The critical slip surfaces obtained in such a manner will be termed the least critical (LCR) and Most critical (MCR) slip surfaces, respectively.

The purpose of the numerical investigations is to determine the following facts:

1. Establishing the convergence and termination criteria, i.e. the criteria to determine if and when a critical failure surface has been attained.
2. The effect of the variation of the nodal displacement increment t on the "most critical" (MCR) and "least critical" (LCR) slip surfaces. The displacement increment controls the speed and the stability of the iterative procedure.
3. The effect of the number of elements, of which the unstable soil mass is composed of, on the MCR and LCR slip surfaces.

4. The effect of the topology of the elements on the MCR and LCR slip surfaces.
5. The effect the degrees of freedom of the nodes have on the the MCR and LCR slip surfaces.
6. The effect of assuming discontinuous normal stresses along the slip surface on the MCR and LCR slip surfaces.
7. The convergence of the MCR and LCR slip surfaces when one starts from two different initial piece-wise linear slip surfaces, all other factors being the same.

By the effect on the critical slip surface is meant the effect on the location of the slip surface, in its global margin of safety and factor of safety.

To examine the above facts, a 2:1 slope having a height of 12 m is chosen. The soil is assumed to be dry and homogenous, having the properties c = 28.7 KN/m2, $\phi = 20°$, $\gamma = 1.89$ KN/m^3. This slope has been analyzed by Fredlund and Krahn (1976) using various conventional methods and by Papantonopoulos (1979) by the generalized limit equilibrium method. The various configurations examined are shown in Fig. 5.1.

5.2 ESTABLISHING THE CONVERGENCE AND TERMINATION CRITERIA

The criteria should pinpoint the critical slip surface, thus terminating the iterations in the computer program. This implies that at a certain stage the global MS of the generated slip surfaces must either stabilise at a certain value or increase with successive number of iterations.

5.2.1 Case Study 1

The configuration shown in Fig. 5.1 (a) is chosen. The objective function is minimised to obtain the MCR slip surface. The global MS was found to decrease successively with the number of iterations (see Fig.5.2), and thus no conclusive criteria could be established, especially since the shape of the MCR slip surface is found to be saw-toothed and thus not compatible with a suitable kinematic mode of sliding (see Fig.5.3). The same trend is observed for the LCR slip surface. To be compatible with an acceptable kinematic mode of sliding, a restriction is imposed on the nodes of the slip surface so as to maintain a concave slip surface. The same procedure is repeated by imposing the concavity condition and the global MS is minimised (MCR slip surface). Fig. 5.4 indicates that, from the eighth iteration onwards, the global MS is found to increase thus, clearly pinpointing the MCR slip surface. The same trend is observed for the LCR slip surface as shown in Fig. 5.5. Thus the criteria for locating the critical slip surface is

clearly established if one imposes the condition that the slip surface be concave.

Table 5.1 shows the comparison between the two cases, i.e. with and without the concavity condition. The initial values of the MS and FS were the same but when the concavity condition is imposed, a 20% increase in the global MS and a 9% increase in the global FS for the MCR slip surface were obtained. This implies that by analysing slopes by the generalised limit equilibrium methods, there exist non concave slip surfaces having lower values of the MS and FS, than those which correspond to the concave slip surfaces.

5.3 VARIATION OF THE NODAL INCREMENTAL DISTANCES

In the proposed method, the most sensitive node is moved a distance of one unit, the others in proportion to their sensitivities. This requires a large number of iterations to arrive at the final critical slip surface, especially if one has chosen the starting slip surface substantially far from the actual one. A study has been carried out by varying the distance moved by the most sensitive node (NDMAX) from one to five units. The optimum value for NDMAX will be the one which gives the least number of iterations for convergence without affecting the global MS and the location of the critical slip surface .

5.3.1 Case Study 2

To find the optimum nodal increment, the configuration shown in Fig. 5.1(b) is studied, and the objective function minimised (MCR slip surface). The nodal increment NDMAX is varied from one to five units. For NDMAX equal to five units, numerical problems were encountered as infeasible solutions were obtained which lead to the abortion of the computer run. This happened, because the element geometry of the slope was destroyed as large displacements were given to the node. The variation of the global MS with the number of iterations, for NDMAX varying from one to four units, can be seen in Fig.5.6. It appears that the global MS converged to the same values regardless of the NDMAX values. The same can be said about the location of the critical slip surfaces, as shown in Fig.5.7, which were found to be identical. From these results, it can be concluded that the optimum nodal increment is four units as the number of iterations required for convergence is the least, about half of that required for NDMAX equal to one unit.

The same trend is noticed when the objective function is maximised (LCR slip surface). The variation of the global MS with the number of iterations for NDMAX equal to one and four units are shown in Fig.5.8. With NDMAX equal to five, infeasible solutions were again obtained. The location of LCR slip surfaces were found to be the same as shown in Fig.5.9. The optimum nodal increment is again found to be four units.

It seems reasonable to assume as a first approximation that NDMAX is a function of the height of the slope. Based on a limited number of case studies examined, where the height of the slope H is 12 m, i.e. 40 ft it can be tentatively concluded that NDMAX should be of the order of one-tenth the height of the slope for faster convergence and numerical stability.

5.4 EFFECT OF THE NUMBER OF ELEMENTS ON THE CRITICAL SLIP SURFACE

To investigate the above effect, all other parameters were kept the same. The configuration shown in Fig. 5.1 (c) and (d) differ only in their number of elements. The initial slip surface for the two configurations is the same. Hence the difference in the global MS and the location of the critical slip surface between the two configurations will be an indication of the effect the number of elements has on the critical slip surface.

5.4.1 Case Study 3

Two configurations were analyzed to investigate the effect on the MCR and LCR slip surfaces.

a) MCR Slip Surface (minimisation of the objective function)

The initial values of the MS and FS for the two configurations were found to be the same. The critical slip surfaces obtained were found to have a difference of 5% and

7.3% between their global MS and FS, respectively, (see Table 5.2, where cases 3A and 3B represent the configurations of Fig.5.1 (c) and (d), respectively). The critical slip surfaces obtained, were found to be different as can be seen from Fig.5.10. The number of iterations required for convergence for cases 3A and 3B were twenty-two and nine respectively.

b) LCR Slip Surface (maximisation of the objective function)

The initial slip surfaces were found to have the same values for the safety index. The least critical slip surfaces for the two configurations were attained after six and nine iterations respectively. The percentage difference in their global MS and FS were found to be 2.5% and 0% respectively, (Table 5.3). Fig. 5.11 shows the location of the critical slip surfaces which were found to coincide.

5.5 EFFECT OF THE TOPOLOGY ON THE CRITICAL SLIP SURFACES

The configurations shown in Fig. 5.1 (b) and (c) are similar in all respects except that they differ in their topology, i.e. the number of elements is the same but their structure is different. The same is the case for the configurations in Fig. 5.1 (e) and (f). All the cases have the same initial slip surface. Hence, the difference in the values of the margin of safety and the location of the

critical slip surface for the two pairs of configurations is an indication of the effect the topology has on the critical slip surface.

5.5.1 Case Study 4

This corresponds to the configuration of Fig. 5.1 (b) and (c).

a) MCR Slip Surface (minimisation of the objective function)

The initial slip surfaces for the two configurations were found to have the same values of the global MS and FS and the percentage difference in the global MS and FS of their critical slip surfaces were found to be 16% and 14% respectively. (Table 5.4.), where cases 4A and 4B correspond to the configuration of Fig.5.1 (b) and (c) respectively. Fig. 5.12 shows the final location of the slip surfaces which did not coincide. The number of iterations required to converge for Case 4A and 4B were twelve and nine respectively.

b) LCR Slip Surface (maximisation of the objective function)

The percentage differences in the MS and FS of their critical slip surfaces were 1.8% for the global MS and 0.5% for the global FS. (Table 5.5). Fig. 5.13 shows that the final slip surfaces are coincident. The number of

iterations required to converge for the two cases were five and six respectively.

5.5.2 Case Study 5

This corresponds to the configuration of Fig. 5.1 (e) and (f).

a) MCR Slip Surface (minimisation of the objective function)

The percentage difference in the global MS of the two critical slip surfaces were found to be less than 1%, (Table 5.6), where case 5A and 5B correspond to the configurations of Fig.5.1 (e) and (f), respectively. The location of the critical slip surfaces which did not coincide is shown in Fig.5.14. The number of iterations required to converge for the two cases were found to be ten.

b) LCR Slip Surface (maximisation of the objective function)

The percentage difference in the global MS of the two critical slip surface is found to be zero. (Table 5.7). Fig. 5.15 shows that the two final slip surfaces are coincident. The number of iterations required for convergence were eight and nine for cases 5A and 5B, respectively.

5.6 THE EFFECT THE DEGREES OF FREEDOM OF THE NODES HAVE ON THE CRITICAL SLIP SURFACE

The following convention is followed in defining the degrees of freedom. If there is no restriction on the movement of the nodes, it has two degrees of freedom. If it is moved in a fixed direction, it has one, and if it is kept stationary, it has zero. The configuration of Fig.5.1(a) is selected and the solution obtained for two cases having different degrees of freedom, but having the same initial slip surface, thus, the difference in the global MS and the location of the slip surface between the two cases is an indication of the effect the degrees of freedom have on the critical slip surface.

5.6.1 Case Study 6

The configuration of Fig. 5.1 (a) is selected. The two cases considered are 6A and 6B. In Case 6A, the nodes on the slope boundary are kept fixed, i.e. 7,8,9 and 10. Nodes 1 and 6 are restricted in their movement to conform with the slope geometry. The nodes along the slip surface, i.e., 2,3,4 and 5, are moved perpendicular to the inclined slope boundary. Thus, the total degrees of freedom for the system of nodes is 6. In Case 6B, the nodes along the slip surface, i.e., 2,3,4 and 5, have the freedom to determine their optimal direction of movement. All other restrictions are the same as in Case 6A. Thus, the total degrees of freedom for this system of nodes is ten and the two cases

differ only in their degrees of freedom. This case is analyzed for the MCR failure surface. The initial MS and FS were found to be the same. The percentage decrease between the initial and final values of the global MS for Case 6B (more degrees of freedom) was found to be approximately one and a half times greater than those of Case 6A (fewer degrees of freedom). (Table 5.8). Thus, with more degrees of freedom one obtains lower values for the global margin of safety. Both cases required thirteen iterations to converge. Fig. 5.16 shows that the final slip surfaces do not deviate much from one another. However if one moves the nodes in vertical or horizontal directions the difference may be substantial in both the values of the margin of safety and the location of the critical slip surfaces.

In the search procedure proposed by Celestino and Duncan (1981), the movement of the nodes is in the same direction, i.e. either vertical or horizontal. Thus, the critical slip surface found will have higher values of the margin of safety than the true one.

5.7 EFFECT OF THE DISCONTINUOUS NORMAL STRESSES ALONG THE SLIP SURFACE ON THE CRITICAL SLIP SURFACE

In all the numerical investigations carried out so far, continuous normal stresses were assumed along the slip surface. By continuous stresses, one means that the stresses corresponding at the node of the two intersection lines along the slip surface are equal to one another. If

this restriction is not imposed, the system will have freedom to assume any values for these normal stresses and a discontinuous stress field will be obtained. The configuration shown in Fig. 5.1 (c) is analyzed by assuming continuous normal distribution in one case and discontinuous normal distribution in the other. Since one starts from the same initial slip surface, the difference in the global MS and the location of the critical slip surface between the two cases will serve as a comparison.

5.7.1 Case Study 7

a) MCR Slip Surface (minimisation of the objective function)

Case 7A corresponds to the configuration in Fig. 5.1(c) assuming discontinuous stress. Case 7B corresponds to the same configuration assuming continuous stresses. Table 5.9 shows that Case 7A gives much lower values of the MS and FS as compared to Case 7B. The location of the critical slip surfaces is shown in Fig. 5.17 and was found to be radically different. The number of iterations required for convergence for Cases 7A and 7B were fifty and twenty-two respectively.

b) LCR Slip Surface (maximisation of the objective function)

Case 7A (discontinuous normal stresses) gives higher values of the safety index i.e. MS and FS, for both the initial and critical slip surface as compared to Case 7B. (Table 5.10). The number of iterations required for convergence for the two cases were nine and eight respectively. Fig. 5.18 shows the critical slip surface.

The reason for obtaining higher values of MS in the maximization of the objective function and lower values for the minimization of the objective function for both the initial and the critical slip surface for the discontinuous case is due to the following. In the formulation of the linear program, less restrictions are imposed on the system as the normal stresses along the slip surface have the freedom to take any values for the discontinuous case. Thus when the objective function is maximised higher values are obtained for the global MS and FS and lower values for the minimisation of the objective function.

5.8 CONVERGENCE OF THE CRITICAL SLIP SURFACES BY STARTING FROM TWO DIFFERENT PIECE-WISE LINEAR SLIP SURFACES

For each of the configurations shown in Fig.5.1, two different initial slip surfaces are assumed and their critical slip surface obtained. The difference between the global MS and the location of the critical slip surface will be an indication of the effectiveness of the algorithm to converge to the same slip surface.

5.8.1 Case Study 8

a) MCR Slip Surface (minimisation of the objective function)

This conforms to the configuration shown in Fig. 5.1 (b). The values of the global MS and FS for the two initial slip surfaces were found to differ by 24.4% and 2.9% respectively. For the critical slip surfaces, the percentage differences in the global MS and FS were found to be 3.2% and 6.9% respectively. (Table 5.11), where cases 8A and 8B correspond to the two different initial slip surfaces as shown in Fig.5.19. As can be seen, the percentage difference in the MS of the two slip surfaces was found to be decreasing. Thus, showing a definite trend for the slip surfaces to converge to the same one. The values of the global FS seem to be diverging, but as mentioned earlier in Chapter 3, decreasing values of MS do not imply decreasing values of FS. Their convergence can be seen in Fig. 5.19 and the two slip surfaces are almost coincident. The number of iterations required for convergence were twelve and nine respectively.

b) LCR Slip Surface (maximisation of the objective function)

The percentage difference between the global MS of the initial and final slip surface for the two cases were found

to be 30% and 6.6% respectively. (Table 5.12). From this, it can be seen that the two slip surfaces are converging. Fig. 5.20 shows that the two surfaces are almost identical. The number of iterations required for convergence for the two cases were found to be five.

5.8.2 Case Study 9

a) MCR Slip Surface (minimisation of the objective function)

This corresponds to the configuration of Fig. 5.1 (c). The percentage difference between the global MS of the initial and final slip surface for the two cases was found to be 24% and 2.9% respectively, confirming that the two initial slip surfaces are converging. (Table 5.13). The Fig. 5.21 shows the critical slip surfaces to be almost identical. The number of iterations required for convergence for the two cases is seventeen and nine, respectively.

b) LCR Slip Surface (maximisation of the objective function)

The percentage difference between the global MS of the initial and the final slip surface for the two cases were found to be 30% and 6% respectively. (Table 5.14). The Fig.5.22 shows that the convergence of the two slip surfaces is satisfactory. The number of iterations required for

convergence for the two cases was found to be six and five, respectively.

5.8.3 Case Study 10

a) MCR Slip Surface (minimisation of the objective function)

This corresponds to the configuration of Fig.5.1 (d). The percentage difference between the values of the MS of the initial and the final slip surfaces for the two cases was found to be 22% and 1%, respectively. (Table 5.15). The convergence of the two slip surfaces can be seen from Fig. 5.23 and a good match is obtained. The number of iterations required for convergence for the two cases were found to be twenty two and twenty respectively.

b) LCR Slip Surface (maximisation of the objective function)

The percentage difference between the values of MS of the initial and the final slip surfaces were found to be 30% and 2.2% respectively. (Table 5.16). The Fig.5.24 shows that a good match is obtained between the two critical slip surfaces. The number of iterations required for convergence were found to be nine and seven respectively.

5.8.4 Case Study 11

a) MCR Slip Surface (minimisation of the objective function)

This corresponds to the configuration of Fig. 5.1(d), but a discontinuous normal stress field along the slip surface is assumed. In this case the percentage difference between the MS of the initial and final slip surfaces remained the same having a value of 3.2%, even though there is a considerable decrease in the values of the MS from the initial to the final slip surface for each of the individual cases. (Table 5.17). This trend is reflected on the location of the critical slip surfaces obtained which were found to be radically different as can be seen from Fig.5.25. Both cases required fifty iterations for convergence.

b) LCR Slip Surface (maximisation of the objective function)

For this case a better convergence was found as compared to the MCR case (see Fig.5.26). The percentage difference between the MS of the initial and the final slip surfaces were found to be 32% and 15% respectively, see Table 5.18. The covergence is not as good as for the other cases examined. Both cases required eight iterations for convergence.

5.8.5 Case Study 12

a) MCR Slip Surface (minimisation of the objective function)

This corresponds to the configuration of Fig. 5.1 (f). The percentage difference between the MS of the initial and the final slip surfaces were found to be 32% and 2.6% respectively as in Table 5.19. Their convergence can be seen from Fig.5.27. Both cases required ten iterations for convergence.

b) LCR Slip Surface (maximisation of the objective function)

The converging behaviour of the slip surfaces is demonstrared by the Table 5.20. In this case the percentage difference between the MS of the initial and the final slip surfaces were found to be 34.6% and 6.9% respectively. The number of iterations required to converge for the two initial slip surfaces were nine and five respectively. Fig. 5.28 indicates that the final critical surfaces have a good match.

5.9 DISCUSSIONS

The convergence criteria were established on the basis of concavity in order to be in conformity with an acceptable kinematic mode of sliding. It was found that by analyzing slope stability problems considering static equilibrium, it is possible to have non-concave slip surfaces. Moreover, the MS of the non-concave slip surface was found to be lower than that of the concave one as can be seen from case study 1A and 1B.

The number of iterations required for the slip surface to converge could be substantially reduced if one finds the optimum values for NDMAX for each slope analysed. For the slope analyzed it was found to be four units, or 1/10 for the NDMAX/H ratio.

The numerical experiments indicate that the number of elements and their topology do not have any appreciable effect on the MS and the location of the least critical slip surface. On the contrary the above factors did influence the location and the values of the global MS for the most critical slip surface. One can select a number of mechanisms of failure which can be accounted for in this proposed "quasi-static" method. Depending on the failure mechanism assumed the number of triangles and topology are automatically decided. Since the MCR slip surface is dependent on the number of the elements and their topology it would be appropriate to analyze the slope for a number of

different mechanism of failures and choose the one that gives the least MS.

Any search, which imposes a restriction on the movement of the nodes, would give higher values of the global MS than the one in which the movements of the node are not restricted.

When discontinuous normal stresses are assumed along the slip surface, radically different slip surfaces are obtained as compared to the one in which continuous normal stress distribution are assumed.

For all the case studies, the convergence obtained by starting from two reasonable but different piece-wise linear surfaces was found to be very satisfactory for the most and the least critical slip surfaces. The only exception was when discontinuous normal stresses were assumed along the slip surface, but in homogenous soil media the normal stress distribution along the slip surface has to be continuous.

Chapter VI

ANALYSIS OF AN ACTUAL SLOPE FAILURE

6.1 CASE INVESTIGATED

The main objective of this analysis is to illustrate the possibilities of the proposed algorithm by conducting a preliminary investigation of a natural clay slope that has failed. For this purpose a natural slope at Rosemere (about 20 km northwest of Montreal) has been selected.

The slope shown in Fig. 6.1 has a height of 11.9 m and makes an angle of 24° with the horizontal. The slope is a result of a 5 m cut in a natural slope. The slide occurred in July 1974, 28 months after the end of the excavation. The soil properties of the clay as reported by Lefebvre and Chahde (1978) are : c' = 8.8 kPa, ϕ = 34.1°, and γ = 16.5 kN/m^3. Fig. 6.1 also shows the lines of equal pore pressure as reported by the same authors.

Working in effective stresses while modifying continuously the geometry is time consuming and cumbersome for the actual computer code. This is due to the fact that this code does not have the capability to automatically update pore pressure variations after each iteration. For this reason, an alternative equivalent scheme combining the submerged unit weight of the soil and the seepage forces has

been used (Cedergren, 1977, pp 117-118). This procedure is explained in detail in the Appendix F.

6.1.1 Analysis of the slope considering post peak soil strength Values

The slope is discretized as shown in Fig. 6.2. At all the interfaces, the effective post peak soil parameters as defined by Lefebvre and Chahde (1978) are considered, i.e. c' = 8.8 kPa, ϕ' = 34.1° The global MS along the slip surface, i.e.lines 5,6,7 and 8, is minimised. The initial margin and factor of safety were found to be 157 kN and 1.29, respectively. The convergence of MCR slip surface was realized after five iterations, and the MS and the FS obtained were found to be 85 kN and 1.24, respectively. The final slip surface is shown in Fig. 6.3, which also shows points measured on the actual failure surface. The stress distribution along the critical slip surface is shown in Fig. 6.4. As can be seen, the maximum stress concentration is along the lines 5 and 6, i.e. at the toe of the slope.

6.1.2 Analysis of the Slope considering Progressive Failure

The above analysis indicates that the slope should be stable, but we know that it failed. One plausible assumption is that the residual strength values for this type of material and for long term conditions (see Law and Lumb 1976) are c' = 0. and ϕ' = 34.1°. Assuming this to be true

one can simulate the progressive failure mechanism as follows:

From the previous analysis, considering post peak soil values, it was noticed that the overstressed zone along the potential failure surface was located at the toe of the slope, i.e. lines 5 and 6, as shown in Fig.6.4. Hence, the initiation of the local failure is assumed to start from the toe and progress toward the top of the slope.

The procedure to simulate the progressive failure will be as follows:

The MS along line 5, i.e. from the toe, will be minimised first considering post peak strength parameters. If the the MS of this line is found to be zero, i.e. FS equal to one, this line could fail locally, and the initiation of local failure could occur. Assuming that this can happen, the MS along the lines 5 and 6 is subsequently minimised considering residual strength parameters for line 5. If the MS along the lines 5 and 6 is found to be zero, both lines could attain the residual strength. The procedure is carried on until all the lines along the slip surface are exhausted, or, at any stage, the MS is not found to be zero, thereby indicating that the propagation of local failure has stopped.

Minimisation of the MS along Line 5 :

The first iteration gave the margin of safety equal to zero, i.e.FS=1. Thus, this line was given residual soil values. The MS of lines 6, 7 and 8 were found to be 25, 31 and 18 kN respectively.

Minimisation of the MS along Lines 5 and 6 :

Line 5 was given residual soil parameters. The MS on lines 5 and 6 was found to be zero in the first iteration. Lines 7 and 8 were found to have the local MS equal to 25 and 14 KN respectively. Thus, line 6 would also have attained residual values.

Minimisation of the MS along Lines 5, 6 and 7 :

Lines 5 and 6 were given residual values. The first iteration was found to give the MS along these lines equal to zero. Thus line 7 would also have attained residual values. The local MS of lines 5,6 and 7 were found to be zero. For line 8, the MS was found to be 4.5 kN.

Minimisation of the MS along Lines 5, 6, 7, and 8 :

Lines 5,6,7 were given residual values. The initial global MS and FS were found to be 71 KN and 1.12, respectively. The critical slip surface was obtained after six iterations having the global MS equal to zero, i.e. FS=1. The local MS of all the lines along the slip surface were found to be zero.

The interesting point to be noted is the propagation of local failure in which the local MS along the slip lines are progressively being reduced to zero. As the failure propagates, the local MS along the subseqent lines were found to be decreasing until the local MS of all the lines along the slip surface were reduced to zero, thereby implying that the progression of local failure will cause the entire slope to fail, refer to Fig.6.5. The critical slip surface obtained closely approximated the points on the actual failure surface.This can be seen in Fig.6.6.

Considering the stability of the slope by assuming the post peak soil strength parameters, the slope was found to be safe. However, the soil strength values could approach the residual strength due to the initiation of progressive failure thereby causing the slope to fail with time. In fact the failure occurred twenty-eight months after the cut was made in the natural slope.

6.1.3 Comparison with Bishop and Janbu Methods

Back-analysis was done on the failed slope by Lefebvre and Chahde (1978). The modified Bishop method was used to analyze the stability of the slope, considering a tension crack of 3.7 m depth to be full of water. The Bishop analysis with a circular failure surface close to the measured one gave a factor of safety of 1.05.

The Janbu method was incorporated with a search for the critical slip surface as proposed by Duncan and Celestino (1981). The program was developed by Trak and Glen (1982). A factor of safety of 1.64 was obtained for the critical slip surface. In this analysis, a tension crack of 3.7m depth to be full of water was also considered. Fig. 6.7 shows the critical slip surface obtained.

No a priori knowledge is known either about the location and depth of the tension crack or the water pressure conditions in the crack when one analyzes the stability of an existing slope. It stands to reason that if the tension crack was not assumed to exist, much higher values of the factor of safety would have been obtained. In the Bishop analysis the failure slip surface was already known. Thus the prediction of a factor of safety equal to 1.05 does not reflect the ability of the searching routine to find the critical slip surface. The Duncan and Celestino search gave a high factor of safety of 1.64 when incorporated in the Janbu analysis.

In the proposed method, an arbitrary slip surface was chosen and progressive failure was simulated. This yielded a FS of 1, i.e. MS = 0, and the critical slip surface obtained was found to be close to the actual one. No tension crack had to be imposed to reduce the factor of safety to be compatible with the knowledge known that the slope had failed.

The information on the prefailure deformations were not available for the Rosemere case study. Hence the failure was assumed to propagate from the toe to the top of the slope.

In other cases of clay slope failures, such as that reported by Eden and Mitchel (1970) and Eden (1972), where cracks appeared at the top and bulging at the toe of the slope, respectively, one can assume the propagation of local failure from top to the toe of the slope to be equally compatible with this type of deformation. This sequence can be easily simulated in the search procedure. Since the final factor of safety was found to be unity, this does not make a difference, as there exists a feasible failure mechanism which might cause the slope to fail.

Chapter VII

CONCLUSIONS AND RECOMMENDATIONS

From the numerical investigations performed, one can conclude that to establish the criterion for pinpointing the critical slip surface, one has to restrict the shape of the slip surface to a concave one, this being compatible with the kinematic mode of sliding failure. It was also seen that, by analyzing the slope by general limit equilibrium methods, one may obtain irregularly shaped slip surfaces having lower margin of safety for the critical slip surfaces than those being concave in shape.

To obtain a fast convergence without affecting the stability of the numerical solutions, it was found that for the analysed problems, the optimal nodal increment for a slope having a height of 12 mt should be equal to one-tenth the height of the slope. Thus, as a tentative first approximation, one may recommend using one-tenth the value of the height of the slope to be analyzed for the optimal nodal increment.

It was observed that the number of triangles and their topology have an effect on the most critical slip surface and no appreciable effect was noticed on the least critical slip surface. A number of failure mechanisms exist for the

slope and each assumed failure mechanism fixes the number of triangles and its topology. Thus, for a more refined analysis, it is recommended that a number of failure mechanisms for the slope be assumed and that the mechanism giving the smallest margin of safety for the most critical slip surface be taken into consideration.

It was found that, if restrictions are imposed on the movements of the nodes, critical slip surfaces obtained will have higher values of margin of safety as compared to the "true slip surface". This implies that freedom should be given to the nodes to move in any of the possible directions.

When discontinuous normal stresses are assumed along the slip surface, the effect on the most critical slip surface was substantial and awkward shapes of the slip surfaces were obtained. The effect on the least critical slip surface was not appreciable. In homogenous continuous soils, the distribution of normal stresses along the slip surface are continuous, and thus continuous normal stress distribution should be assumed.

It was seen that by keeping all factors the same, and by starting with two different trial slip surfaces, the convergence of the slip surfaces for the MCR and LCR slip surfaces were found to be remarkably good. The only exception was in the MCR slip surface when discontinuous normal stresses along the slip surface were assumed.

When the case of a natural slope failure at Rosemere was analyzed by the proposed method, it indicated that the slope could fail progressively and the critical slip surface obtained by it closely approximated that of the actual failure surface.

For a more refined analysis of the slope, it is recommended that a number of possible failure mechanisms for the slope be chosen and analyzed for both short-term and long-term stability. For the long-term stability, it should also be analyzed by simulating progressive failure for c-ϕ soils.

In conclusion, it can be said that the proposed procedure takes into account the following considerations :

1. No a priori assumption about the shape of the initial slip surface has to be made.
2. A rigorous mathematical approach is used to locate the critical slip surface.
3. An easy check on the validity of the results can be obtained after each iteration.
4. A concrete criterion is established to indicate if and when the critical slip surface is obtained.
5. Any mechanism of failure can be easily simulated.
6. The search procedure gives quick convergence.

REFERENCES

Baker, R. & Garber, M., (1978), 'Theoretical analysis of the stability of slopes'. Geotechnique, Vol. 28, No. 4, pp. 395-411.

Biarez, J.,(1961), 'Contribution a l'etude des properietes mechaniques des Sols et des materiaux pulverulents', thesis presented to the University of Grenoble, Grenoble, France.

Bishop, A.W., (1955), 'The use of the slip circle in the stability analysis of slopes'. Geotechnique, Vol. 5, No. 1, 1955, pp. 7-17.

Bishop, A.W., (1967), 'Progressive failure with special reference to the mechanism causing it'. Geotechnical Conference, Oslo, Vol. II pp. 142-150

Bjerrum, L., (1967), 'Progressive failure in slopes of overconsolidated plastic clay and clay shales'. ASCE, J. of the soil Mech. and found. Div., Vol. 93, SMS, pp. 8-49,

Boutrop, E. & Lovell, C., (1980), 'Searching techniques in slope stability analysis'. Mechanics of Landslides and Slope Stability. Eng. Geol., Vol. 16, pp. 51-61.

Carter, R.K., (1971), 'Computer oriented slope stability analysis by method of slices'. Thesis Purdue University, Ind.

Castillo, E. & Revilla, J., (1977), 'The calculus of variation applied to stability of slopes'. Geotechnique, Vol. 1, pp. 11-26.

Cedergren, H., (1977), 'Seepage, Drainage and flownets', 2nd.ed.

Celestino, T. & Duncan, J., (1981), 'Simplified search for noncircular slip surfaces'. Proceedings of the tenth international Conference on Soil Mechanics and Foundation Engg. Stoçkholm Vol. 1, pp-391-415.

Chen, W.F., (1975), 'Limit Analysis and Soil Plasticity' Elsevier, Amsterdam.

Chen, W.F. & Snitbhan, N., (1975), 'On slip surface and slope stability analysis'. Japanese Society of Soil Mechanics and Foundation Engg. Vol. 15, No. 3, pp. 41-48.

Dantzig, G.B., (1963), 'Linear Programming and Extensions'. Princeton Univ. Press, Princeton, N.J.

De Josselin De Jong, G., (1981), 'A variational fallacy'. Geotechnique, Vol. 31, No. 2, pp. 289-290.

Eden, W.J. and Mitchel, R.J., (1970), 'The mechanics of landslides in Leda clay'. Canadian Geotechnical Journal, 7, pp. 285-296.

Eden, W.J., (1972), 'Some Observations at le Coteau landslide, Gatineau, Quebec'. Canadian Geotechnical journal, 9, pp. 508-514.

Fellenius, W. (1936)., 'Calculation of the stability of earth dams'. Trans. Second Cong. on large Dams 4, Washington.

Fredlund, D.G. & Krahn, J., (1976). 'Comparison of Slope Stability Analysis'. 29th Can. Geot. Conf., Vancouver, B.C., pp. VIII - 58 a 74.

Frohlich, O.K., (1955), 'General Theory of Stability of Slopes'. Geotechnique, Vol. 5, No. 1, Session 1/6, pp. 35-47.

Gass, S.I., (1966), 'Linear Programming'. McGraw-Hill Book Co.

Goldstein, M.N., (1969), 'Applications of Calculus of Variations to Investigations of Bases and Slopes'. Osnovaniya, Fundamenty; Mekhanika Gruntov, No. 1, pp. 2-6, Jan-Feb.,(traduction en anglais).

Horn, J., (1961), 'Slope stability analysis'. ASCE Transaction, vol 126, pp 217-232.

Janbu, N., (1954), 'Application of Composite Slip Surfaces for Stability Analysis'. Proceedings of the European Conference on Stability of Earth Slopes, Stockholm, Vol. 3, pp. 43-49.

Janbu, N., Bjerrum, L. & Kjaernsli, B. (1956), 'Stabilitetsberegning for fyllinger skjaeringer og naturlige skraninger', Norwegian Geotechnical Institute Publication No. 16, Oslo, Norway.

Kopacsy, I., (1961), 'Distribution des constraintes a la rupture forme de la surface de glissement et hauteur theorique des talus' C.R., 5e Congr. de Mec. des Sols et des Tr.de Fond., pp. 641-650

Law, T.K. & Lumb, P., (1976), 'A limit equilibrium analysis of Progressive failure in the Stability of Slopes'. Rev. Can. Geotech Vol. 15, No. 1, Feb. 1978.

Lefebvre, G. and Chahde, J., (1978). 'Analyse de la rupture d'une pente de deblai dans la region de Rosemere', Quebec. Rapport Geo-78-03, section de geotechnique, Universite de Sherbrooke, P.Q.

Lefebvre, G., (1981), 'Strength and Slope Stability in Canadian soft clay deposits'. Rev. Can. Geotech., Vol. 18, No. 3, Aug. 1981.

Lowe, J., III & Karafiath, L. (1960), 'Stability of Earth Dams Upon Drawdown', Proceedings First Pan-American Conference on Soil Mechanics and Foundation, Mexico City, Vol. 2, pp. 537-552.

Morgenstern, N.R. & Price, V.E., (1965), 'The Analysis of the Stability of General Slip Surfaces'. Geotech, Vol. 15, No. 1 pp. 79-93.

Morgenstern, N.R. & Price, V.E., (1967). 'A Numerical Method for solving the equations of Stability of General Slip Surfaces'. Computer J., 9, pp. 388-393.

Narayan, C.G.P., Ramamurty, T. & Bhatkar, V.P., (1976), 'Slope Stability Analysis by Variational Techniques', Indian Geotechnical Society, Vol. 6. No. 2, pp. 67-90.

Narayan, C.G.P., Ramamurty, T. & Bhatkar, V.P., (1977), 'Variational Method for Slope Stability Analysis'. C.R. 9e Congr. Int. de Mec. des Sols et des Tr. des Fond., Tokyo, pp. 139-142.

Papantonopoulos, C. & Ladanyi, B., (1973), 'Analyse de la stabilite des talus rocheux par une methode generalisee de l'equilibre limite'. C.R., du 9e Symp. Can. de mec. des roches, Montreal, pp. 167-187.

Papantonopoulos, C., (1979), 'Analyse a la rupture des Rocheux par discretisation et Programmation Lineaire'. Ph.D thesis Ecole Polytechnique.

Papantonopoulos, C., (1984), 'Determination de la surface de glissement la plus critique par la methode generalisee de calcul a la rupture'. (Manuscript to be published). International Symposium on Landslides, Toronto.

Seed, H.B., & Sultan, H.A., (1966), 'Stability Analysis for Sloping Core Embankments'. ASCE Conference on the Stability of Slopes and Embankments.

Sherard, J.L., Woodward, R.J., Gizienski, S.F., & Clevenger, W.A., (1963), 'Earth and Earth-Rock dams'. John Wiley & Sons, Inc., New York.

Siegel, R.A., (1975), 'Computer Analysis of General slope stability Problems'. Thesis Purdue University, Ind.

Skempton, A., (1964), 'Longterm stability of clay slopes'. Geotech, Vol. 14, pp. 75-102.

Spencer, E. (1967), 'A Method of Analysis of the stability of Embankments Assuming Parallel interslice forces', Geotechnique, 17, pp. 11-26.

Taylor, D.W., (1948), 'Fundamentals of soil mechanics', John Wiley & Sons, Inc. New York.

Terzaghi, K., (1962), 'Stability of steep slopes in hard unweathered Rock'. Geotech, Vol. 12, pp. 251-270.

U.S. Army Corps of Engineers (1970), 'Engineering and Design, Stability of Earth and Rock-Fill Dams', Department of the Army, Corps of Engineers, Engineer Manual, EM 1110-2-1902, April.

Vajda, S., (1961), 'Mathematical Programming'. Adison-Wesley Publ. Co. Inc.

Whitman, R.V., & Bailey, A., (1967) 'Use of computers for slope stability analysis'. Proc of the ASCE, July 1967, SM 4. pp 475-497.

Whitman, R.V., & Moore, P.J., (1963), 'Thoughts concerning the Mechanics of slope stability analysis'. Proc of the 2nd Pan American Conf on soil mechanics and foundation engg, Brazil, Vol. 1, pp. 391-411.

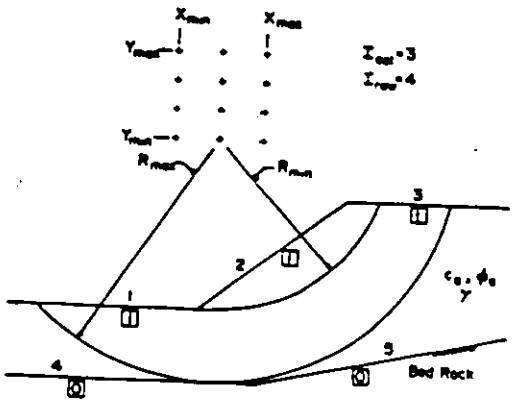

Fig. 2.1 Grid search parameters for circular surface analysis. (Carter 1971)

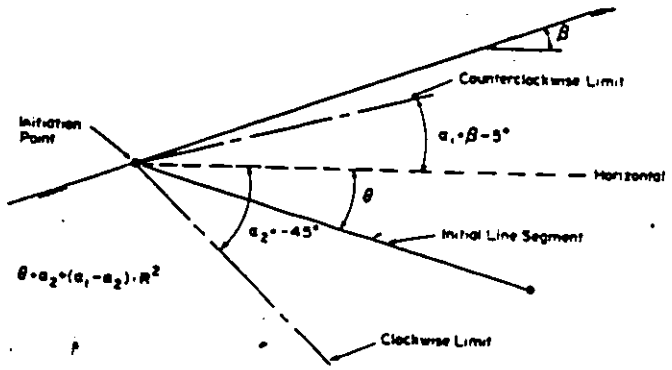

Fig. 2.2 Selecting the initial line segment (Siegel 1975)

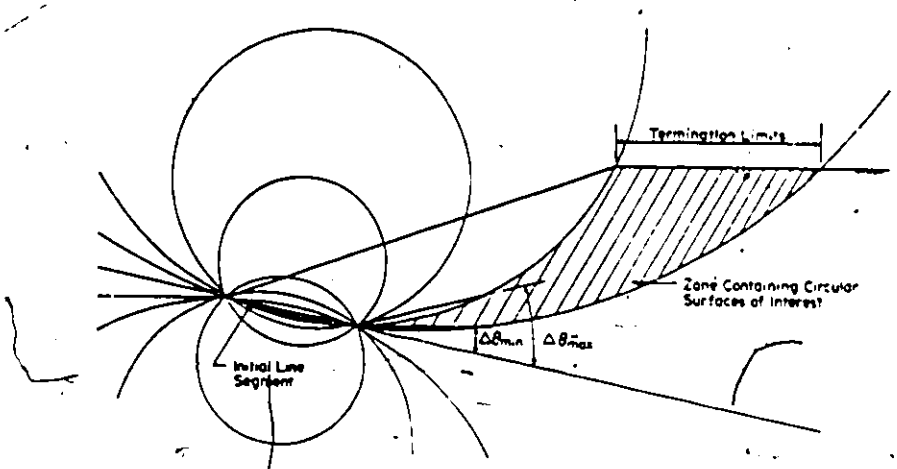

Fig. 2.3 Family of circles having initial line segment as a chord. (Siegel 1975)

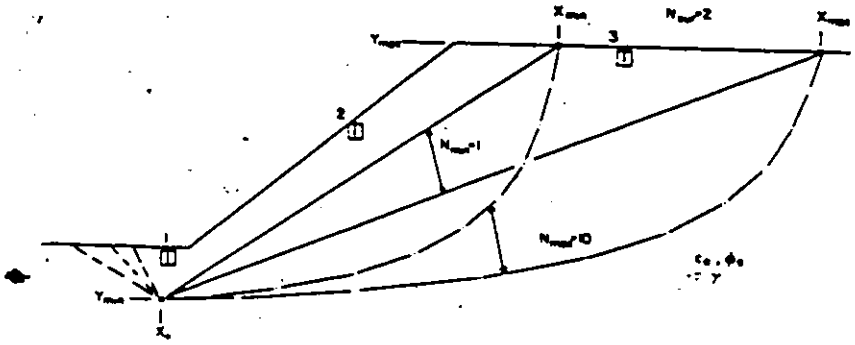

Fig. 2.4 Irregular search parameters for irregular surface analysis. (Carter 1971)

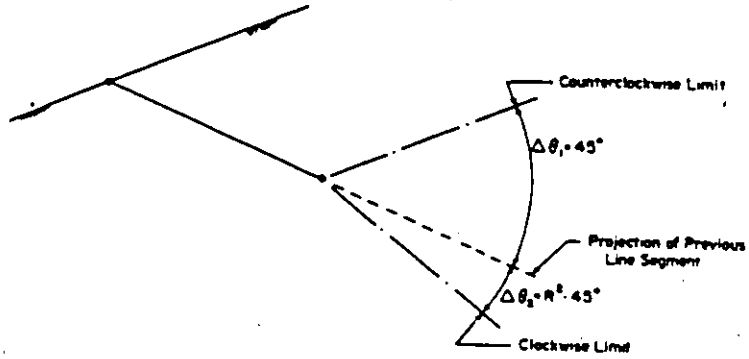

Fig. 2.5 Direction limits for successive line segments of irregular surface. (Siegel 1975)

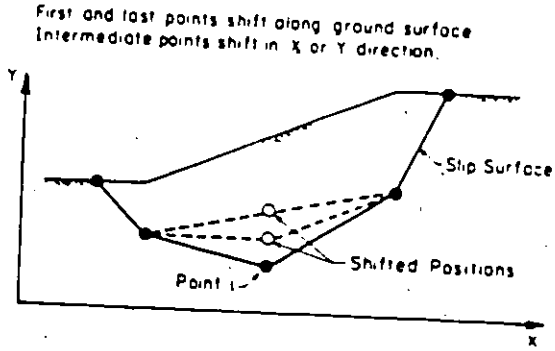

Fig. 2.6 Shifting points on the slip surface (Celestino and Duncan 1981)

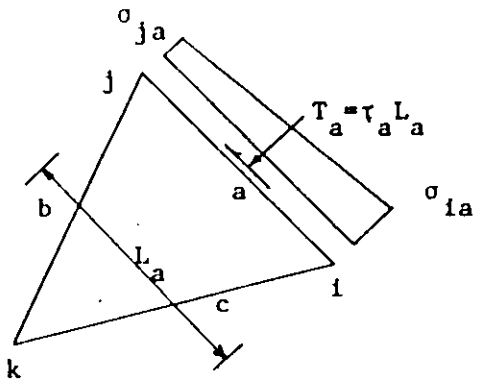

Fig.3.1 Stress distribution on the side a

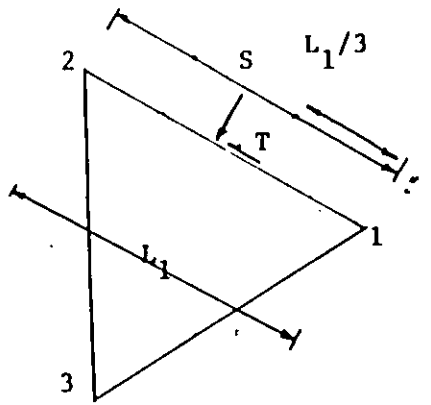

Fig.3.2 Equivalent force at the interface

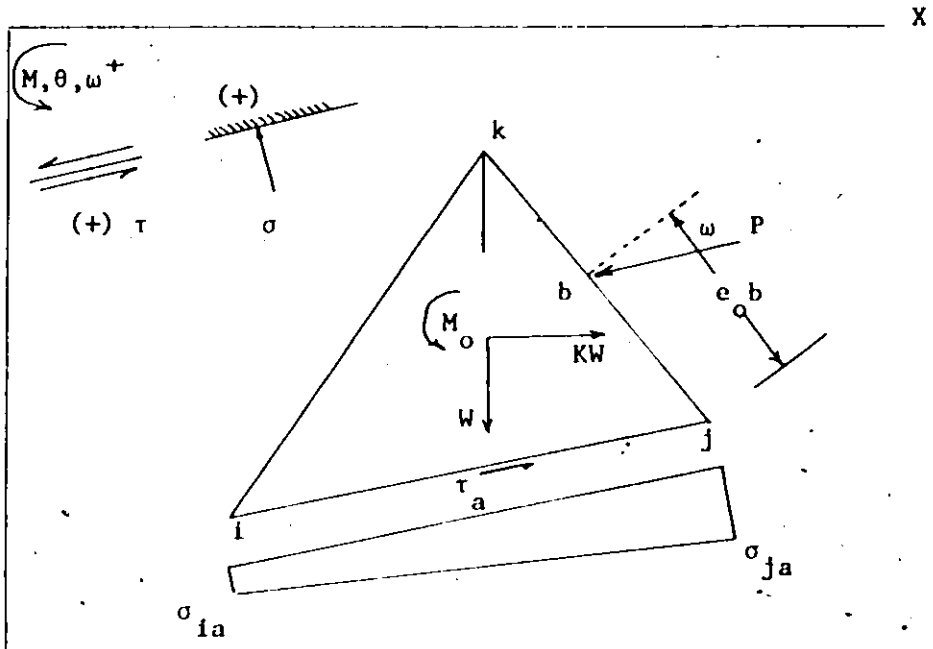

Fig.3.3 Stresses and their sign conventions

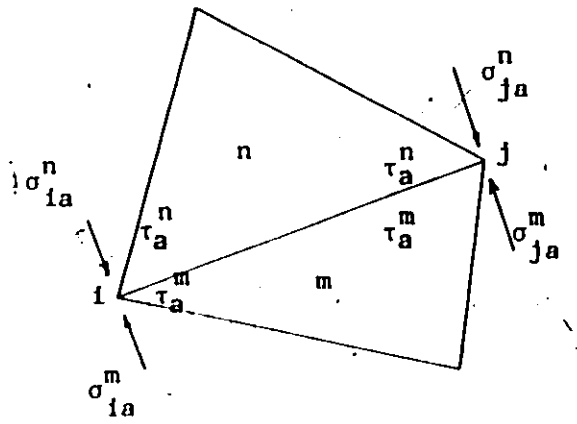

Fig.3.4 Equilibrium condition at the interface

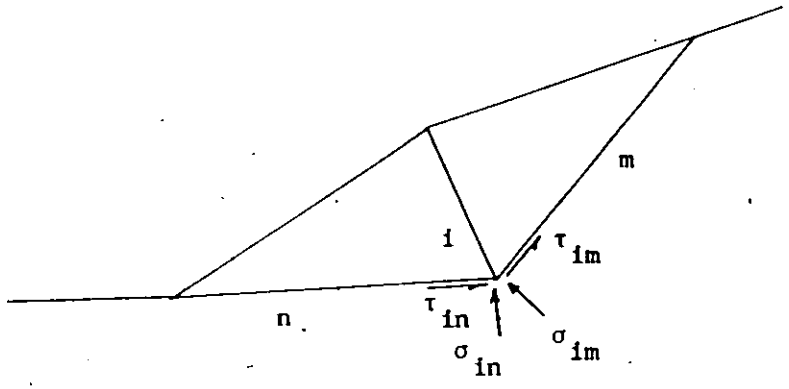

Fig.3.5 Additional relation at the node

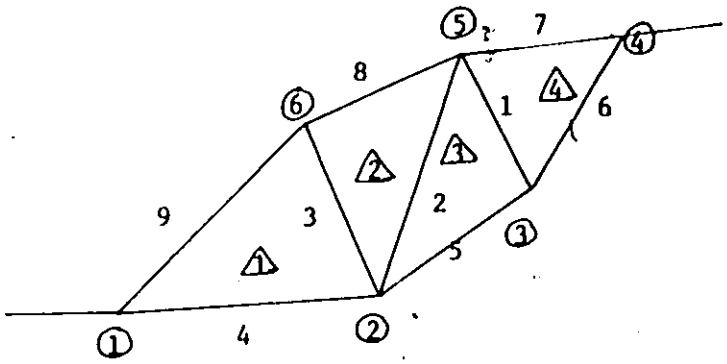

Fig.3.6 Decomposition of the unstable region

$$\begin{bmatrix} [A1] & [I] & [0] \\ [A2] & [0] & [I] \end{bmatrix} \begin{bmatrix} \\ X \\ \\ \end{bmatrix} \begin{bmatrix} B1 \\ \hline B2 \end{bmatrix}$$

Fig.3.7 Constraints in the linear programme

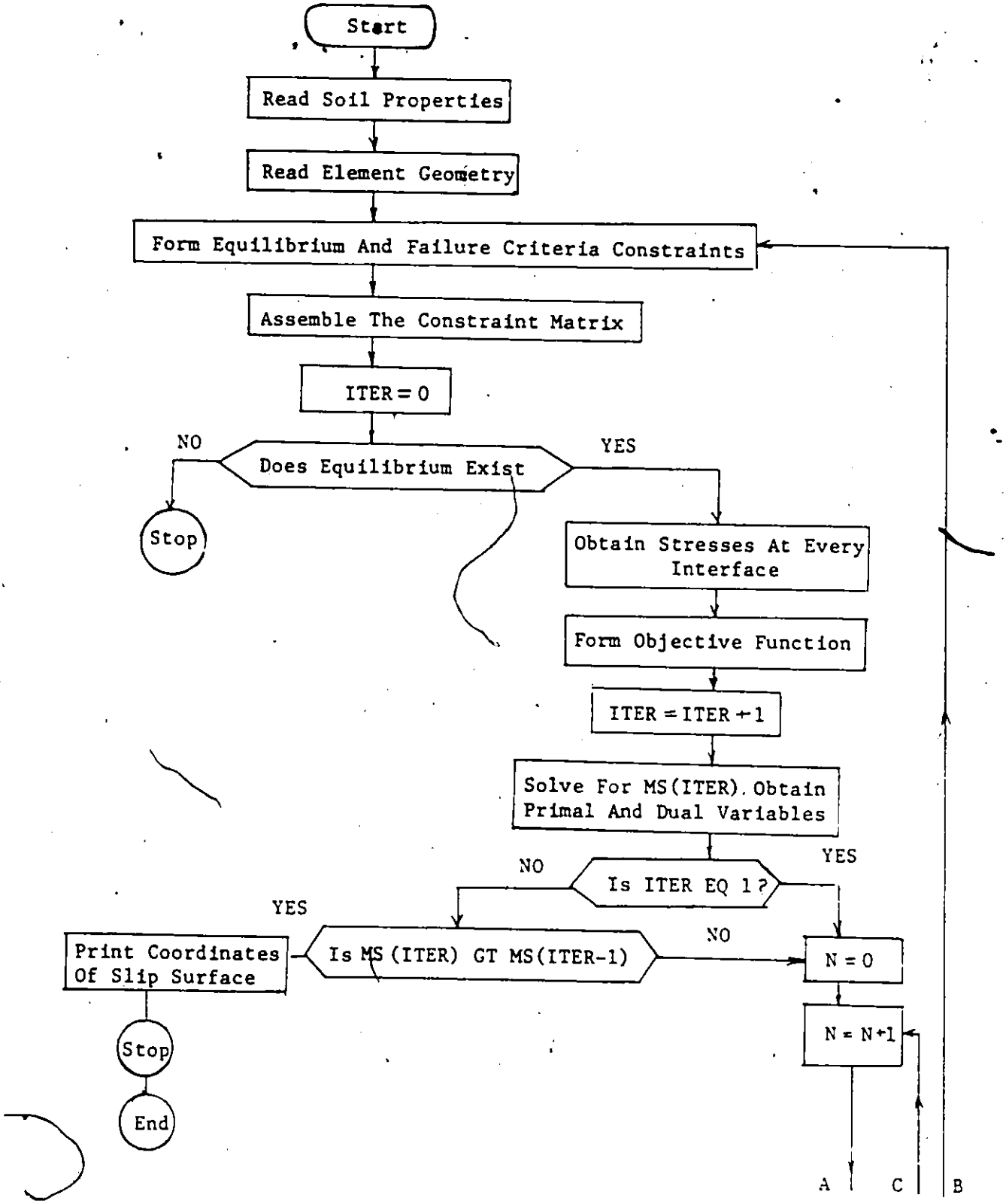
Start
Read Soil Properties
Read Element Geometry
Form Equilibrium And Failure Criteria Constraints
Assemble The Constraint Matrix
ITER = 0
NO
Does Equilibrium Exist
YES
Stop
Obtain Stresses At Every Interface
Form Objective Function
ITER = ITER + 1
Solve For MS(ITER). Obtain Primal And Dual Variables
NO
Is ITER EQ 1 ?
YES
YES
Print Coordinates Of Slip Surface
Is MS (ITER) GT MS(ITER-1)
NO
N = 0
N = N+1
Stop
End
A
C
B

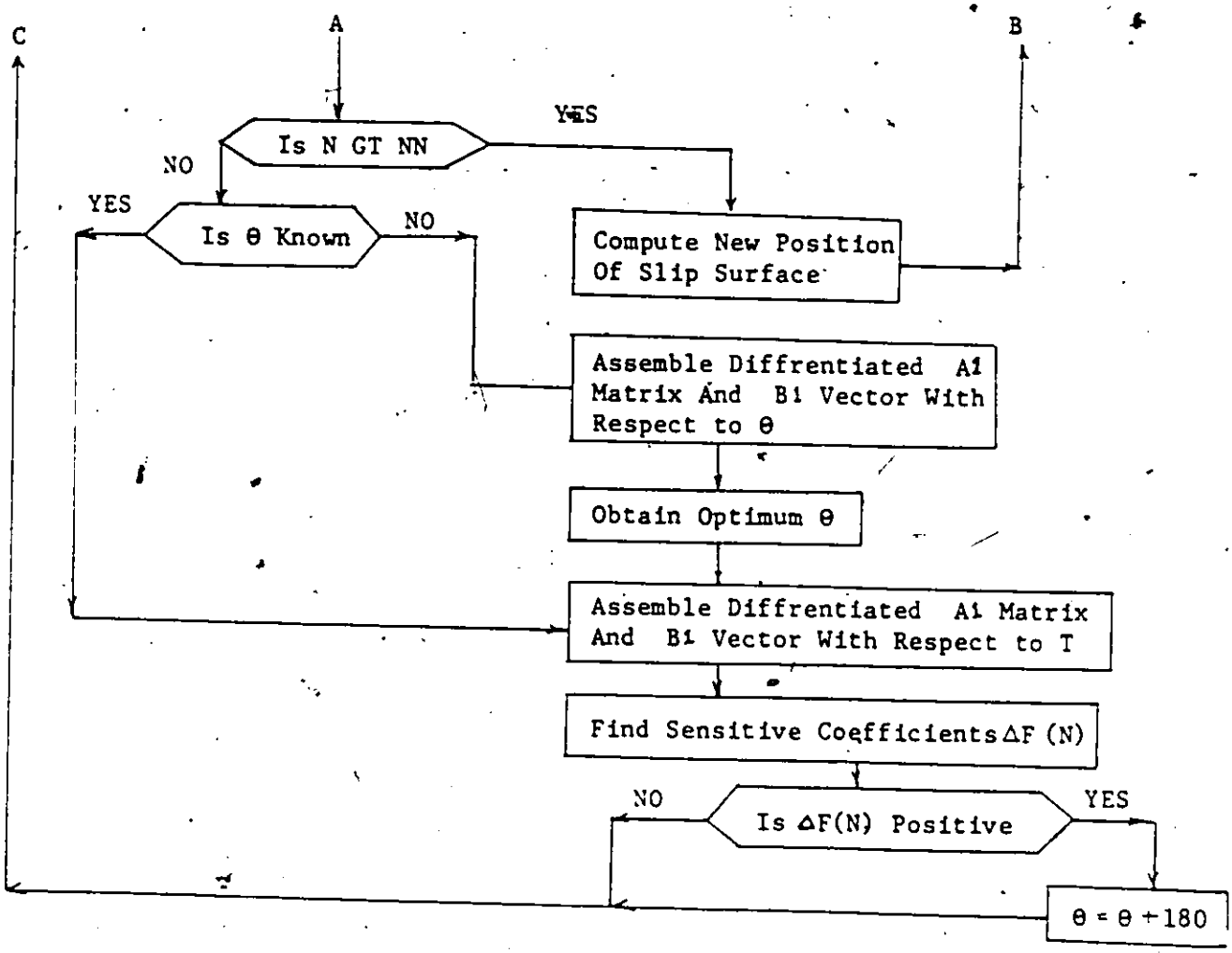

NN - Number of nodes on the Slip surface
θ - Optimum angle of movement
ΔF - Sensitive Coefficient of the node
ITER - Iteration Number
MS - Margin of Safety

Fig.4.1 Flow chart of the search Procedure

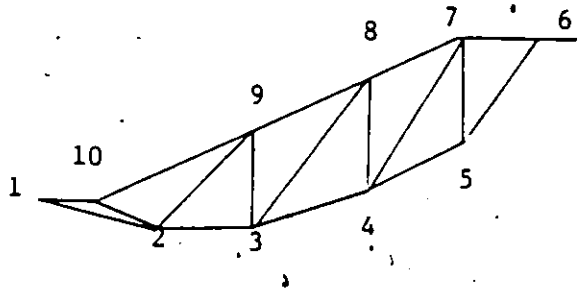

(a)

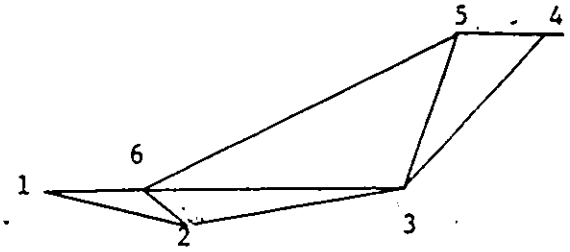

(b)

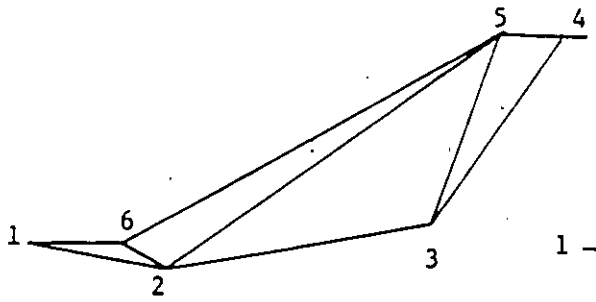

(c)

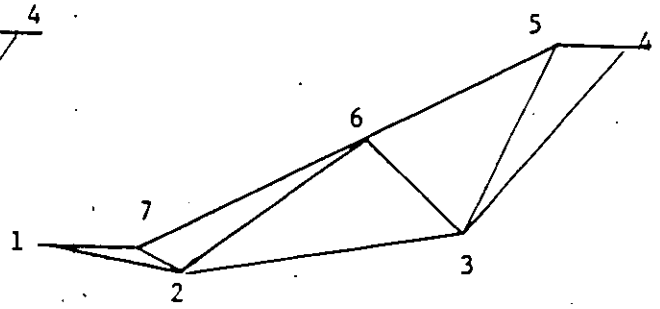

(d)

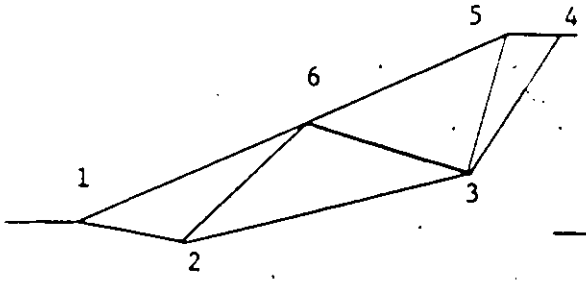

(e)

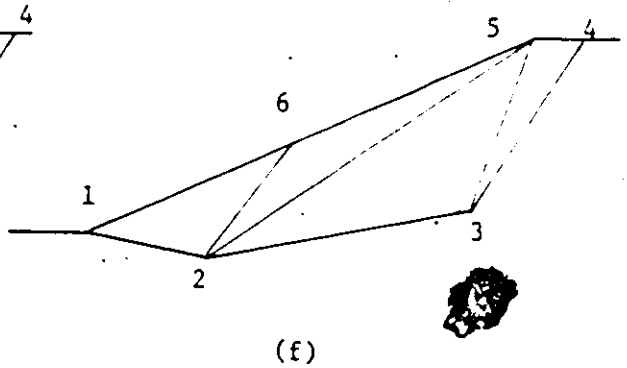

(f)

Fig.5.1 Configurations of the slope studied

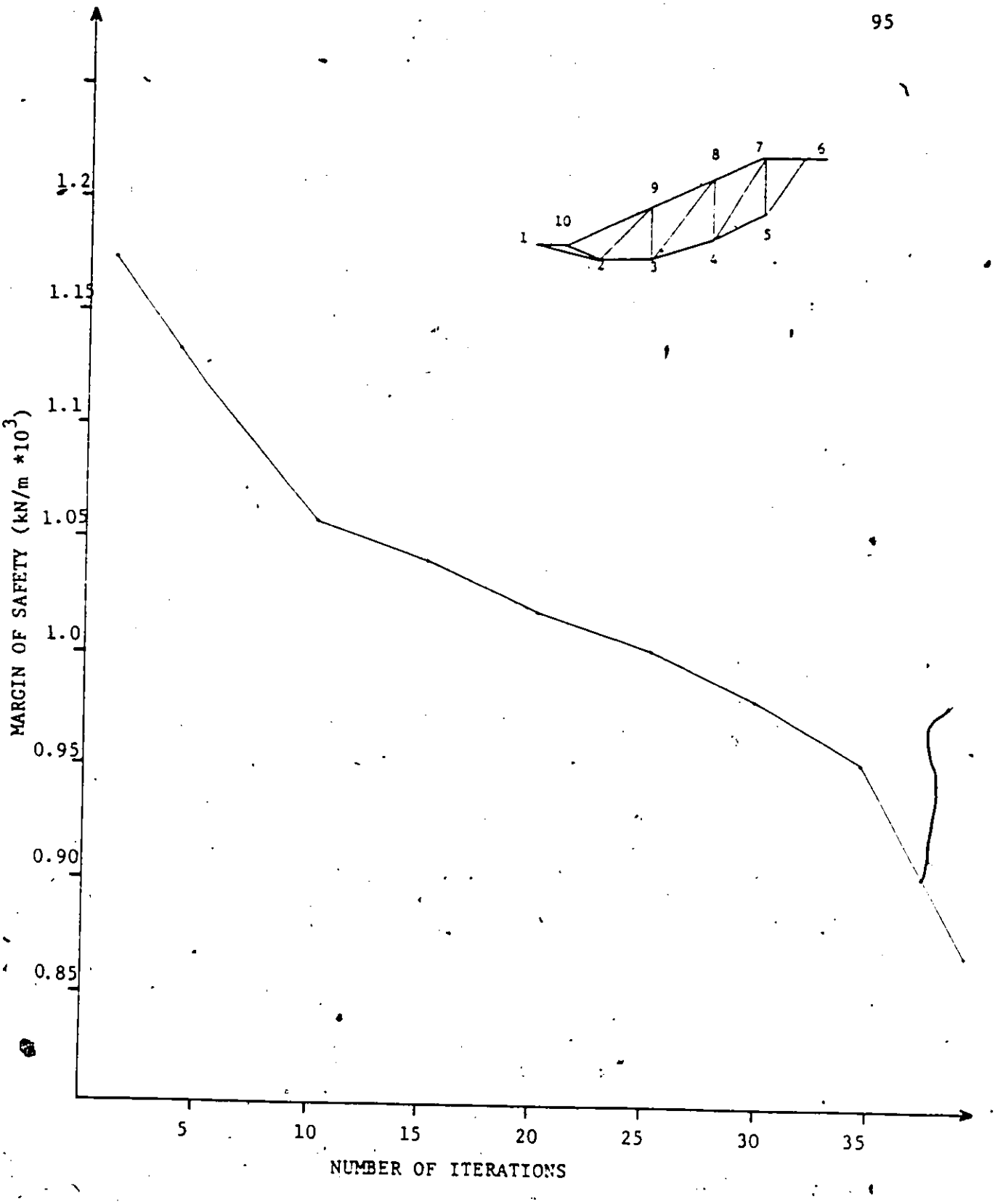

Fig. 5.2 MS vs number of iterations for non concave slip surface

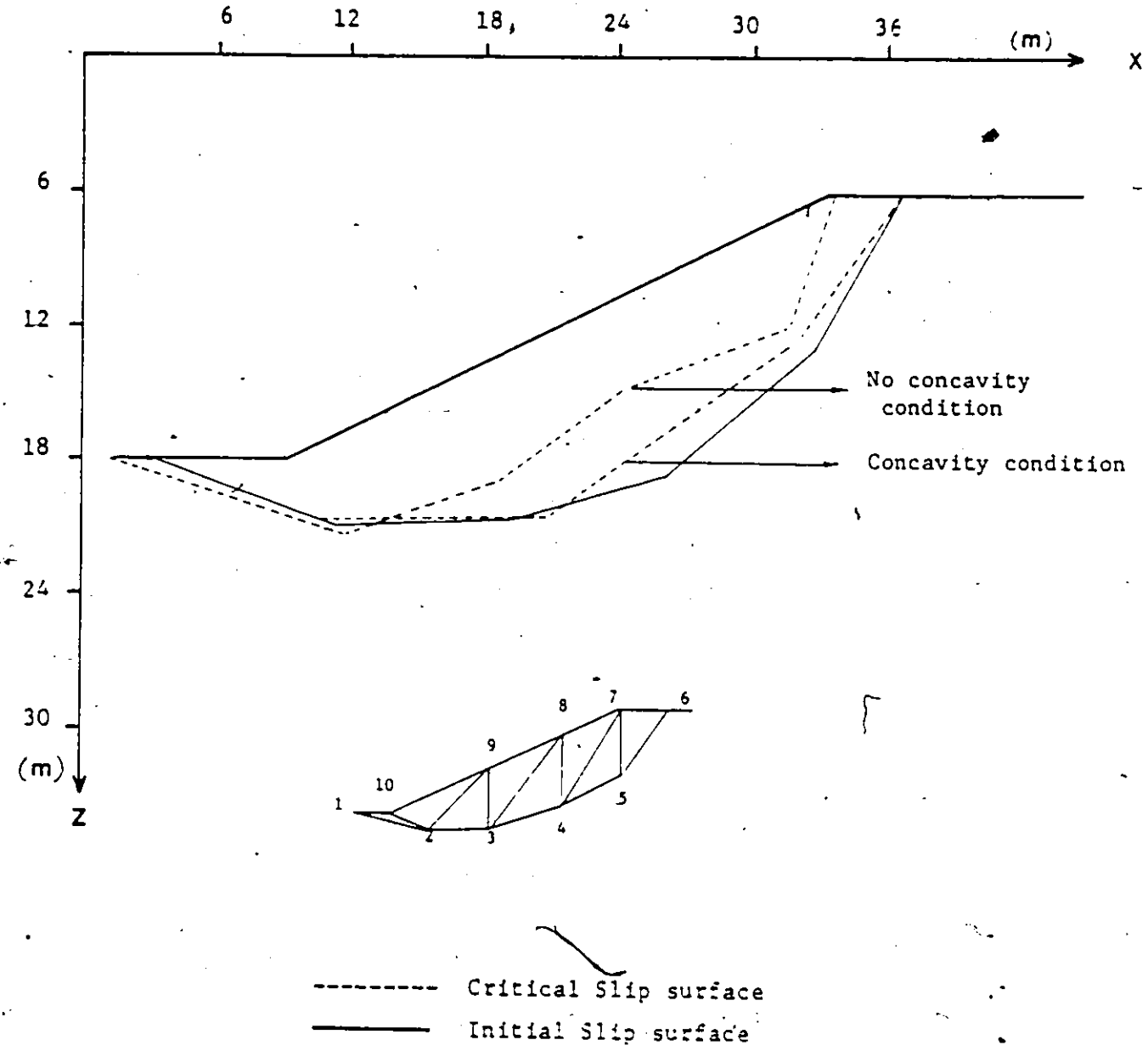

Fig. 5.3 Comparison of the shape of the MCR slip surface with and without the concavity condition

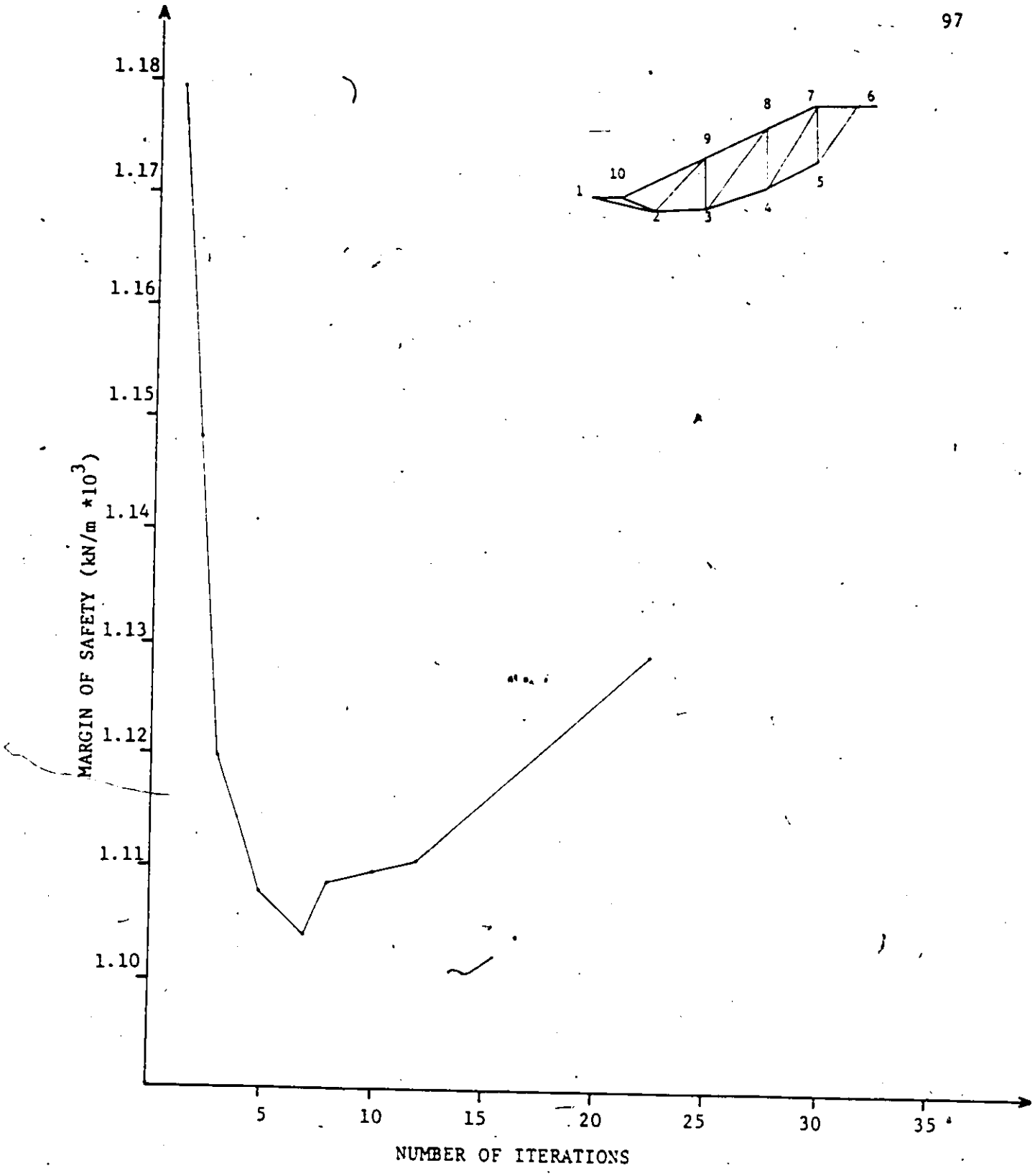

Fig. 5.4 MS vs number of iterations for concave slip surface (MCR)

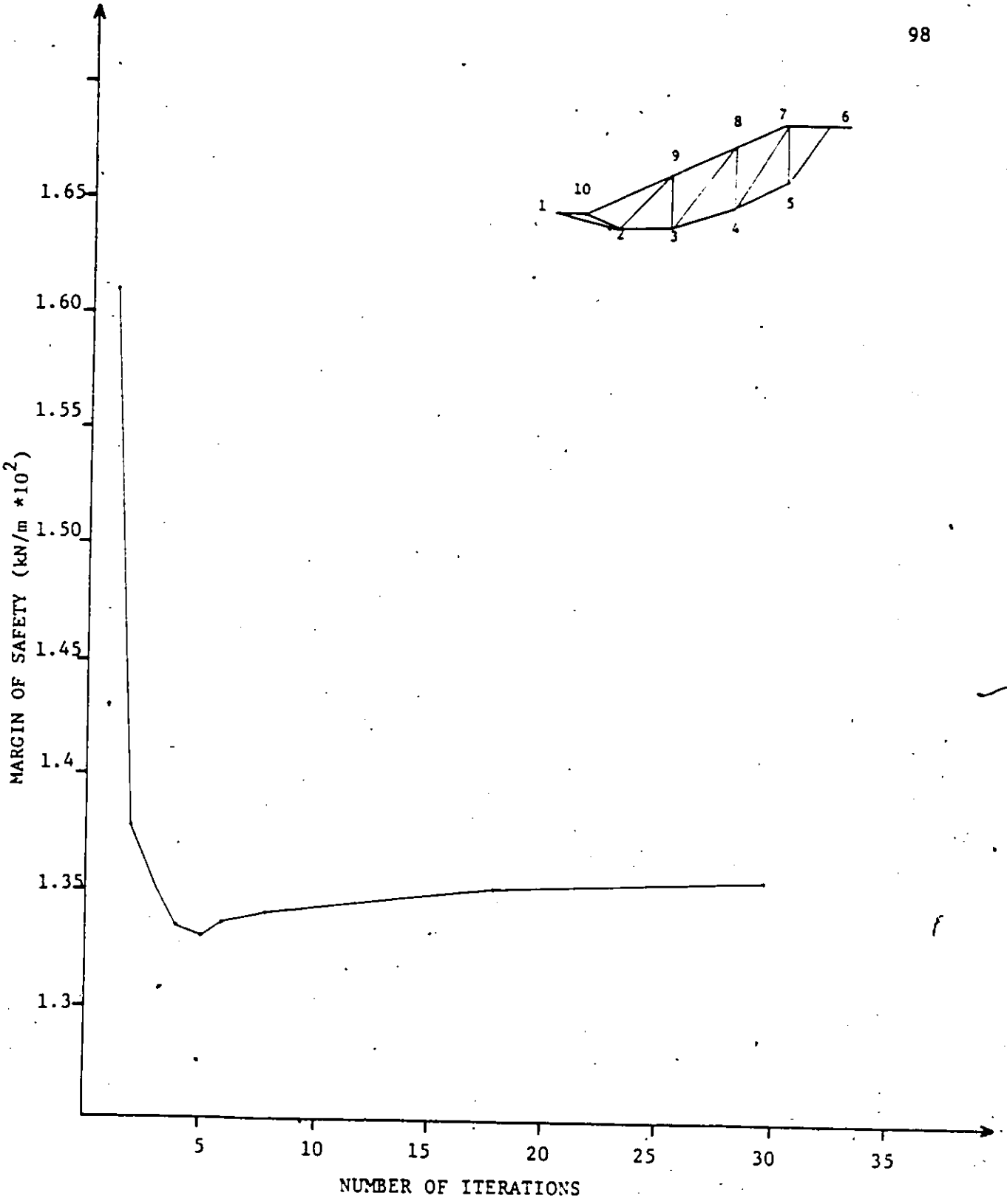

Fig. 5.5 MS vs number of iterations for concave slip surface (LCR)

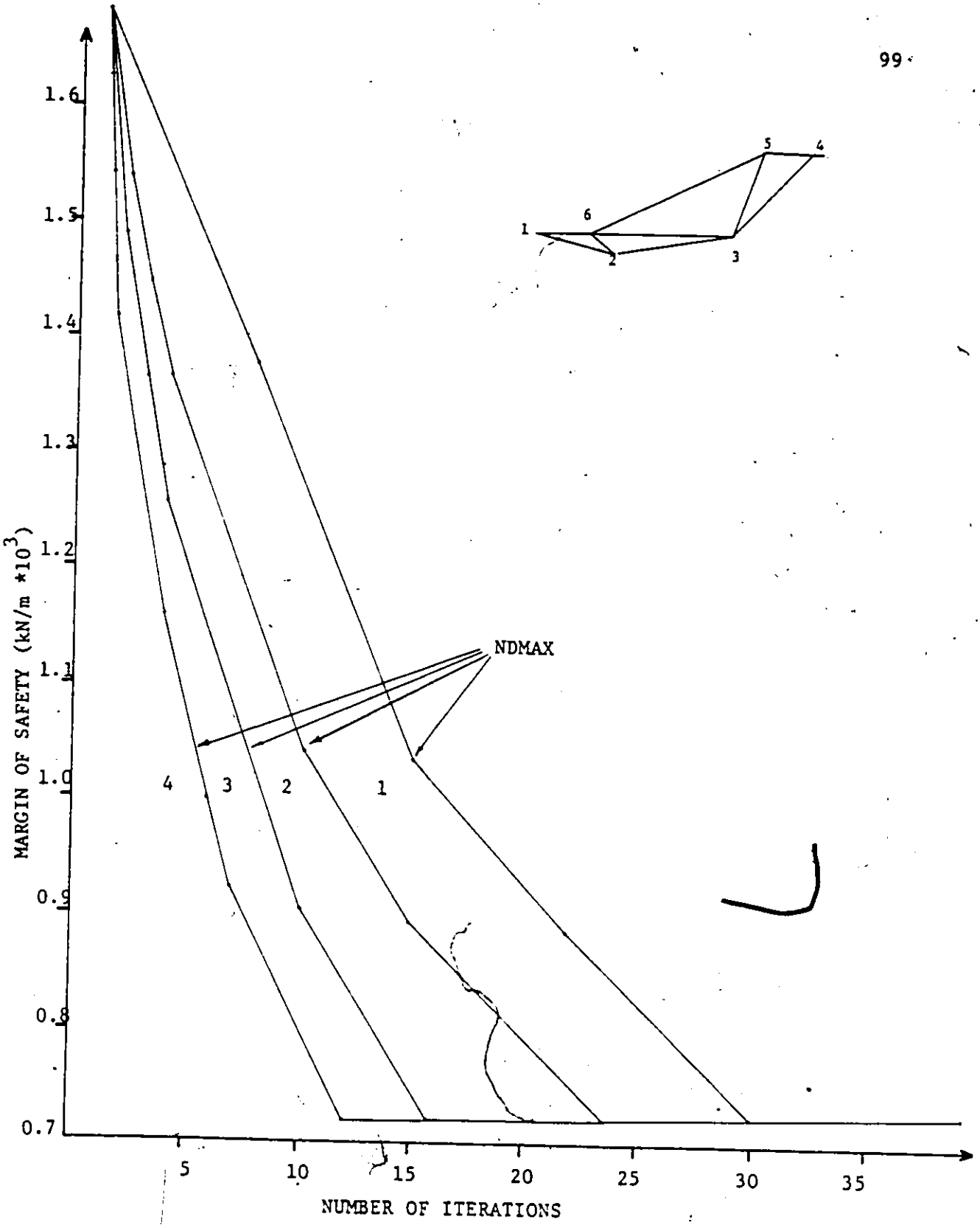

Fig.5.6 MS vs number of iterations for different values of NDMAX (MCR)

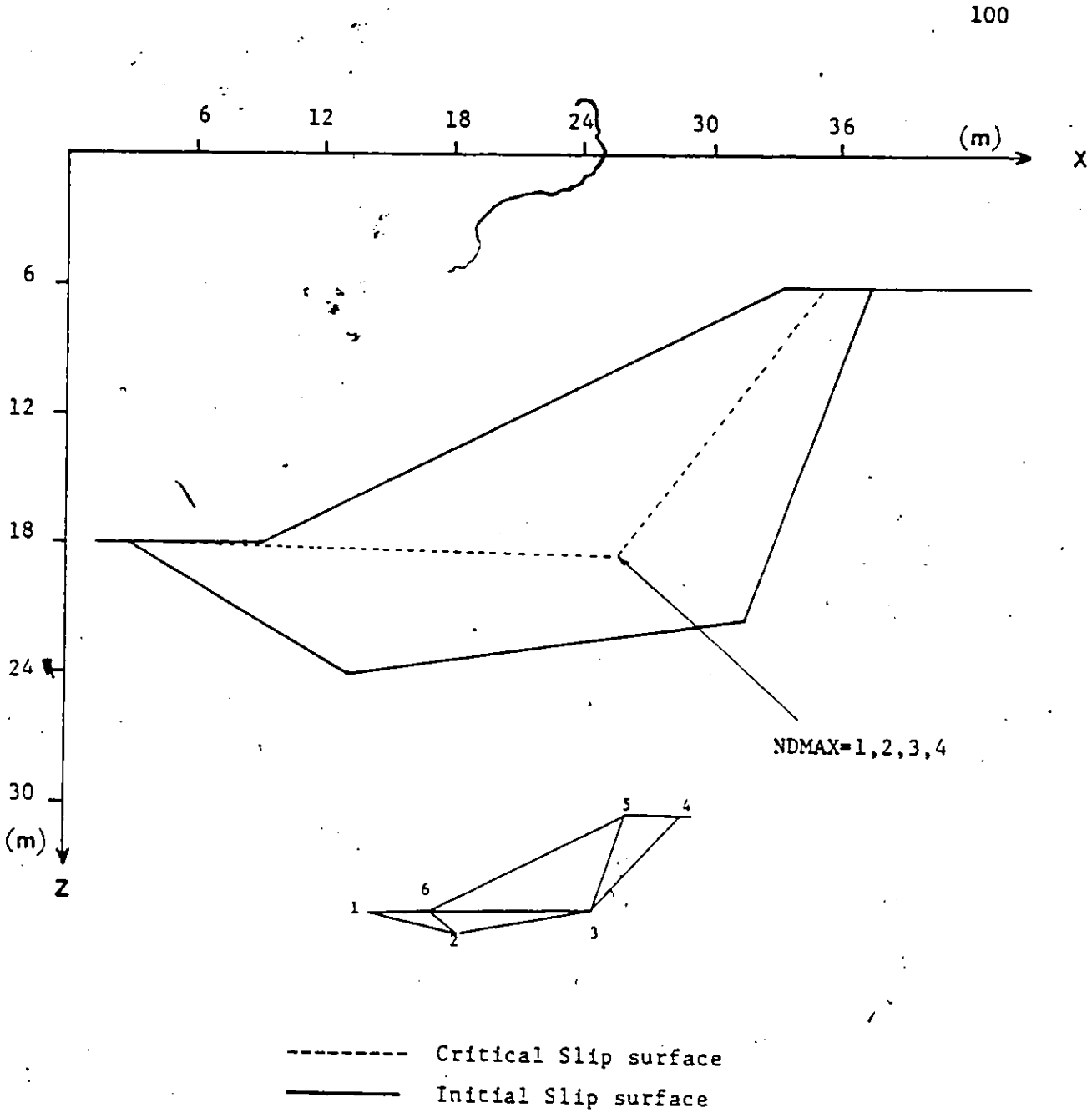

Fig.5.7 Comparison of the location of the MCR slip surface for different values of NDMAX

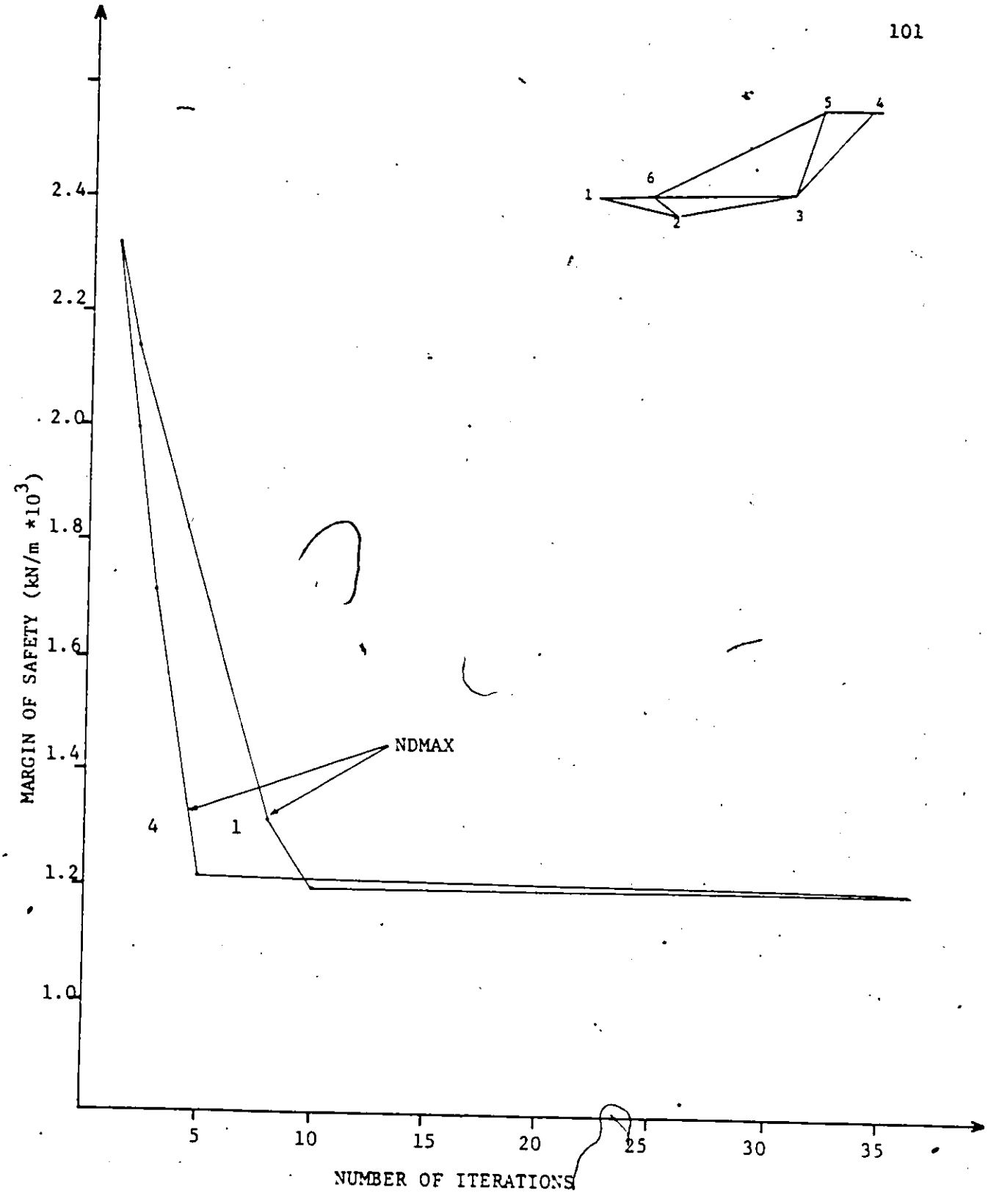

Fig. 5.8 MS vs number of iterations for different values of NDMAX (LCR)

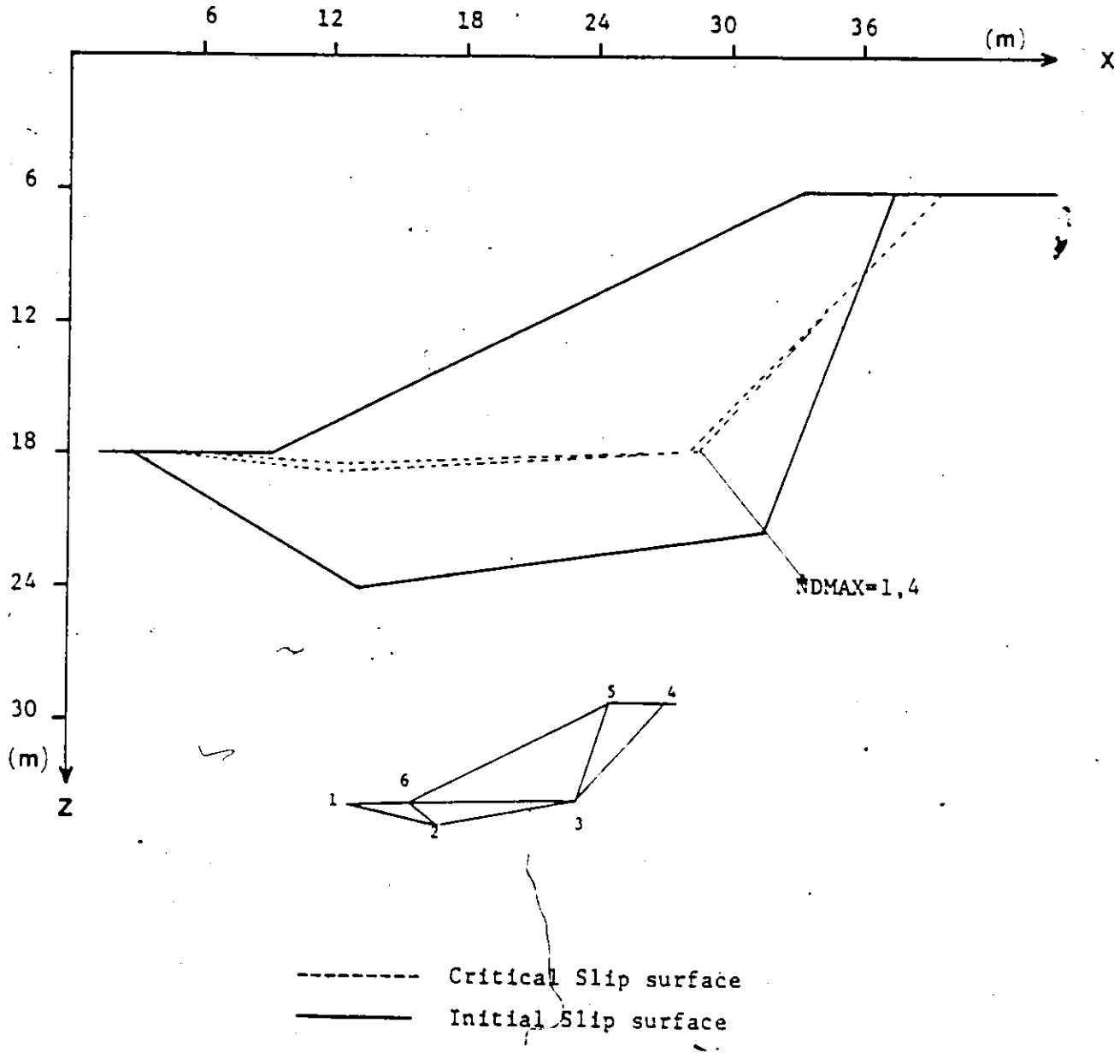

Fig.5.9 Comparison of the location of the LCR slip surface for different values of NDMAX

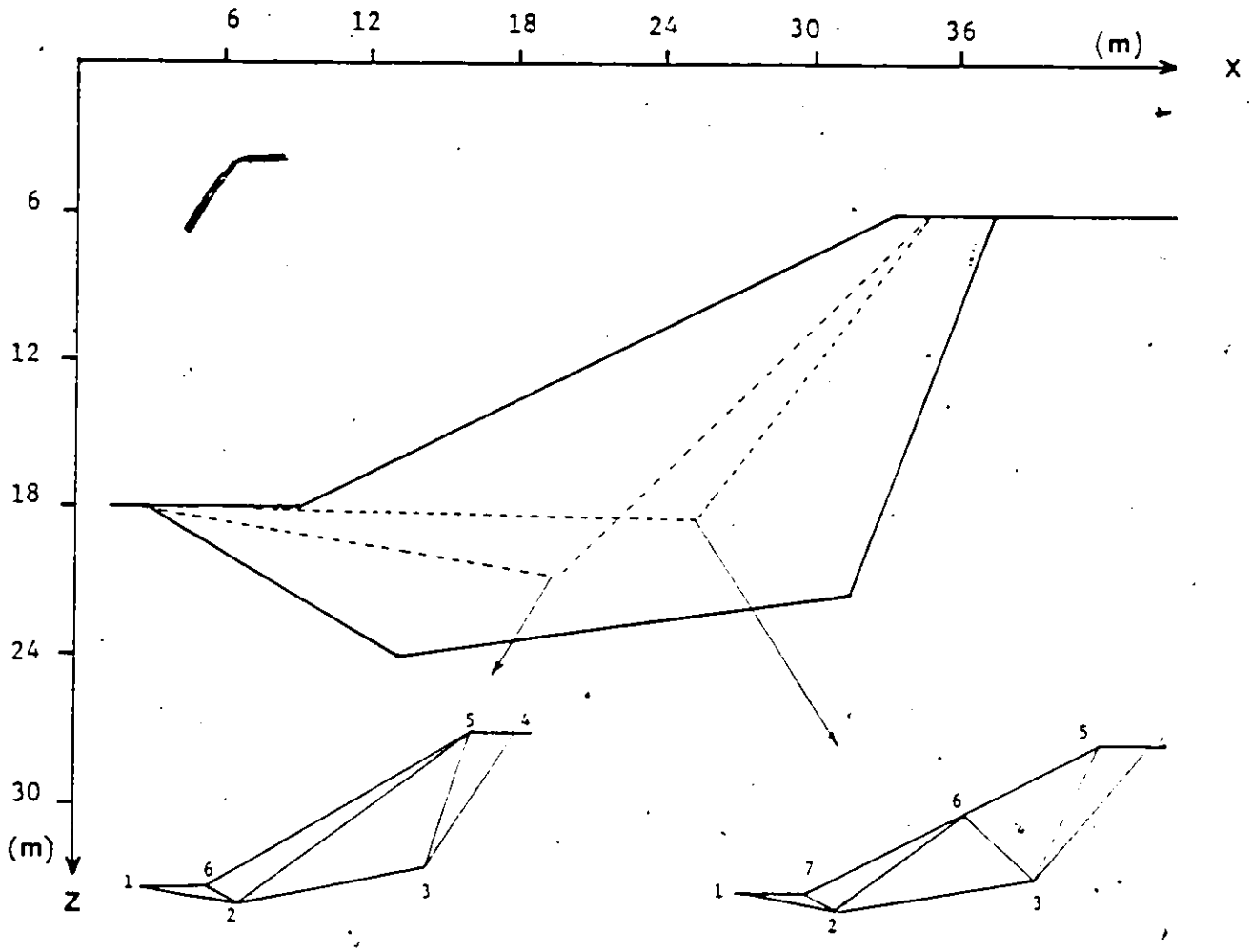

--------- Critical Slip surface

——————— Initial Slip surface

Fig. 5.10 Effect of the number of elements on the location of the MCR slip surface

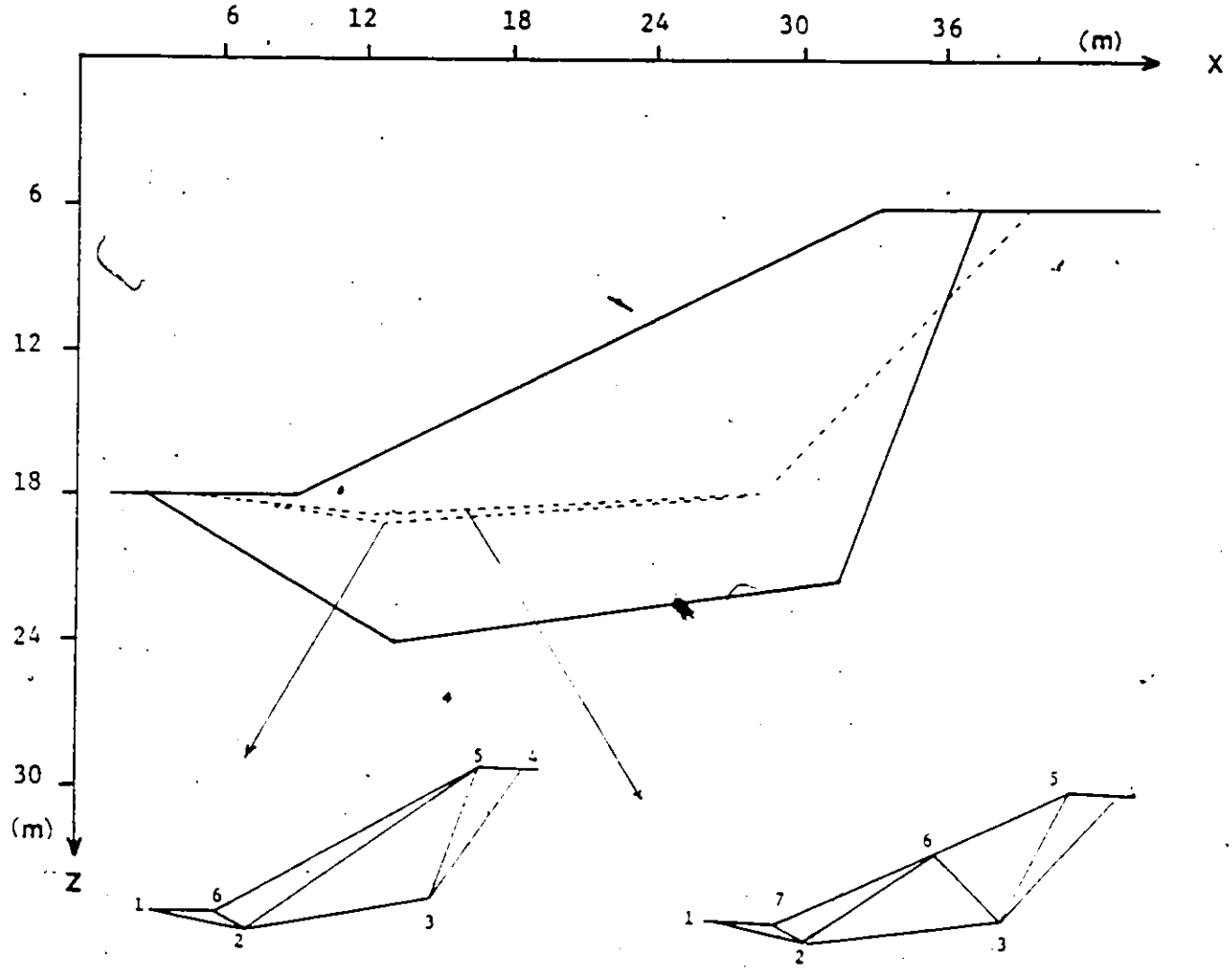

--------- Critical Slip surface

——— Initial Slip surface

Fig. 5.11 Effect of the number of elements on the location of the LCR slip surface

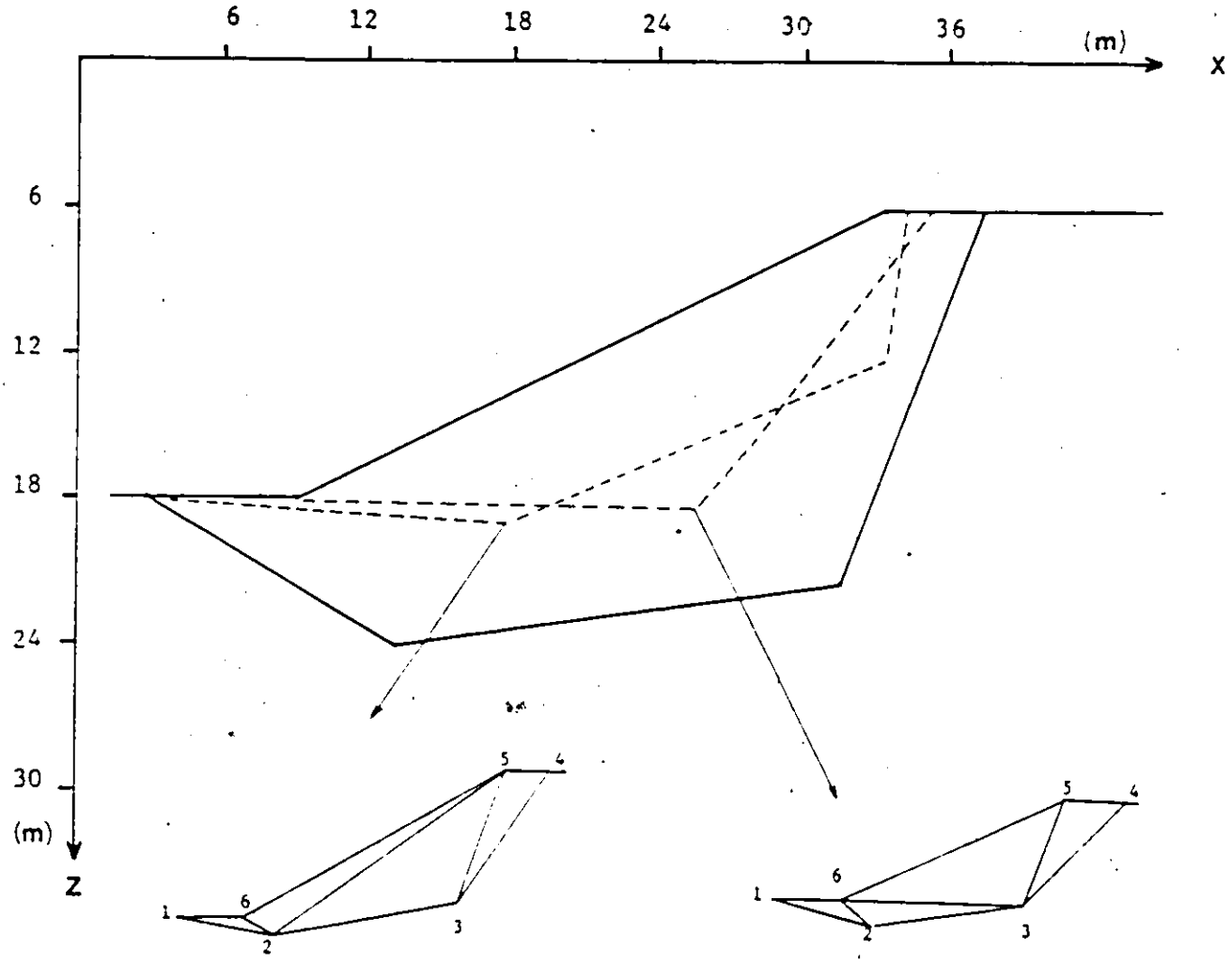

--------- Critical Slip surface

——— Initial Slip surface

Fig. 5.12 Effect of the topology on the location of the MCR slip surface case study 4(a)

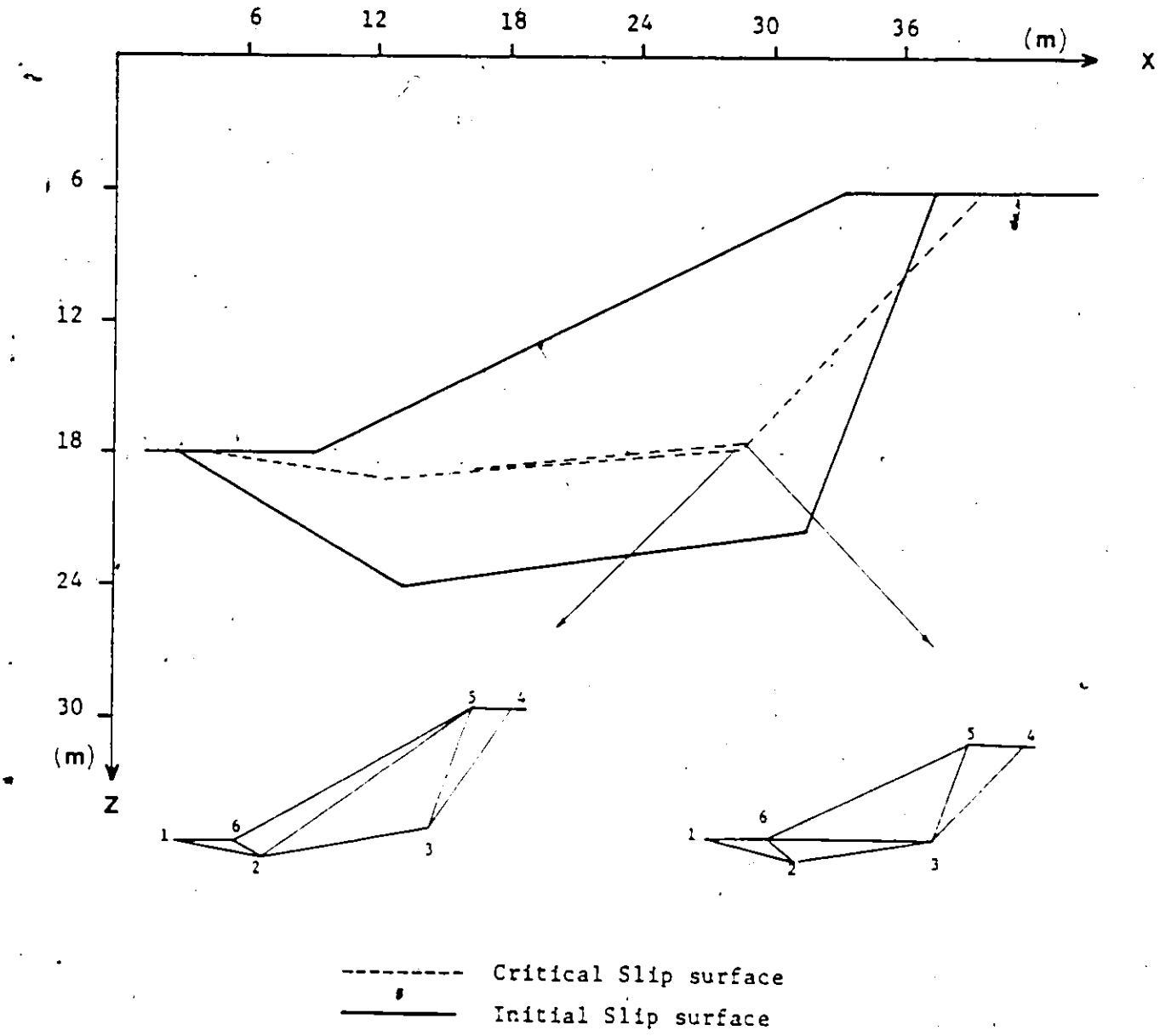

Fig. 5.13 Effect of the topology on the location of the LCR slip surface case study 4(b)

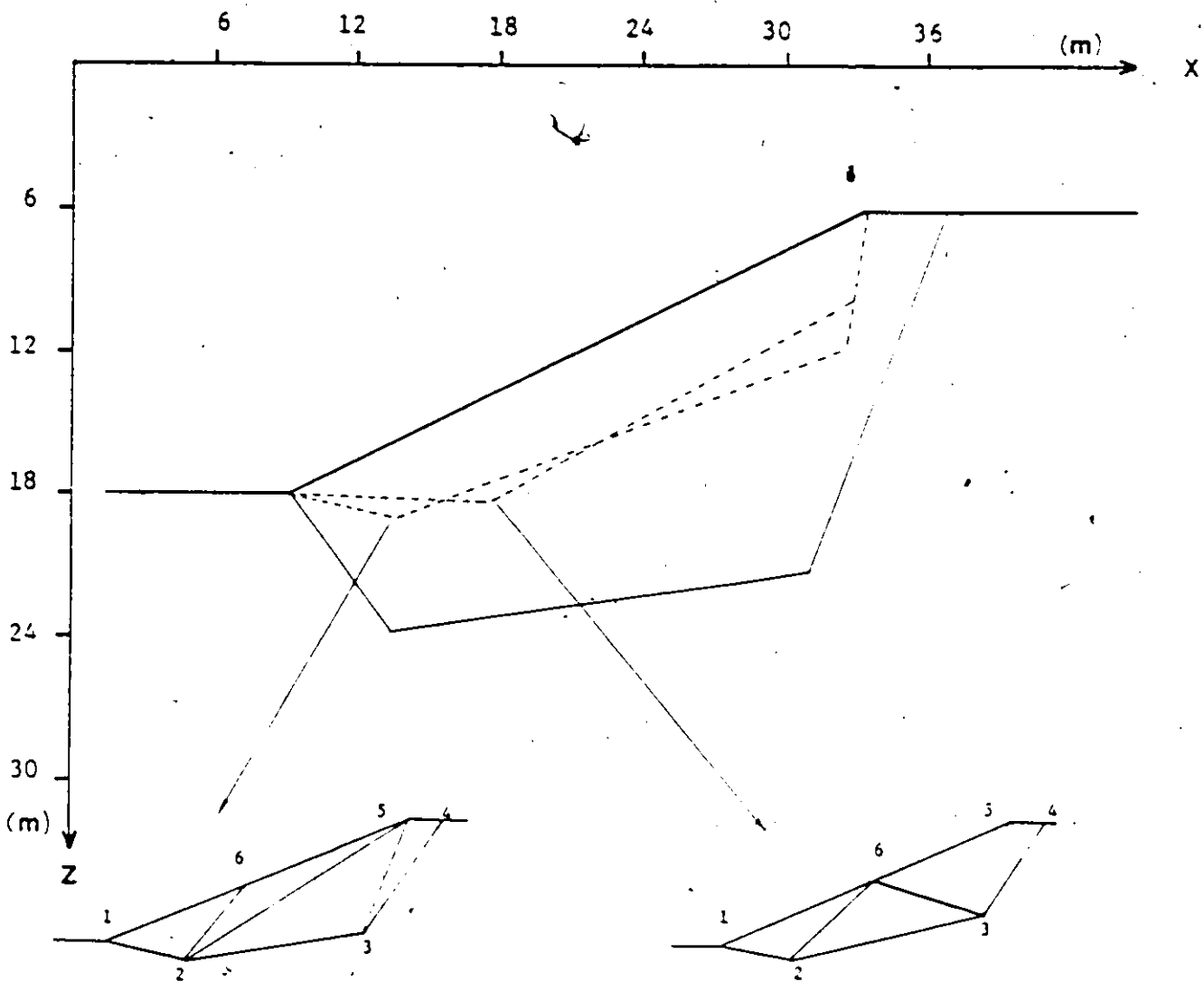

Fig. 5.14 Effect of the topology on the location of the MCR slip surface case study 3(a)

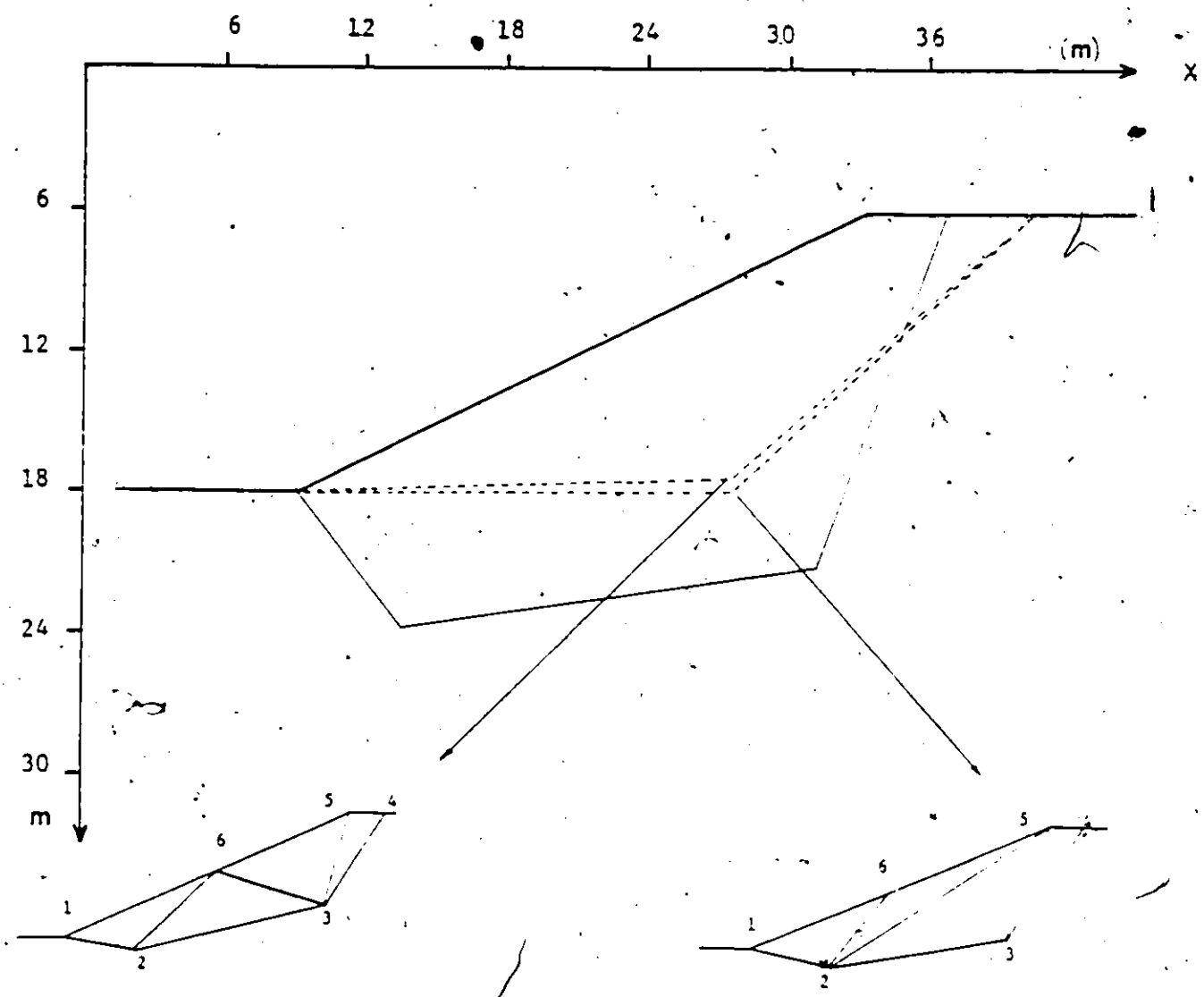

Fig. 5.15 Effect of the topology on the location of the LCR slip surface case study 5(b)

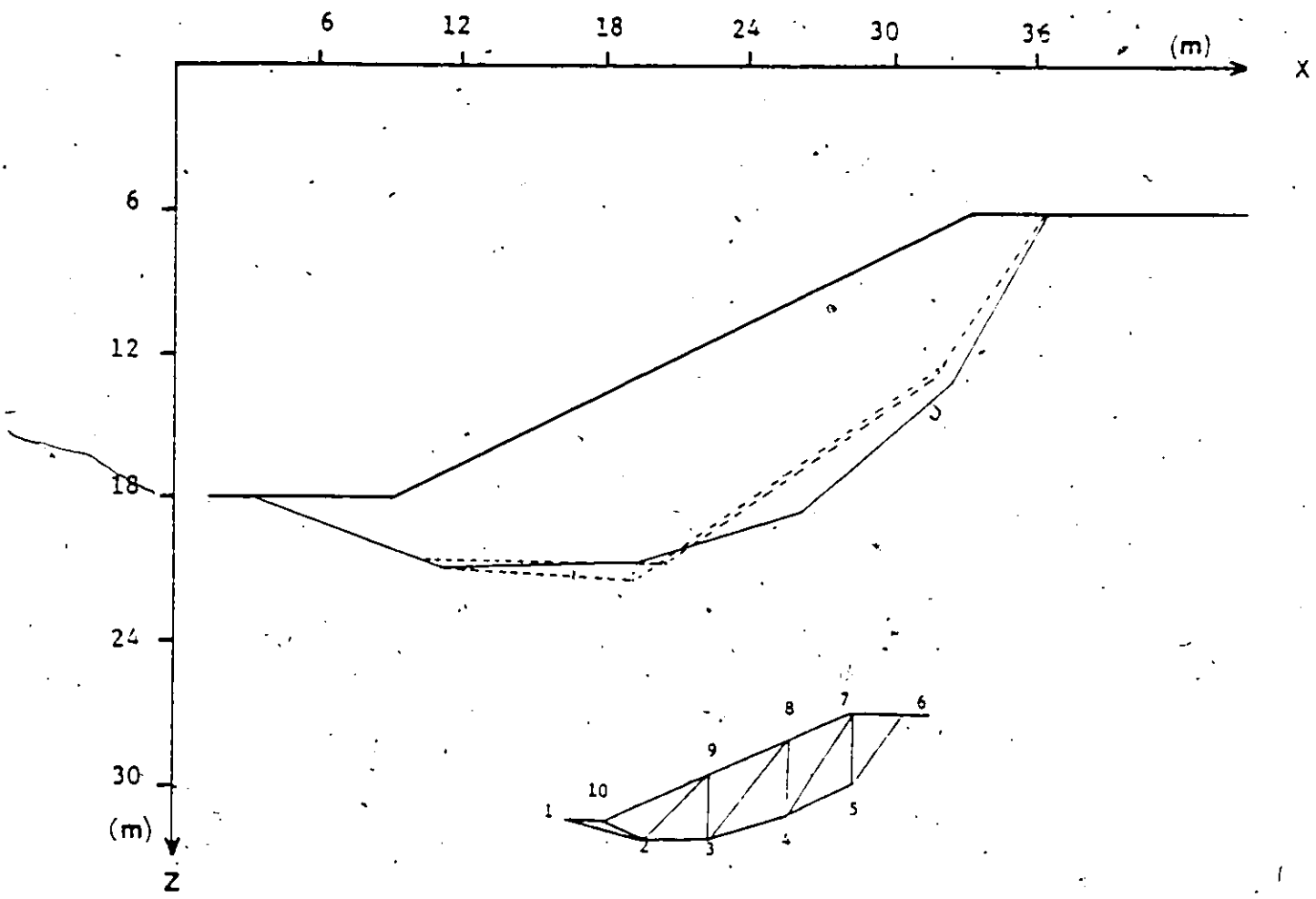

--------- Critical Slip surface

——————— Initial Slip surface

Fig. 5.16 Effect the degrees of freedom have on the MCR slip surface

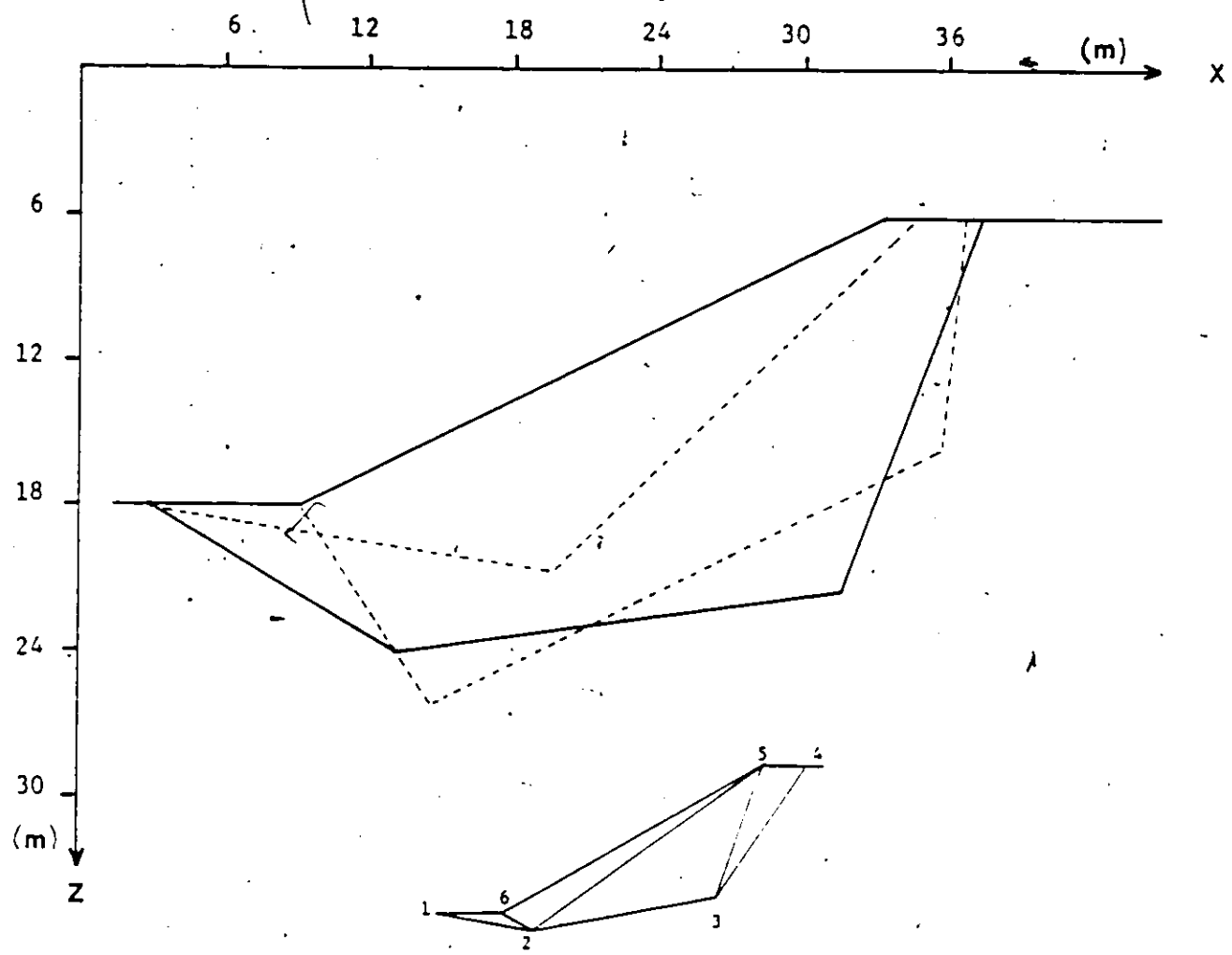

Fig. 5.17 Effect of discontinuous normal stress on the location of the MCR slip surface

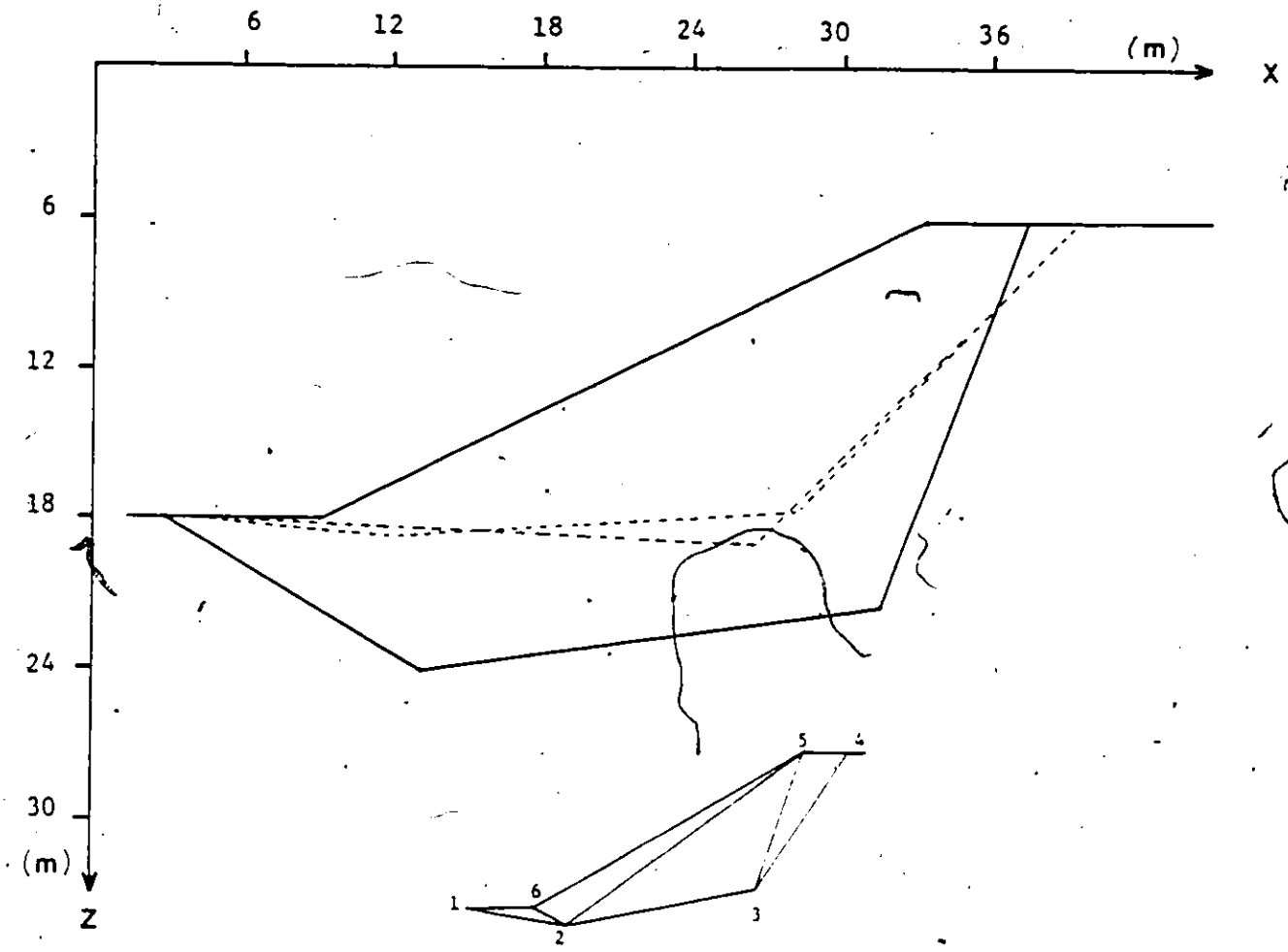

--------- Critical Slip surface

——— Initial Slip surface

Fig. 5.18 Effect of discontinuous normal stress on the location of the LCR slip surface

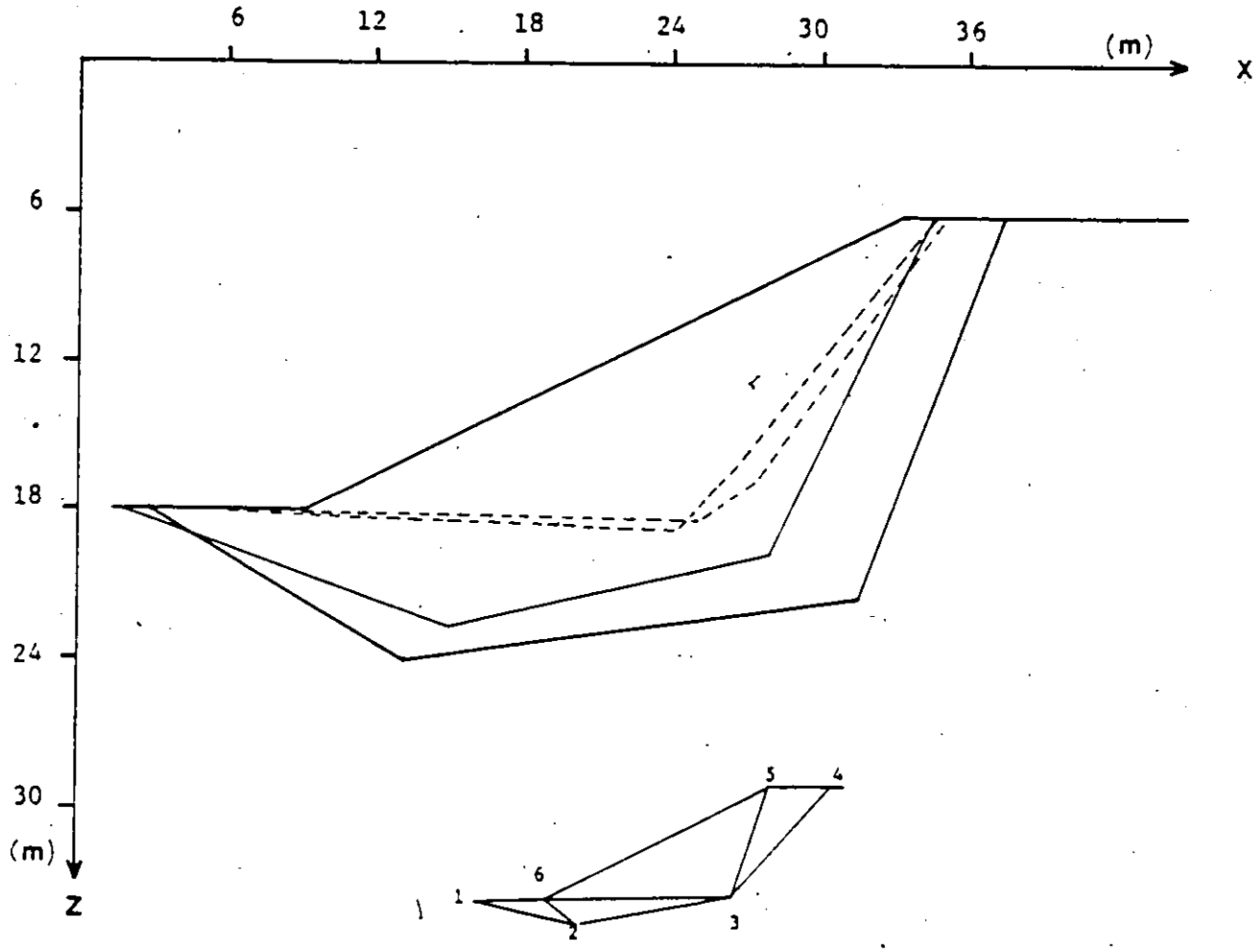

--------- Critical Slip surface

——————— Initial Slip surface

Fig. 5.19 Location of MCR slip lines starting from different trial slip surfaces case study 8(a)

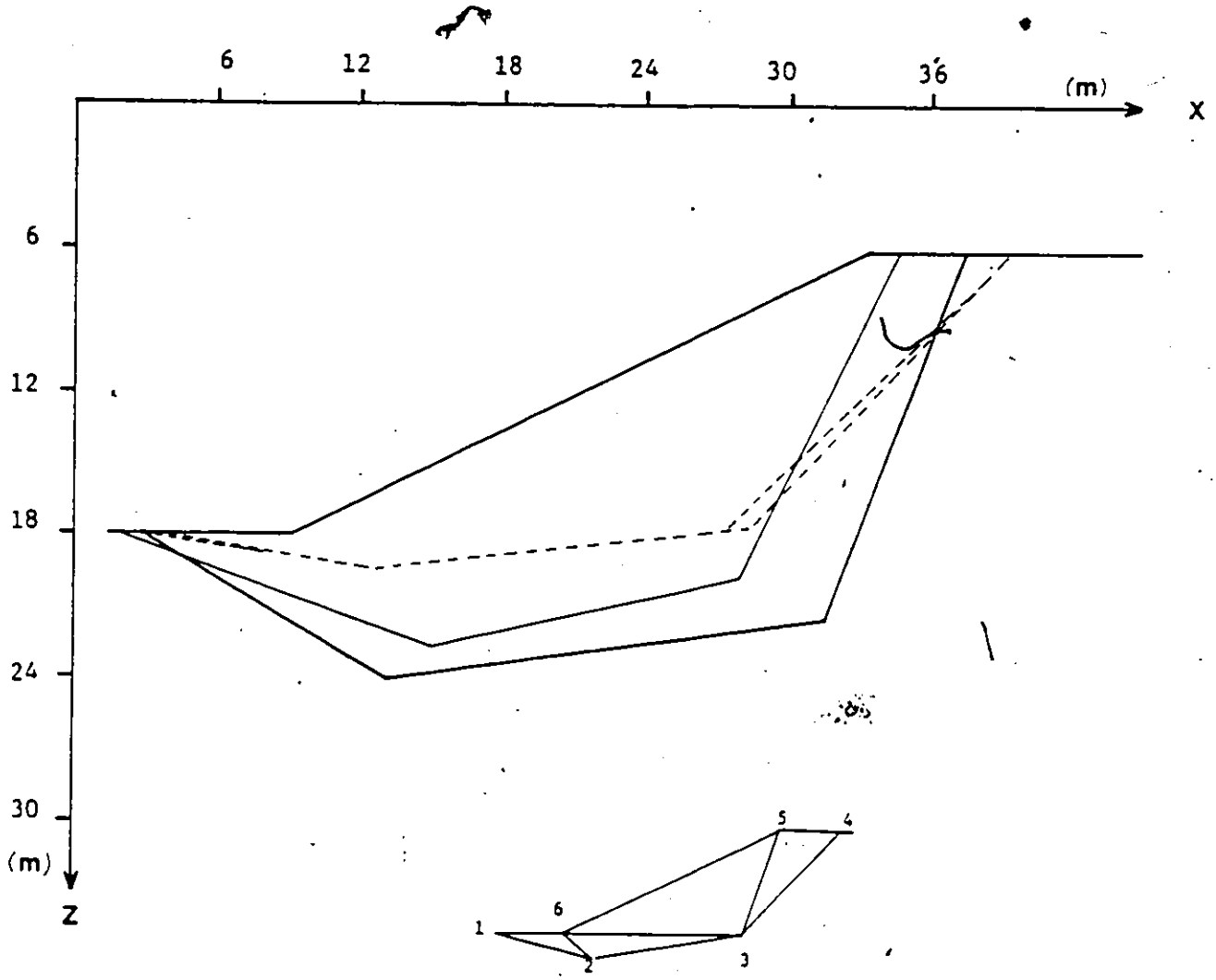

--------- Critical Slip surface

——— Initial Slip surface

Fig. 5.20 Location of LCR slip lines starting from different trial slip surfaces case study 8(b)

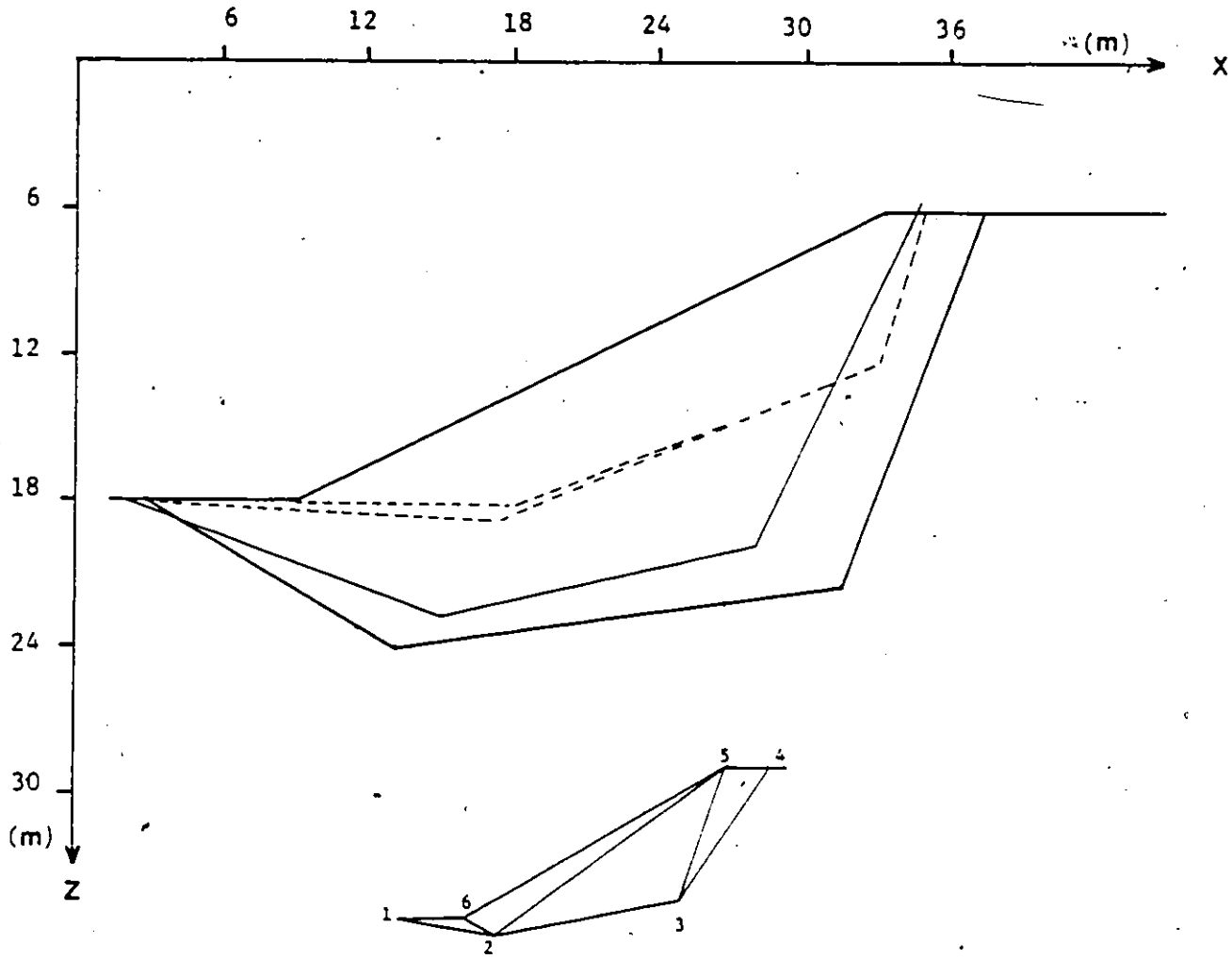

--------- Critical Slip surface

——————— Initial Slip surface

Fig. 5.21 Location of MCR slip lines starting from different trial slip surfaces case study 9(a)

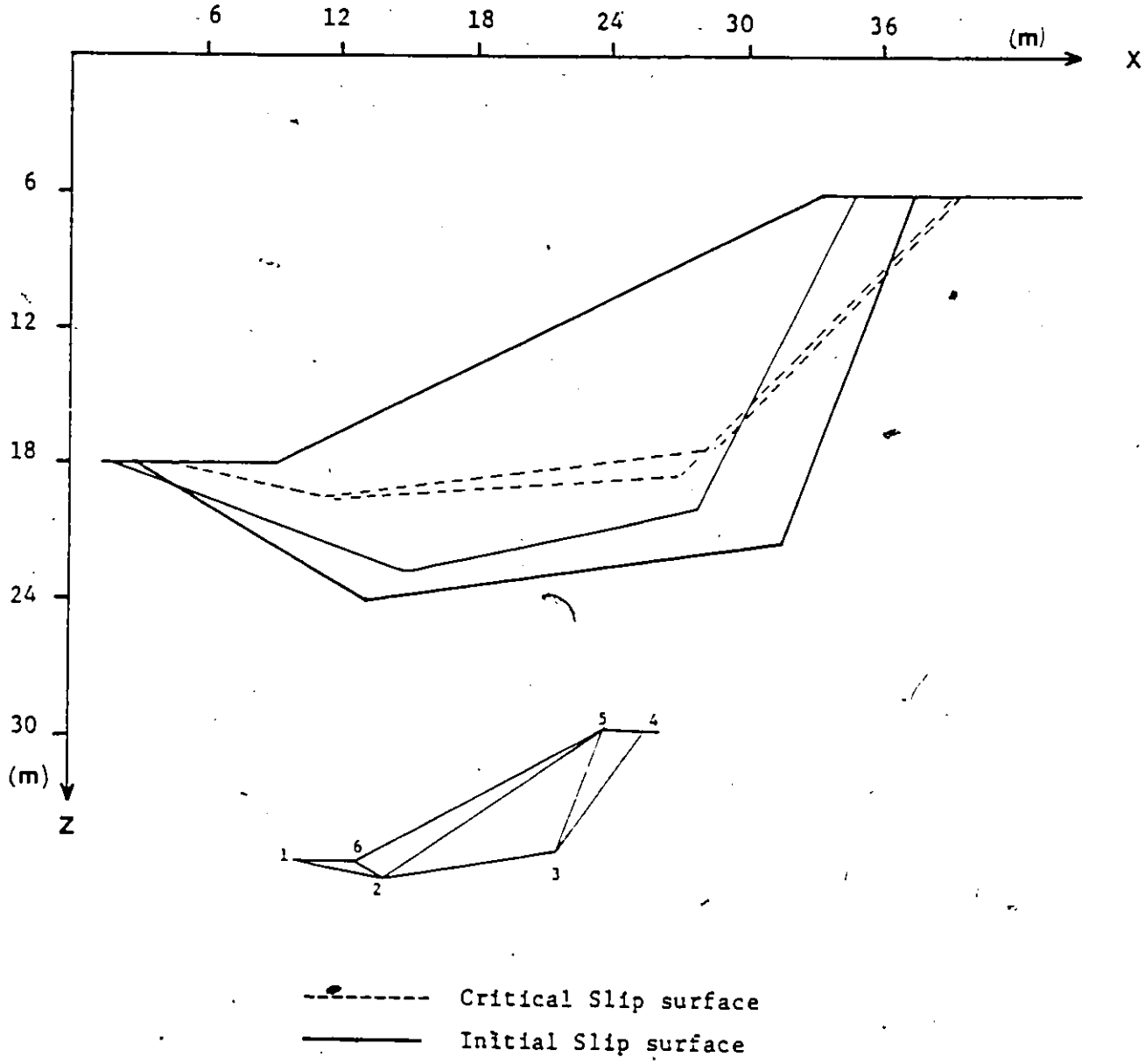

Fig. 5.22 Location of LCR slip lines starting from different trial slip surfaces, case study, 9(b)

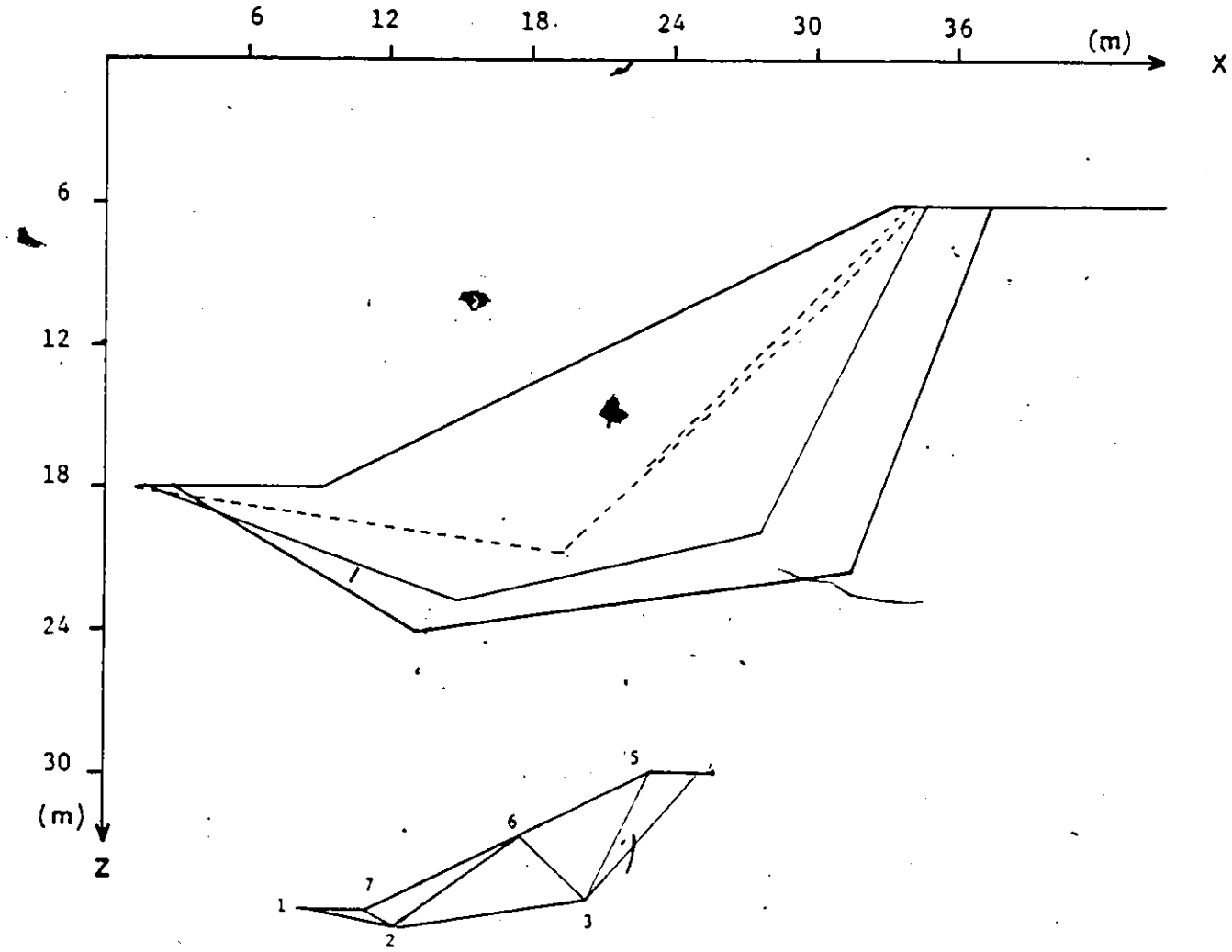

--------- Critical Slip surface

——————— Initial Slip surface

Fig. 5.23 Location of MCR slip lines starting from different trial slip surfaces case study 10(a)

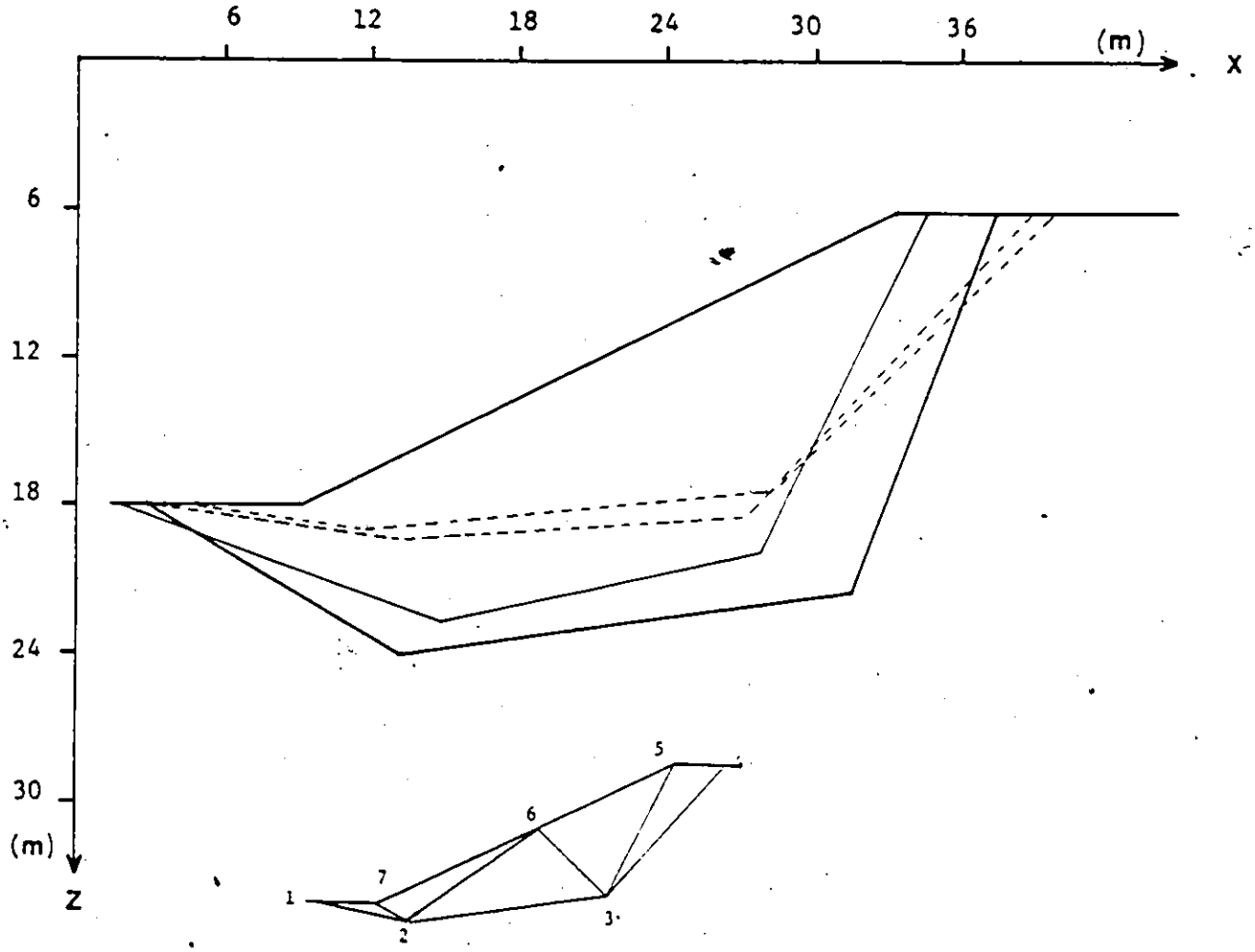

--------- Critical Slip surface

——— Initial Slip surface

Fig. 5.24 Location of LCR slip lines starting from different trial slip surfaces case study 10(b)

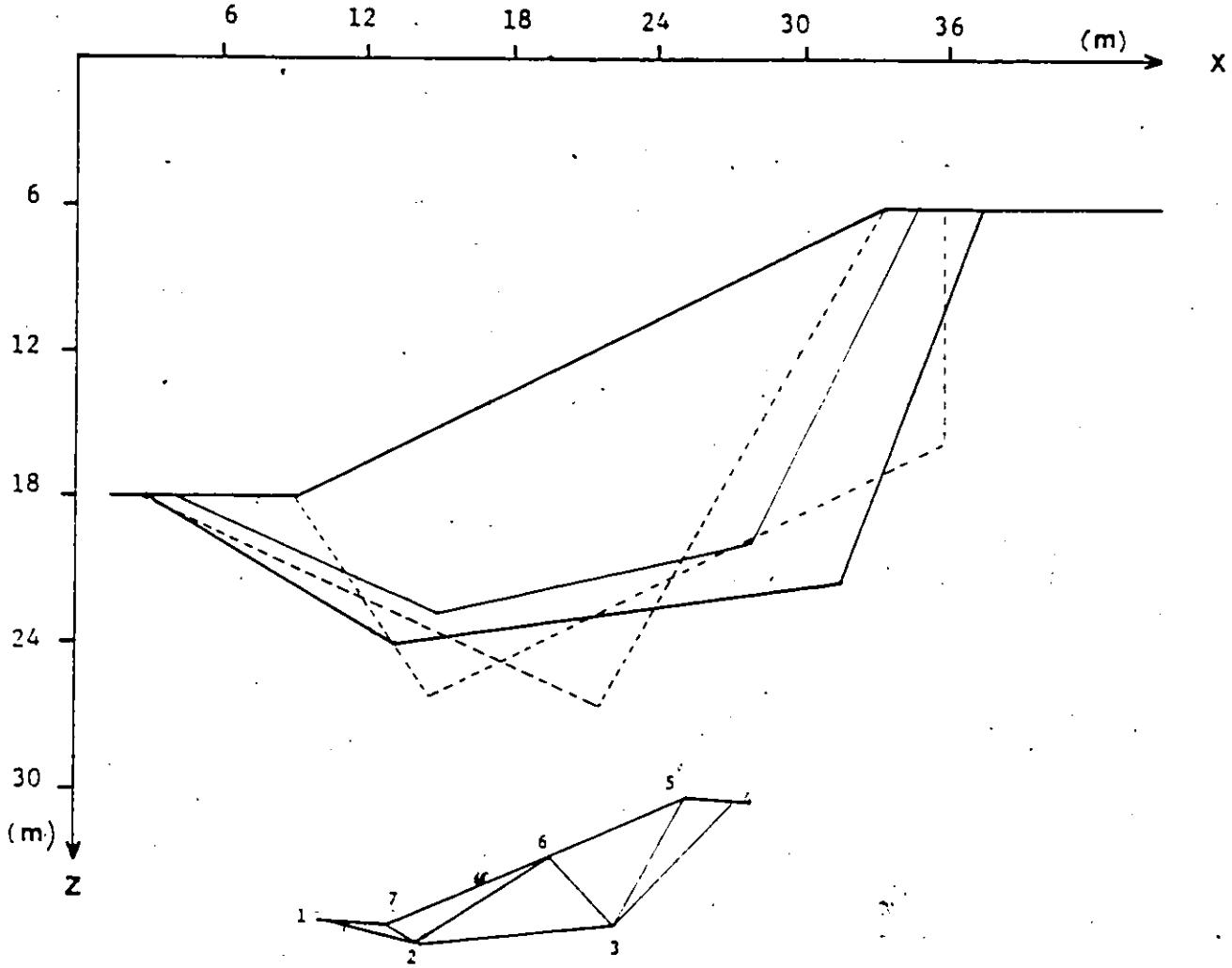

--------- Critical Slip surface

——— Initial Slip surface

Fig. 5.25 Location of MCR slip lines starting from different trial slip surfaces case study 11(a)

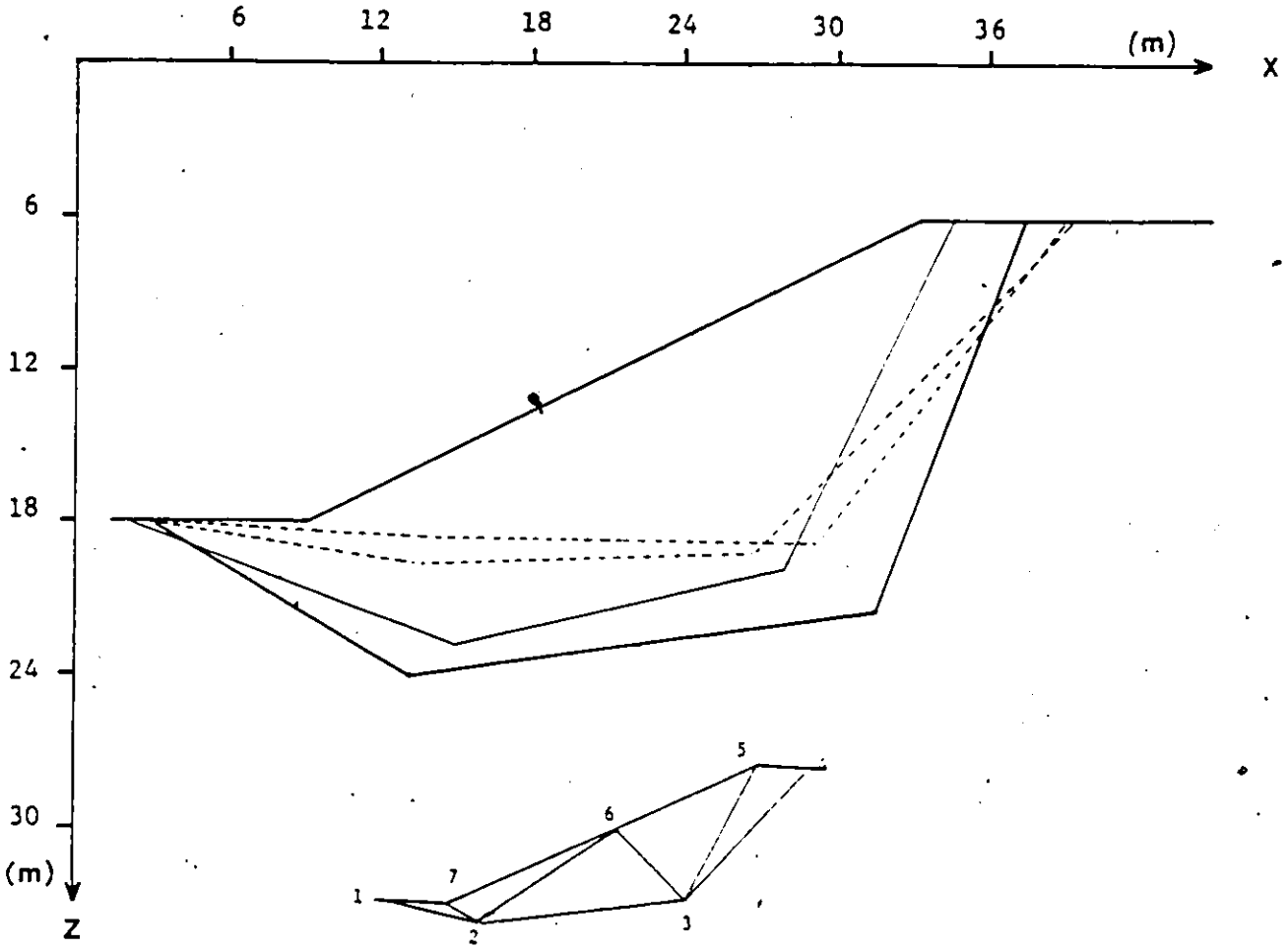

--------- Critical Slip surface

——————— Initial Slip surface

Fig. 5.26 Location of LCR slip lines starting from different trial slip surfaces case study 11(b)

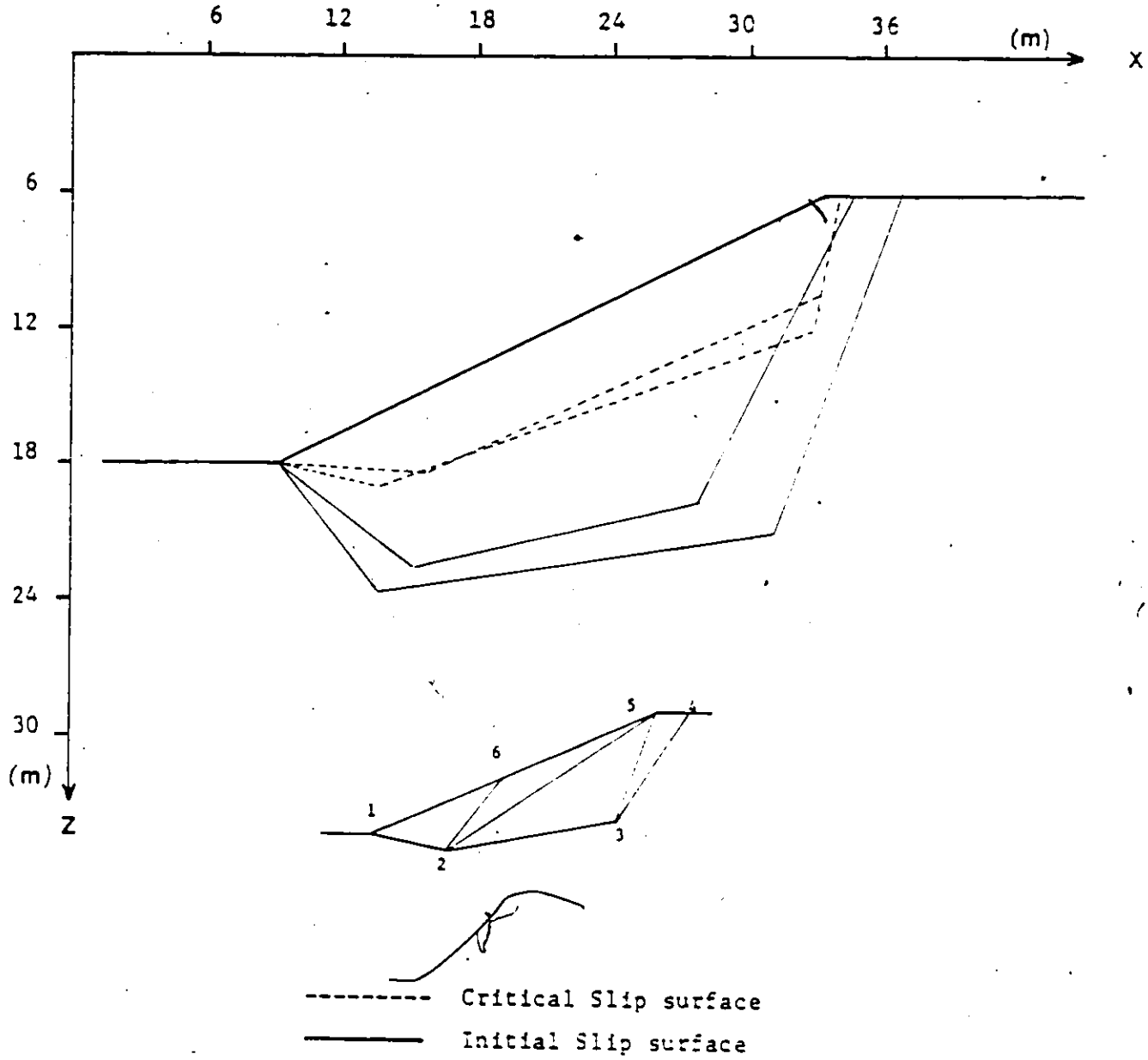

Fig. 5.27 Location of MCR slip lines starting from different trial slip surfaces case study 12(a)

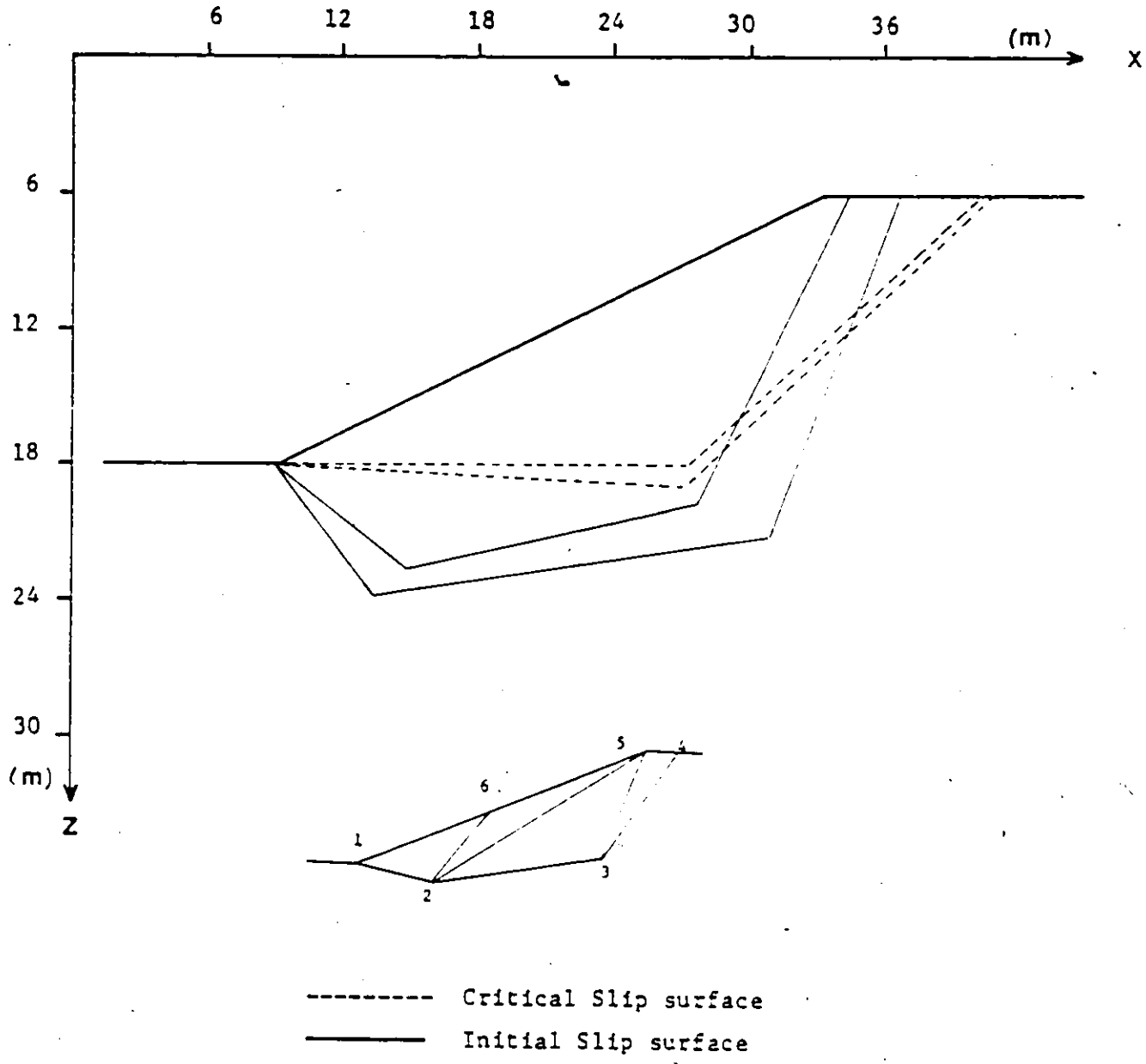

Fig. 5.28 Location of LCR slip lines starting from different trial slip surfaces case study 12(b)

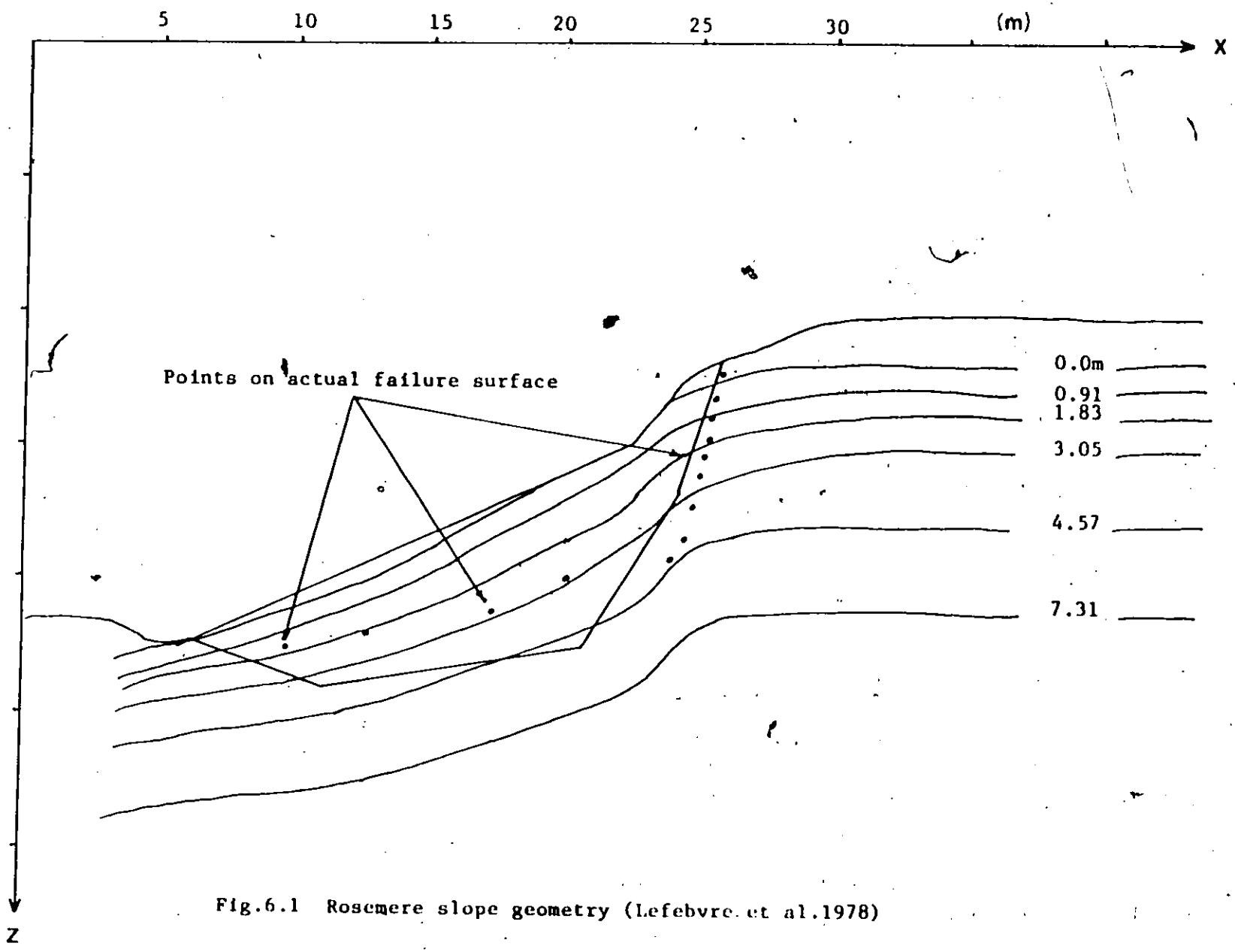

Fig.6.1 Rosemere slope geometry (Lefebvre et al.1978)

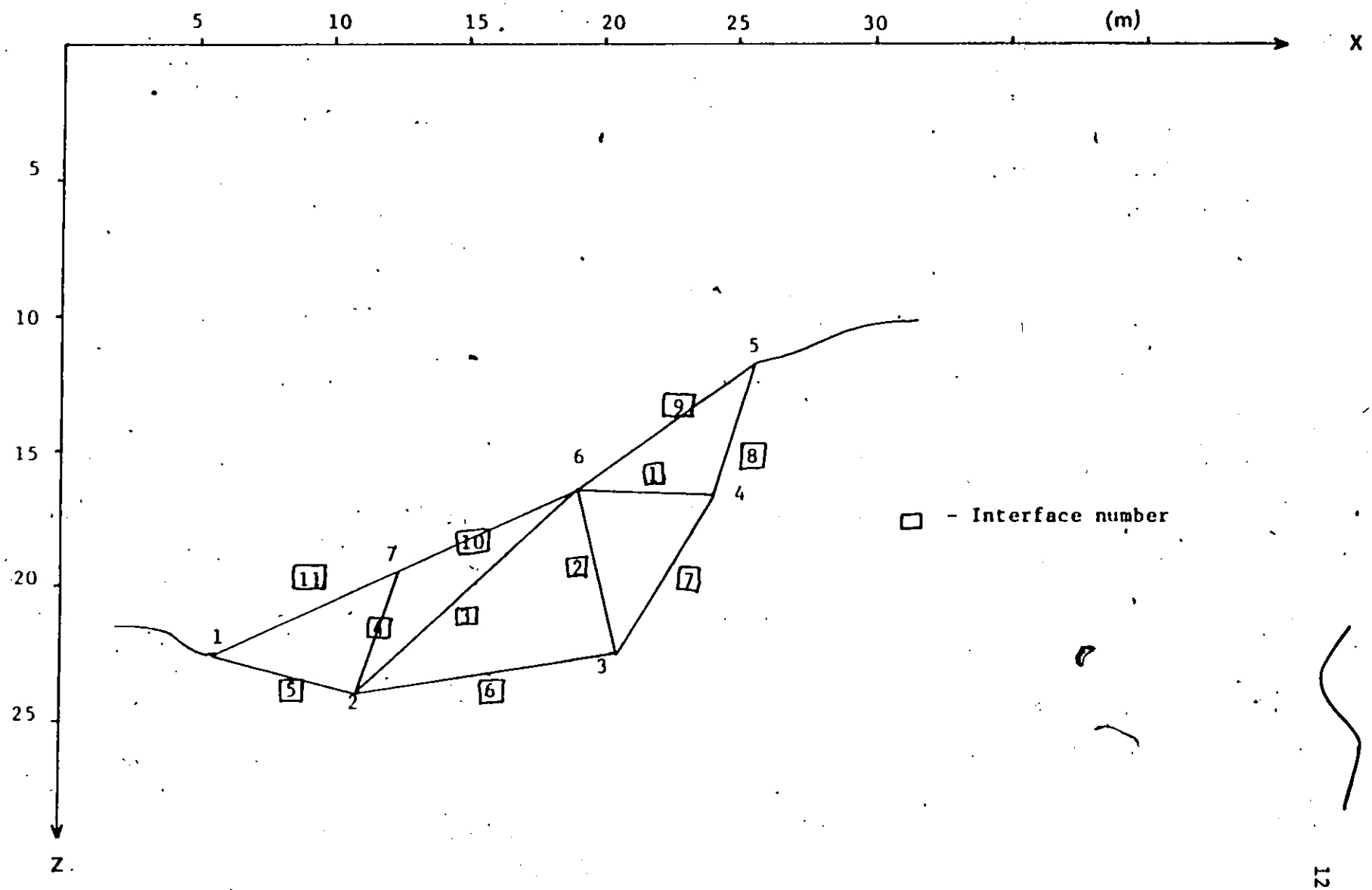

Fig.6.2 Discretisation of the Rosemere slope

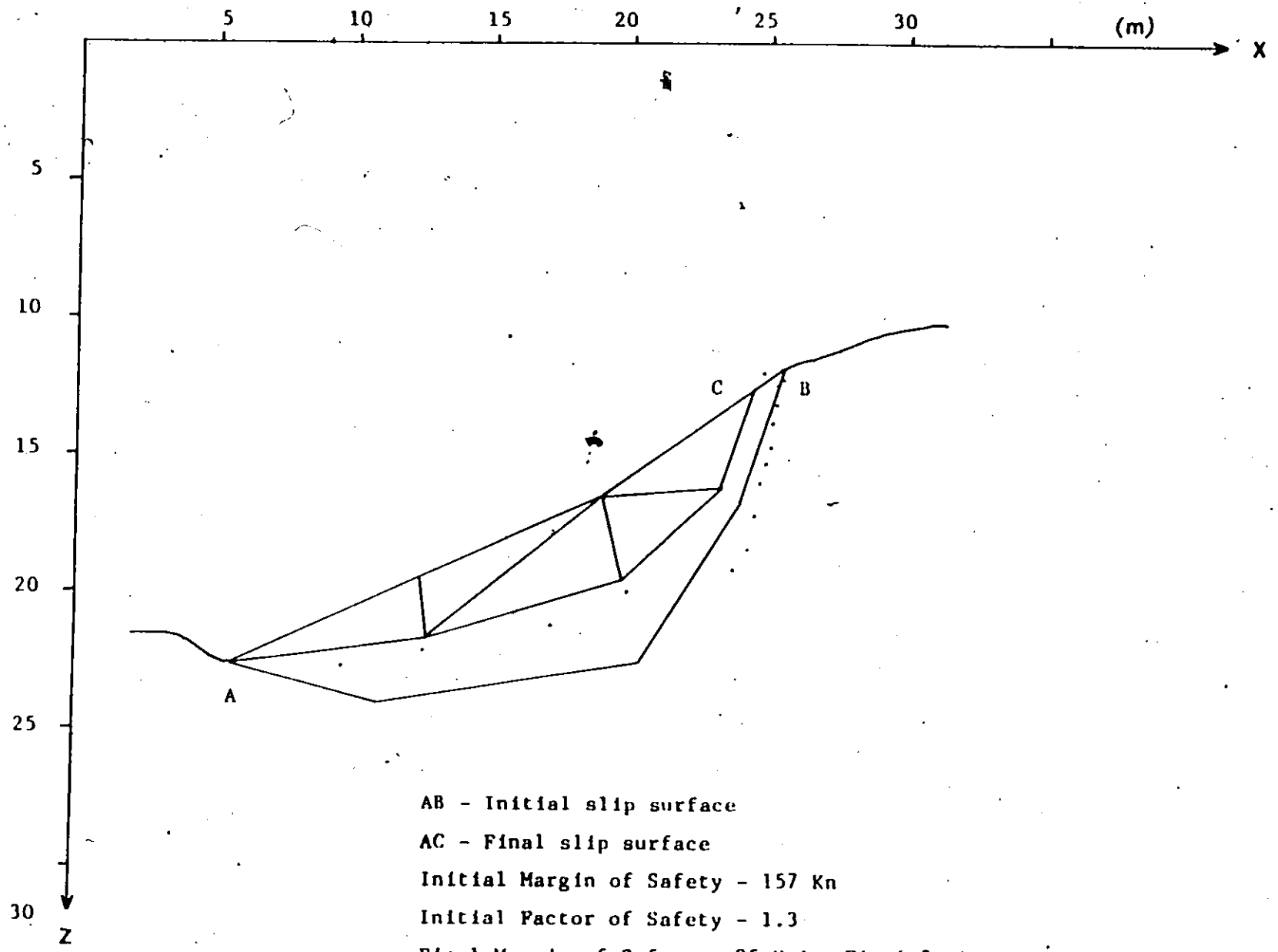

AB - Initial slip surface

AC - Final slip surface

Initial Margin of Safety - 157 Kn

Initial Factor of Safety - 1.3

Final Margin of Safety - 85 Kn

Final Factor of Safety - 1.2

Fig.6.3 Location of the MCR slip surface considering peak soil strength

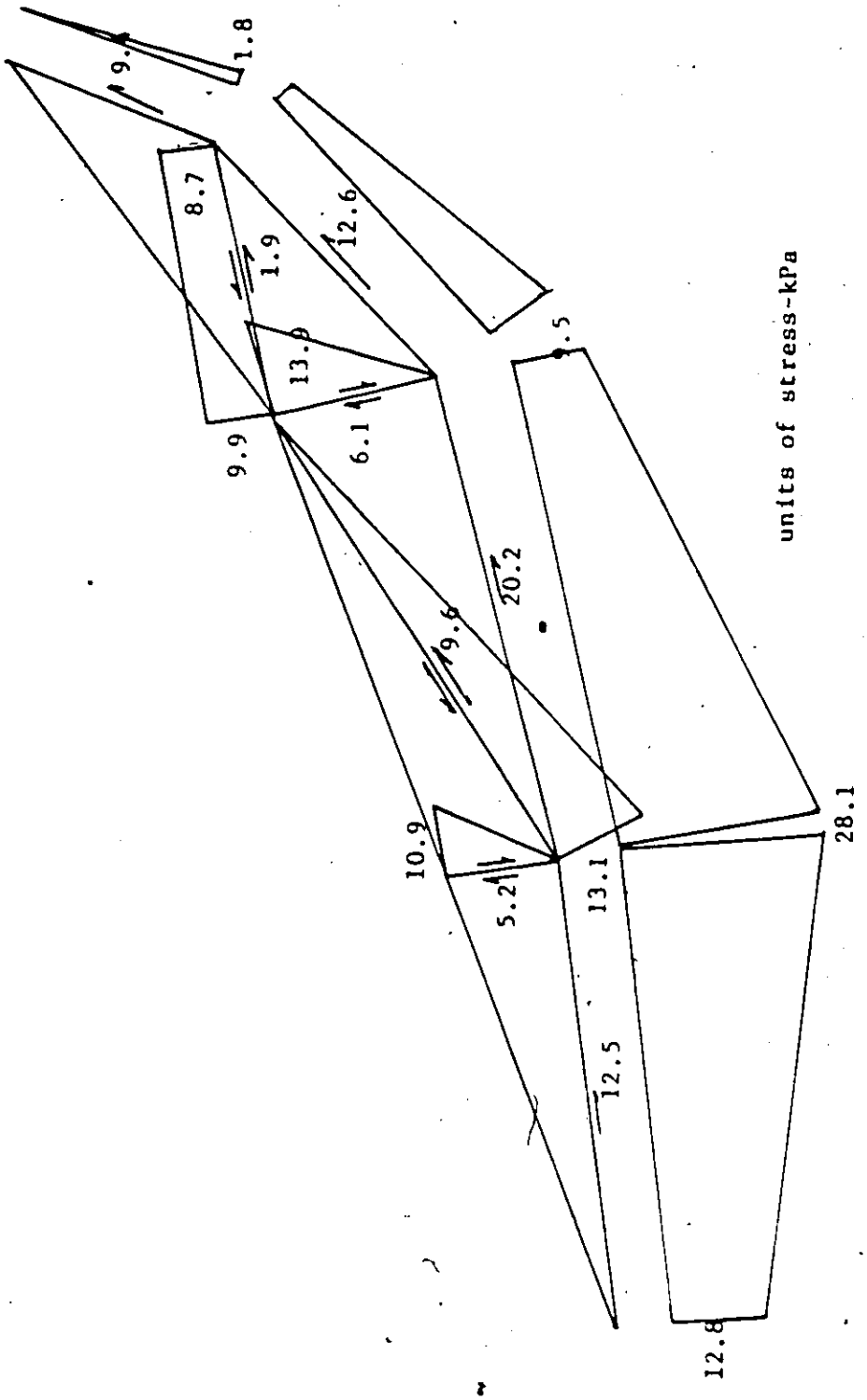

Fig.6.4 Distribution of stresses for the Rosemere slope

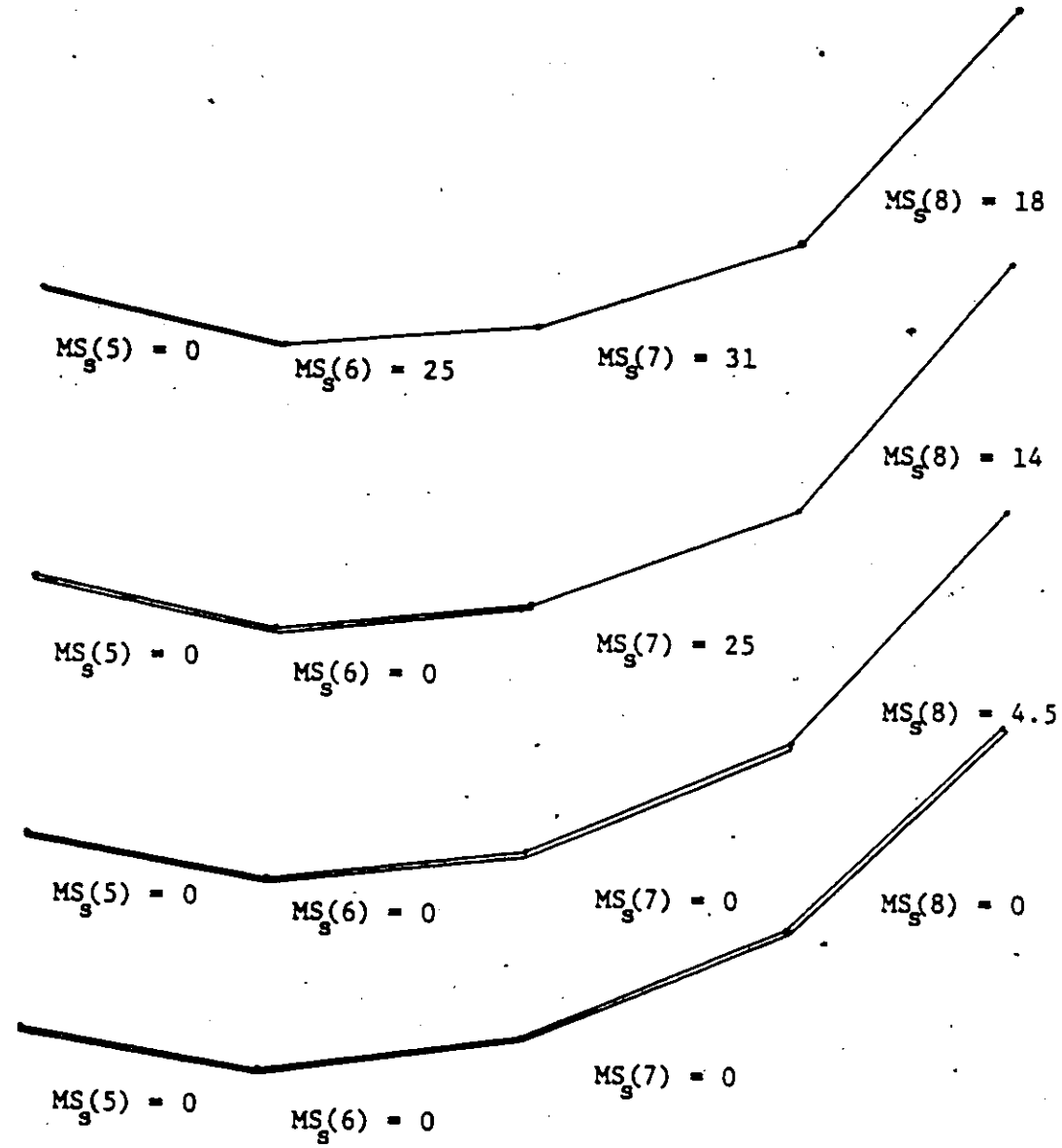

Units of MS_s in kN.

Fig.6.5 Propagation of local failure.

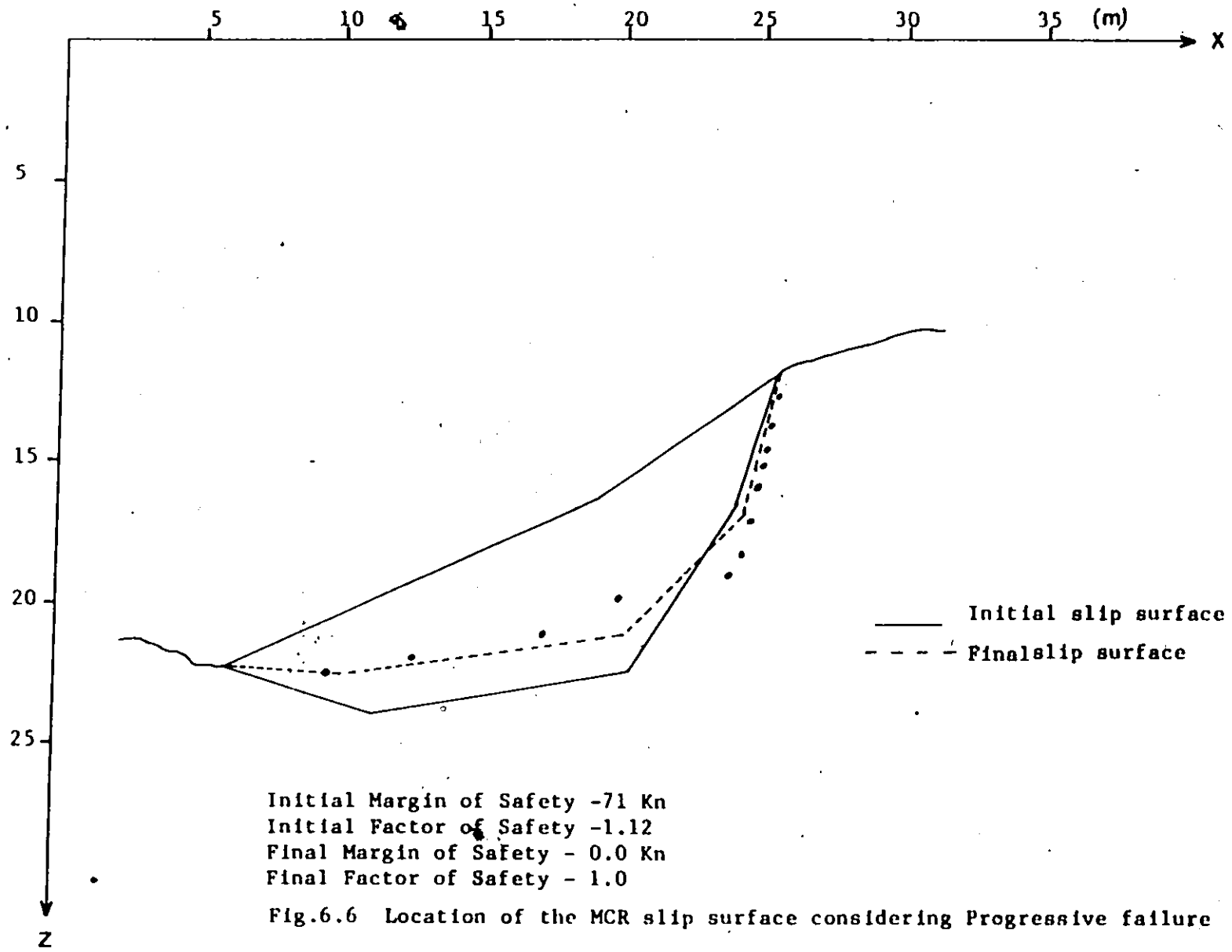

Initial Margin of Safety -71 Kn
Initial Factor of Safety -1.12
Final Margin of Safety - 0.0 Kn
Final Factor of Safety - 1.0

Fig.6.6 Location of the MCR slip surface considering Progressive failure

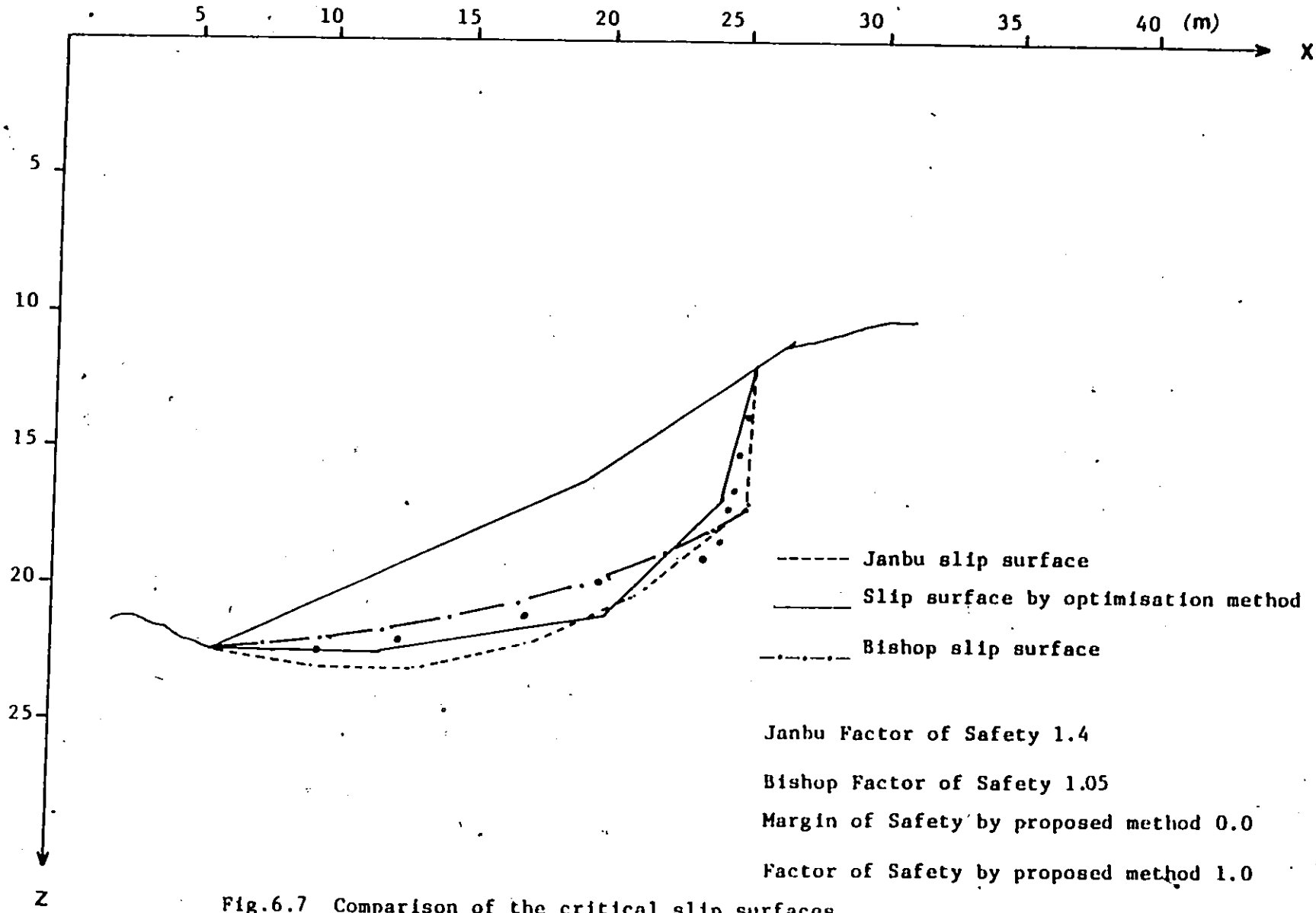

Fig.6.7 Comparison of the critical slip surfaces Obtained by various methods

Table 3.1 Equilibrium equations for the triangular element (Papantonopoulos)

$\{t\}^T$	σ_{ia}	σ_{ja}	τ_a	σ_{jb}	σ_{kb}	τ_b	σ_{kc}	σ_{ic}	τ_c		$\tilde{Y}$	P_1	P_2	$R(u)$	M_0	
ΣF_z	X_{ij}	X_{ij}	$-Z_{ij}/2$	X_{jk}	X_{jk}	$-Z_{jk}/2$	X_{ki}	X_{ki}	$-Z_{ki}/2$	=	β	$-2\sin\theta_b$	$2\cos\theta_b$	$-2R_1$	0	(1)
ΣF_x	Z_{ij}	Z_{ij}	$X_{ij}/2$	Z_{jk}	Z_{jk}	$X_{jk}/2$	Z_{ki}	Z_{ki}	$X_{ki}/2$	=	KE	$2\cos\theta_b$	$2\sin\theta_b$	$2R_2$	0	(2)
ΣM_G	M_b	$-M_c$	E/2	M_c	$-M_a$	E/2	M_a	$-M_b$	E/2		0	$-6\eta_1$	$-6\eta_2$	$-6R_3$	$-6M_0$	(3)
				[S']							(W)	(Q_1)	(Q_2)	(R)	(M)	

Table4.1 Diffrentiated [Al] matrix With respect to θ by moving node i

	side a			side b			side c		
	σ_{ia}	σ_{ja}	τ_a	σ_{jb}	σ_{kb}	τ_b	σ_{kc}	σ_{ic}	τ_c
F_z	$t.\cos\theta$	$t.\cos\theta$	$\frac{t.\sin\theta}{2}$	0	0	0	$-t.\cos\theta$	$-t.\cos\theta$	$-\frac{t.\sin\theta}{2}$
F_x	$-t.\sin\theta$	$-t.\sin\theta$	$\frac{t.\cos\theta}{2}$	0	0	0	$t.\sin\theta$	$t.\sin\theta$	$-\frac{t.\cos\theta}{2}$
M_G	$\frac{d(M_b)}{d\theta}$	$-\frac{d(M_c)}{d\theta}$	$\frac{1}{2}.\frac{d(E)}{d\theta}$	$\frac{d(M_c)}{d\theta}$	$-\frac{d(M_a)}{d\theta}$	$\frac{1}{2}.\frac{d(E)}{d\theta}$	$\frac{d(M_a)}{d\theta}$	$-\frac{d(M_b)}{d\theta}$	$\frac{1}{2}.\frac{d(E)}{d\theta}$

Table 4.2 Diffrentiated [A1] matrix with respect to θ by moving node j

	side a			side b			side c		
	σ_{ia}	σ_{ja}	τ_a	σ_{jb}	σ_{kb}	τ_b	σ_{kc}	σ_{ic}	τ_c
F_z	$-t.\cos\theta$	$-t.\cos\theta$	$\frac{-t.\sin\theta}{2}$	$t.\cos\theta$	$t.\cos\theta$	$\frac{t.\sin\theta}{2}$	0	0	0
F_x	$t.\sin\theta$	$t.\sin\theta$	$\frac{-t.\cos\theta}{2}$	$-t.\sin\theta$	$-t.\sin\theta$	$\frac{t.\cos\theta}{-2}$	0	0	0
M_G	$\frac{d(M_b)}{d\theta}$	$\frac{-d(M_c)}{d\theta}$	$\frac{1}{2}.\frac{d(E)}{d\theta}$	$\frac{d(M_c)}{d\theta}$	$\frac{-d(M_a)}{d\theta}$	$\frac{1}{2}.\frac{d(E)}{d\theta}$	0	0	0

Table 4.3 Diffrentiated [Al] matrix with respect to θ by moving node k

	side a			side b			side c		
	σ_{ia}	σ_{ja}	τ_a	σ_{jb}	σ_{kb}	τ_b	σ_{kc}	σ_{ic}	τ_c
F_z	0	0	0	$-t.\cos\theta$	$-t.\cos\theta$	$\frac{-t.\sin\theta}{2}$	$t.\cos\theta$	$t.\cos\theta$	$\frac{t.\sin\theta}{2}$
F_x	0	0	0	$t.\sin\theta$	$t.\sin\theta$	$\frac{-t.\cos\theta}{2}$	$-t.\sin\theta$	$-t.\sin\theta$	$\frac{t.\cos\theta}{2}$
M_G	$\frac{d(M_b)}{d\theta}$	$\frac{-d(M_c)}{d\theta}$	$\frac{1}{2}.\frac{d(E)}{d\theta}$	$\frac{d(M_c)}{d\theta}$	$\frac{-d(M_a)}{d\theta}$	$\frac{1}{2}.\frac{d(E)}{d\theta}$	$\frac{d(M_a)}{d\theta}$	$\frac{-d(M_b)}{d\theta}$	$\frac{1}{2}.\frac{d(E)}{d\theta}$

Table4.4 Diffrentiation of {Bl} vector with respect toθ by moving node i,j,k

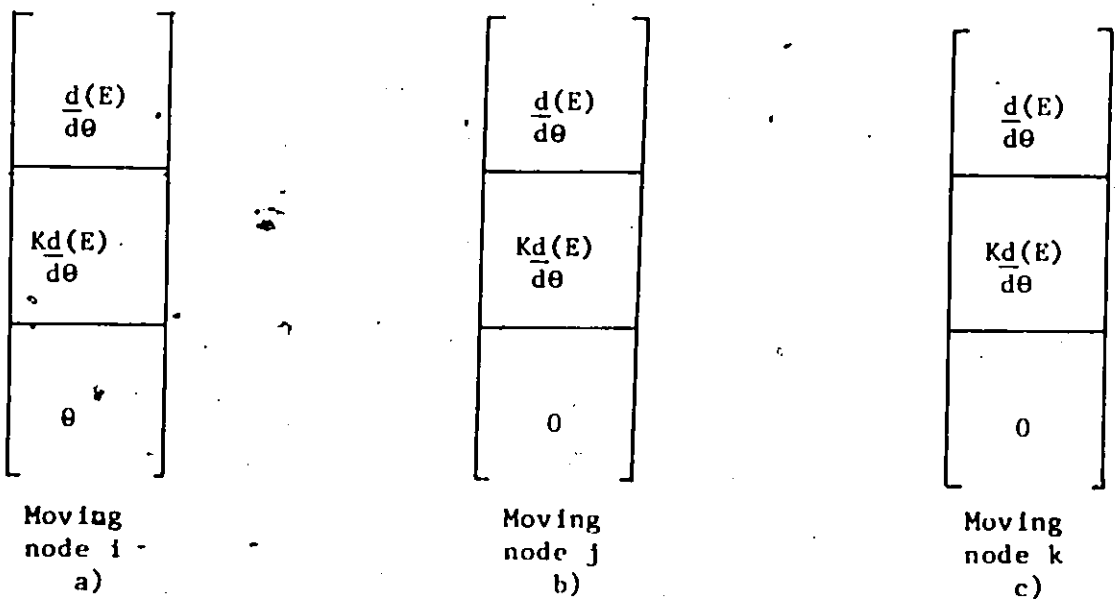

Table 4.5 Diffrentiated [A1] matrix with respect tot by moving node i

	side a			side b			side c		
	σ_{ia}	σ_{ja}	τ_a	σ_{jb}	σ_{kb}	τ_b	σ_{kc}	σ_{ic}	τ_c
F_z	$\sin\theta$	$\sin\theta$	$-\frac{\cos\theta}{2}$	0	0	0	$-\sin\theta$	$-\sin\theta$	$\frac{\cos\theta}{2}$
F_x	$\cos\theta$	$\cos\theta$	$\frac{\sin\theta}{2}$	0	0	0	$-\cos\theta$	$-\cos\theta$	$-\frac{\sin\theta}{2}$
M_G	$\frac{d(M_b)}{dt}$	$-\frac{d(M_c)}{dt}$	$-\frac{1}{2}\cdot\frac{d(E)}{d\theta}$	$\frac{d(M_c)}{dt}$	$-\frac{d(M_a)}{dt}$	$\frac{1d(E)}{2dt}$	$\frac{d(M_a)}{dt}$	$-\frac{d(M_b)}{dt}$	$\frac{d(E)}{dt}$

Table4.6 Diffrentiated [Al] matrix with respect tot by moving node j

	side a			side b			side c		
	σ_{ia}	σ_{ja}	τ_a	σ_{jb}	σ_{kb}	τ_b	σ_{kc}	σ_{ic}	τ_c
F_z	$-\sin\theta$	$-\sin\theta$	$\frac{\cos\theta}{2}$	$\sin\theta$	$\sin\theta$	$-\frac{\cos\theta}{2}$	0	0	0
F_x	$-\cos\theta$	$-\cos\theta$	$-\frac{\sin\theta}{2}$	$\cos\theta$	$\cos\theta$	$\frac{\sin\theta}{2}$	0	0	0
M_G	$\frac{d(M_b)}{dt}$	$-\frac{d(M_c)}{dt}$	$\frac{1}{2}.\frac{d(E)}{dt}$	$\frac{d(M_c)}{dt}$	$-\frac{d(M_a)}{dt}$	$\frac{1}{2}.\frac{d(E)}{dt}$	$\frac{d(M_a)}{dt}$	$-\frac{d(M_b)}{dt}$	$\frac{1}{2}.\frac{d(E)}{dt}$

Table 4.7 Diffrentiated [Al] matrix With respect tot by moving node k

	side a			side b			side c		
	σ_{ia}	σ_{ja}	τ_a	σ_{jb}	σ_{kb}	τ_b	σ_{kc}	σ_{ic}	τ_c
F_z	0	0	0	$-\sin\theta$	$-\sin\theta$	$\frac{\cos\theta}{2}$	$\sin\theta$	$\sin\theta$	$\frac{-\cos\theta}{2}$
F_x	0	0	0	$-\cos\theta$	$-\cos\theta$	$\frac{-\sin\theta}{2}$	$\cos\theta$	$\cos\theta$	$\frac{\sin\theta}{2}$
M_G	$\frac{d(M_b)}{dt}$	$\frac{-d(M_c)}{dt}$	$\frac{1}{2}\cdot\frac{d(E)}{dt}$	$\frac{d(M_c)}{dt}$	$\frac{-d(M_a)}{dt}$	$\frac{1}{2}\cdot\frac{d(E)}{dt}$	$\frac{d(M_a)}{dt}$	$\frac{-d(M_b)}{dt}$	$\frac{1}{2}\cdot\frac{d(E)}{dt}$

Table 4.8 Diffrentiation of {B1} vector with respect to t by moving node i,j,k

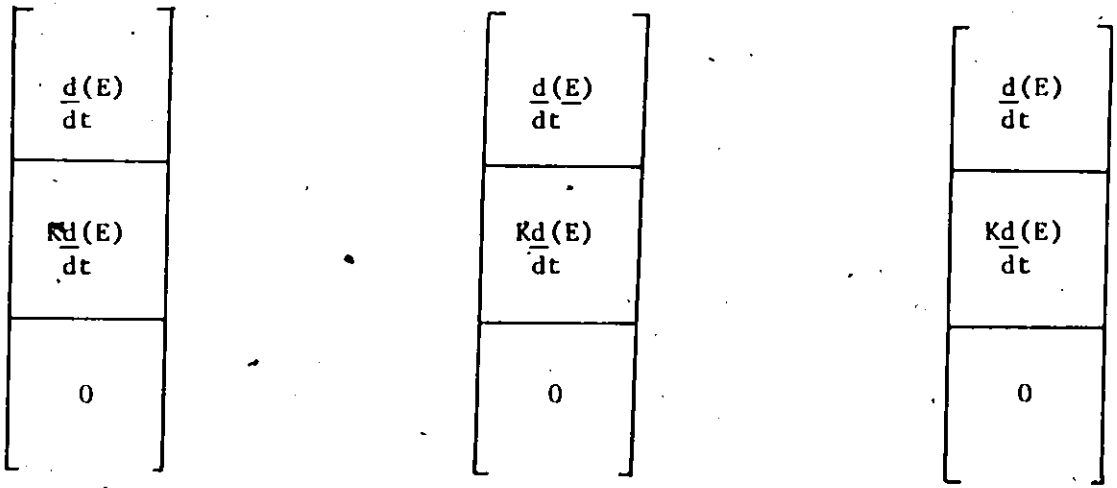

Table 5.1 Comparison of the MS and FS of the MCR slip line with and without the concavity condition

Case Number	Initial MS	Initial FS	Final MS	Final FS	% decrease in MS	% decrease in FS
1A	1180	1.95	878	1.76	25.6	9.7
1B	1180	1.95	1103	1.93	6.5	1.0
% difference in Slip surface	0.0	0.0	20.4	8.8	-	-

Units MS Kn/m

Table 5.2 Effect of the number of elements on the MS and FS of the MCR slip.surface

Case Number	Initial MS	Initial FS	Final MS	Final FS	% decrease in MS	% decrease in FS
3A	1761	2.10	975	2.01	44.6	4.2
3B	1761	2.10	1027	2.17	41.7	3.2
% difference in Slip surface	0.0	0.0	5.0	7.3	-	-

Units MS Kn/m

Table 5.3 Effect of the number of elements on the MS and FS of the LCR slip surface

Case Number	Initial MS	Initial FS	Final MS	Final FS	% decrease in MS	% decrease in FS
3A	2345	2.43	1260	2.06	46.3	15.2
3B	2345	2.43	1228	2.06	47.6	15.2
% difference in Slip surface	0.0	0.0	2.5	0.0	-	-

Units MS Kn/m

Table 5.4 Effect of the topology on the MS and FS of the MCR slip surface

Case Number	Initial MS	Initial FS	Final MS	Final FS	% decrease in MS	% decrease in FS
4A	1761	2.10	819	1.73	95.3	17.6
4B	1761	2.10	975	2.01	44.6	4.2
% difference in Slip surface	0.0	0.0	16	13.9	-	-

Units MS Kn/m

Table 5.5 Effect of the topology on the MS and FS of the LCR slip surface

Case Number	Initial MS	Initial FS	Final MS	Final FS	% decrease in MS	% decrease in FS
4A	2345	2.43	1283	2.05	45.3	15.6
4B	2345	2.43	1260	2.06	46.3	15.2
% difference in Slip surface	0.0	0.0	1.8	0.5	-	-

Units MS Kn/m

Table 5.6 Effect of the topology on the MS and FS of the MCR slip surface

Case Number	Initial MS	Initial FS	Final MS	Final FS	% decrease in MS	% decrease in FS
5A	1904	2.64	708	1.93	62.8	26.9
5B	1904	2.64	715	1.81	62.4	31.4
% difference in Slip surface	0.0	0.0	0.97	6.2	-	-

Units MS Kn/m

Table Table 5.7 Effect of the topology on the MS and FS of the LCR slip surface

Case Number	Initial MS	Initial FS	Final MS	Final FS	% decrease in MS	% decrease in FS
5A	3341	5.65	1002	1.96	70.0	65.3
5B	3341	5.65	1002	1.97	70.0	65.1
% difference in Slip surface	0.0	0.0	0.0	0.5	-	-

Units MS Kn/m

Table 5.8 Effect the degrees of freedom have on the MS and FS of the MCR slip surface

Case Number	Initial MS	Initial FS	Final MS	Final FS	% decrease in MS	% decrease in FS
6A	1180	1.95	1135	1.91	3.8	2.1
6B	1180	1.95	1102	1.92	6.6	1.5
% difference in Slip surface	0.0	0.0	2.9	0.5	-	-

Units MS Kn/m

Table 5.9 Effect of discontinuous normal stress on the MS and FS of the MCR slip surface

Case Number	Initial MS	Initial FS	Final MS	Final FS	% decrease in MS	% decrease in FS
7A	1126	1.51	483	1.18	57.0	21.8
7B	1761	2.10	1027	2.17	41.7	3.2
% difference in Slip surface	36.0	28.0	53.0	45.6	-	-

Units MS Kn/m

Table 5.10 Effect of the discontinuous normal stress on the MS and FS of the LCR slip surface

Case Number	Initial MS	Initial FS	Final MS	Final FS	% decrease in MS	% decrease in FS
7A	2694	4.42	1392	2.21	48.3	50.0
7B	2345	2.43	1228	2.06	47.6	15.2
% difference in Slip surface	12.9	45.0	11.8	6.8	-	-

Units MS Kn/m

Table 5.11 Comparison of MS and FS of the MCR slip line starting from different trial surfaces Case Study - 8(a)

Case Number	Initial MS	Initial FS	Final MS	Final FS	% decrease in MS	% decrease in FS
8A	1761	2.1	819	1.73	95.3	17.6
8B	1332	2.04	846	1.86	38	10.6
% difference in Slip surface	24.4	2.9	3.2	6.9	-	-

Units MS Kn/m

Table 5.12 Comparison of MS and FS of the LCR slip line starting from different trial surfaces Case Study - 8(b)

Case Number	Initial MS	Initial FS	Final MS	Final FS	% decrease in MS	% decrease in FS
8A	2345	2.43	1283	2.05	45.3	15.6
8B	1643	2.27	1153	2.0	30	12
% difference in Slip surface	29.9	6.6	10	2.4	-	-

Units MS Kn/m

Table 5.13 Comparison of the MS and FS of the MCR slip line starting from different trial surfaces Case Study - 9(a)

Case Number	Initial MS	Initial FS	Final MS	Final FS	% decrease in MS	% decrease in FS
9A	1761	2.1	975	2.01	44.6	4.2
9B	1332	2.04	967	2.12	27.4	-3.8
% difference in Slip surface	24.3	2.9	0.8	5.0	-	-

Units MS Kn/m

Table 5.14 Comparison of the MS and FS of the LCR slip line starting from different trial surfaces Case Study - 9(b)

Case Number	Initial MS	Initial FS	Final MS	Final FS	% decrease in MS	% decrease in FS
9A	2345	2.43	1260	2.06	46.3	15.2
9B	1632	2.22	1184	2.02	27.4	9
% difference in Slip surface	30.4	8.6	6	1.9	-	-

Units MS Kn/m

Table 5.15 Comparison of the MS and FS of the MCR slip line starting from different trial surfaces Case Study - 10(a)

Case Number	Initial MS	Initial FS	Final MS	Final FS	% decrease in MS	% decrease in FS
10A	1761	2.1	1027	2.17	41.7	-3.2
10B	1366	2.08	1038	2.28	24	-8.8
% difference in Slip surface	22.4	0.95	0.98	0.46	-	-

Units MS Kn/m

Table 5.16 Comparison of the MS and FS of the LCR slip line starting from different slip surfaces Case Study - 10(b)

Case Number	Initial MS	Initial FS	Final MS	Final FS	% decrease in MS	% decrease in FS
10A	2345	2.43	1228	2.06	47.6	15.2
10B	1643	2.27	1202	2.01	26.9	11.5
% difference in Slip surface	30	6.6	2.2	2.4	-	-

Units MS Kn/m

Table 5.17 Comparison of the MS and FS of the MCR slip line starting from different trial slip surfaces Case Study - 11(a)

Case Number	Initial MS	Initial FS	Final MS	Final FS	% decrease in MS	% decrease in FS
11A	1126	1.51	483	1.18	57	21.8
11B	1090	1.73	499	1.19	54.2	31.2
% difference in Slip surface	3.2	12.7	3.2	0.84	-	-

Units MS Kn/m

Table 5.18 Comparison of the MS and FS of the LCR slip line starting from different trial surfaces Case Study - 11(b)

Case Number	Initial MS	Initial FS	Final MS	Final FS	% decrease in MS	% decrease in FS
11A	2694	4.42	1392	2.21	48.3	50
11B	1831	2.89	1187	2.02	35.2	30
% difference in Slip surface	32	34.6	14.7	8.6	-	-

Units MS Kn/m

Table 5.19 Comparison of the MS and FS of the MCR slip line starting from different trial surfaces Case Study - 12(a)

Case Number	Initial MS	Initial FS	Final MS	Final FS	% decrease in MS	% decrease in FS
12A	1939	2.7	715	1.81	63.1	32.9
12B	1319	2.04	696	1.91	47.2	6.4
% difference in Slip surface	32	24.4	2.6	5.2	-	-

Units MS Kn/m

Table 5.20 Comparison of the MS and FS of the LCR slip line starting from different trial surfaces Case Study - 12(b)

Case Number	Initial MS	Initial FS	Final MS	Final FS	% decrease in MS	% decrease in FS
12A	3341	5.65	1002	1.97	70	65.1
12B	2183	3.31	1076	1.86	50.7	43.8
% difference in Slip surface	34.6	41.4	6.9	5.6	-	-

Units MS Kn/m

Appendix A

CONVENTIONAL LIMIT EQUILIBRIUM METHODS

1. FELLENIUS METHOD : This method is applicable only to circular failure surfaces. Fig.A.1(a) shows the formulation of the method.

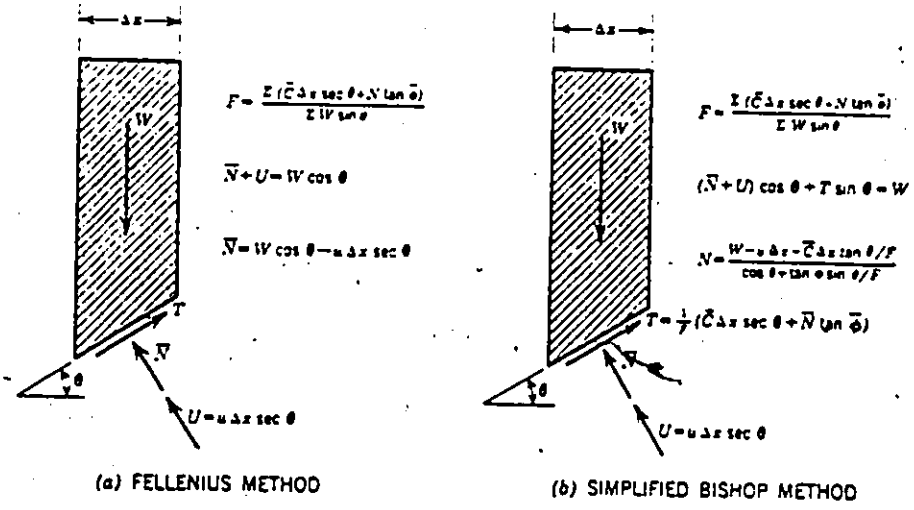

Fig. A.1 Derivation of the resultant normal effective force (After Whitman and Bailey)

Fellinius (1936) defined safety factor in terms of moments about the centre of the failure arc. The denominator of the equation for F is an exact expression for the moment of the weight of the soil in the failure mass. (The radius R has

been cancelled from numerator and denominator). The numerator is the moment of the shear stresses along the failure surface, and involves the unknown distribution of N along that surface. Thus far there is no error in the formulation. The difficulty begins with the attempt to evaluate N. Fig.A.1(a) gives the expression for N. The implied assumption can be stated as: the resultant of all forces on the sides of a slice acts parallel to the bottom of the slice. If this condition were actually met on all slices, each slice would be in equilibrium in the direction normal to its respective part of the failure surface. The expression for N (and hence for F) would then be accurate. In actuality, this condition is not met for all slices, and hence some of the slices are not in equilibrium and the computed F is approximate.

2. SIMPLIFIED BISHOP METHOD : This method is applicable only to circular failure surfaces. The Simplified Bishop method (1955) involves exactly the same definition of safety factor as the Fellinius Method. However, a different scheme is used to evaluate N. As shown in Fig.A.1(b), this is done by summing the vertical components of the forces. Now the implied assumption is: the resultant of all forces on the sides of the slice acts horizontally, i.e. this resultant has no vertical component.

Again, if this condition were met on all sides, the expression for N (and hence for F) would be accurate. This condition generally is not met for all slices, and so the computed F is in error.

3. MORGENSTERN-PRICE METHOD : In this method Morgestern and Price (1965) proposed the following procedure for reducing the indeterminate problem to a determinate one. A function f(x) is assumed which relates to the side forces E(x), and X(x) as :

$$\tan\alpha(x) = \frac{X(x)}{E(x)} = \lambda f(x) \qquad \text{A.1}$$

The function f(x) describes the pattern by which $\alpha(x)$ varies from interface to interface. Fig.A.2 illustrates several simple possible patterns.

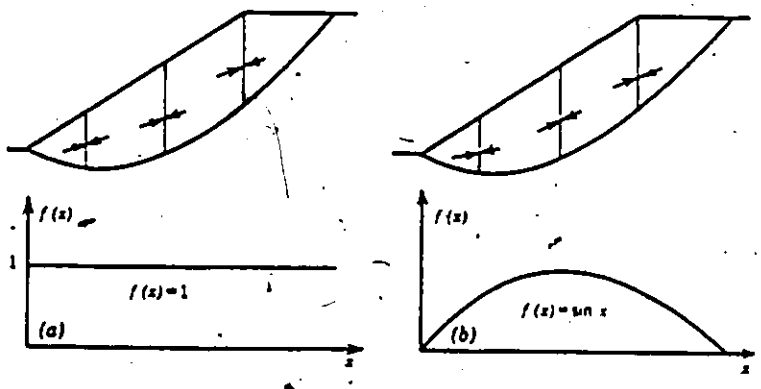

Fig. A.2 Examples of interslice force functions

However, any type of pattern may be used. The unknown parameter λ determines the magnitude of α. Assuming the pattern f(x) amounts to making n-1 assumptions regarding n-1 values of. One more unknown, λ, has been introduced, so that in effect n-2 assumptions have been made. This leaves 3n unknowns with 3n equations (see Fig.A.3).

	(a) Unknowns associated with force equilibrium
n	resultant normal forces $\bar{N}$ on the base of each slice or wedge
1	safety factor, which permits the shear forces T on the base of each slice to be expressed in terms of $\bar{N}$
n-1	resultant normal forces $\bar{E}$ on each interface between slices or wedges
n-1	angles α which express the relationships between the shear force X and the normal force E on each interface
3n-1	unknowns, versus 2n equations
	(b) Unknowns associated with moment equilibrium
n	co-ordinates a locating the resultant $\bar{N}$ on the base of each wedge or slice
n-1	co-ordinates b locating the resultant $\bar{E}$ on each interface between wedges or slices
2n-1	unknowns, versus n equations
	(c) Total unknowns
5n-2	unknowns versus 3n equations.

Fig. A.3 Unknowns and equations for n slices (After Whitman and Bailey)

The user of this method must exercise his judgement and intuition in the assumption of a function f(x). That is, he must estimate how the angle $\alpha(x)$ will change throughout the free body. However, the actual magnitude of these angles are computed as part of the solution. Other quantities also computed as part of the solution are the forces E and X on the sides of slices, the distance b, (b defines the point

of application of the normal force on the side of a slice), the forces N and T (or stresses and) along the failure surface, and the factor of safety, F (see Fig.A.4).

Some assumptions regarding f(x) may lead to distribution of stresses along the failure arc that seem totally unreasonable in the light of intuition. Some f(x) will result in large values of b which imply that the line of action of side forces E falls outside the failure mass; or that the values of X exceed the shear resistance available along vertical planes.

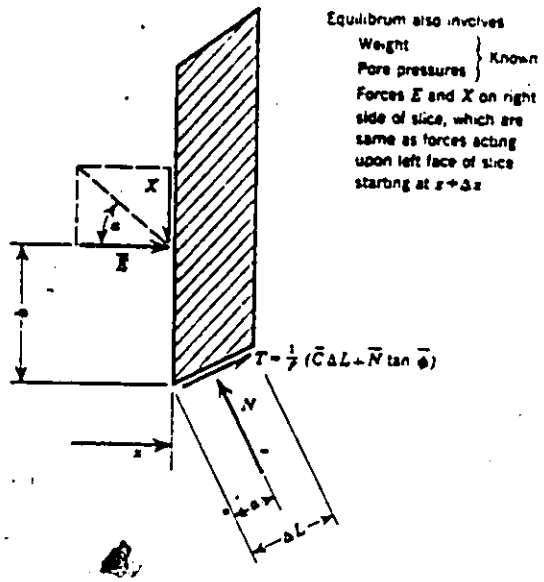

Fig. A.4 Forces acting upon a slice (After Whitman and Bailey)

All these results are unreasonable, but all other solutions must be regarded as correct. Thus this method does not free the engineer from making a judgement, but it gives far more information on which to base the judgement.

4. SPENCER METHOD : This method is a special case of the Morgenstern-Price method. Spencer (1967) assumes a constant relationship between the magnitude of the interslice shear and normal forces.

$$\frac{X}{E} = \tan\theta \qquad \text{A.2}$$

where, θ = angle of the resultant interslice force from the horizontal.

The assumption corresponds to putting the interslice force function f(x) equal to 1, and λ equal to $\tan\theta$.

5. JANBU SIMPLIFIED METHOD : In this method the interslice shear forces are assumed to be zero by Janbu (1954). The normal force equation is the same as in Bishop's Simplified method. The factor of safety is computed from the horizontal force equilibrium equation. Then an empirical correction factor is multiplied by the computed factor of safety in an attempt to account for the effect of the interslice shear forces. The empirical correction factor is related to the shear strength properties and the shape of the slip surface. In this method the moment equilibrium is not satisfied. The empirical correction factor generally increases the factor of safety by up to approximately 10 percent.

6. JANBU GENERALIZED METHOD : In this method Janbu(1954, 1956) includes the effect of interslice forces by making an assumption regarding the point at which the interslice forces act, i.e. the line of thrust. The factor of safety equation is derived from horizontal force equilibrium. The interslice shear forces are computed from the summation of the moments about the centre of the base of each slice. Once the safety factor has been obtained it is possible to plot the computed interslice shear and normal forces and determine a corresponding side force function. This method indirectly satisfies the moment equilibrium.

7. FORCE EQUILIBRIUM METHODS :

a. Lowe and Karafiath Method: In this method (1960) the direction of the resultant of each interslice force is assumed to be equal to the average of the surface and slip surface slopes. The factor of safety is computed from force equilibrium equations.

b. Corps of Engineers Method: In the Corps of Engineers method (1970) the direction of the resultant interslice force is assumed to be equal to the average surface slope. This appears to be interpreted as either equal to the average slope between the extreme entrance and exit of the failure surface or the changing slope of the ground surface. The factor of safety is computed from force equilibrium equations.

Appendix B

EQUILIBRIUM EQUATIONS FOR THE GENERALISED LIMIT EQUILIBRIUM METHOD (GLEM)

Appendix B is an abbreviated form of Appendix E taken from Papantonopoulos (1979).

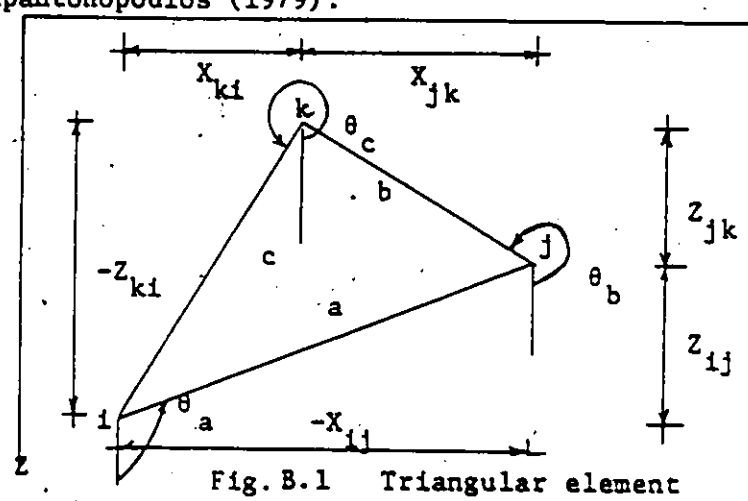

Fig. B.1 Triangular element

a) Relationship between the coordinates of the nodes i, j and k, the sides a, b and c, and the angles θ_a, θ_b and θ_c.

For simplicity of the notations we have

$$Z_{ij} = Z_i - Z_j \;,\; Z_{jk} = Z_j - Z_k \;,\; Z_{ki} = Z_k - Z_i$$
$$X_{ij} = X_i - X_j \;,\; X_{jk} = X_j - X_k \;,\; X_{ki} = X_k - X_i \qquad (B.1)$$

From Fig. B.1

$$\sin\theta_a = -\frac{X_{ij}}{a} \;,\; \sin\theta_b = -\frac{X_{jk}}{b} \;,\; \sin\theta_c = -\frac{X_{ki}}{c} \;, \qquad (B.2)$$

$$\cos\theta_a = -\frac{Z_{ij}}{a} \;,\; \cos\theta_b = -\frac{Z_{jk}}{b} \;,\; \cos\theta_c = -\frac{Z_{ki}}{c} \;, \qquad (B.3)$$

$$\mathrm{tg}\,\theta_a = \frac{X_{ij}}{Z_{ij}} \;,\; \mathrm{tg}\,\theta_b = -\frac{X_{jk}}{Z_{jk}} \;,\; \mathrm{tg}\,\theta_c = \frac{X_{ki}}{Z_{ki}} \;, \qquad (B.4)$$

$$a^2 = Z_{ij}^2 + X_{ij}^2 \;,\; b^2 = Z_{jk}^2 + X_{jk}^2 \;,\; c^2 = Z_{ki}^2 + X_{ki}^2 \qquad (B.5)$$

b) Relations between the coordinates of the nodes and the area of the triangle.

$$E = Z_i X_{jk} + Z_j X_{ki} + Z_k X_{ij} = Z_{ki} X_{ij} - Z_{ij} X_{ki}$$
$$= Z_{ij} X_{jk} - Z_{jk} X_{ij} \qquad (B.6)$$
$$= Z_{jk} X_{ki} - Z_{ki} X_{jk}$$

$$M_c = Z_{ij} Z_{jk} + X_{ij} X_{jk}\ ,\ M_a = Z_{jk} Z_{ki} + X_{jk} X_{ki}\ ,\ M_c = Z_{ki} Z_{ij} + X_{ki} X_{ij} \qquad (B.7)$$

$$M_b + M_c = - X_{ij}^2 - Z_{ij}^2 = - a^2$$
$$M_c + M_a = - X_{jk}^2 - Z_{jk}^2 = - b^2 \qquad (B.8)$$
$$M_a + M_b = - X_{ki}^2 - Z_{ki}^2 = - c^2$$

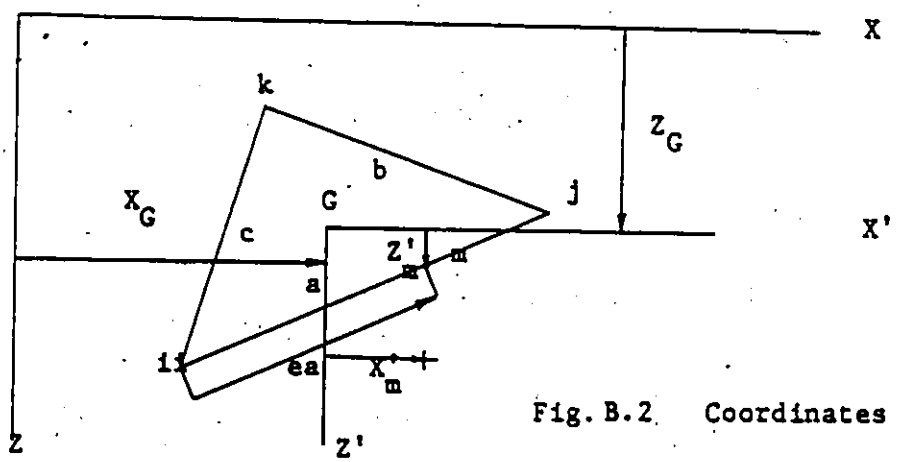

Fig. B.2 Coordinates Z_m and X_m

c) Coordinates of any point m on the side of the triangle. Fig B.2

The centroid of the triangle is given by

$$Z_G = \frac{1}{3} (Z_i + Z_j + Z_k)\ ,\ X_G = \frac{1}{3} (X_i + X_j + X_k) \qquad (B.9)$$

Let the point m be at a distance ea on the side a from the node i, where $0 < e < 1$. Then

$$Z_m' = Z_i - ea \sin(\theta_a - 90) - Z_G = Z_i + ea \cos\theta_a - Z_G$$
$$X_m' = X_i - ea \cos(\theta_a - 90) - Z_G = X_i + ea \sin\theta_a - Z_G$$

Using the relation of equation B.2 and B.3 we obtain

$$Z_m' = Z_i - eZ_{ij} - Z_G \text{ and } X_m' = X_j - eX_{jk} - X_G \qquad (B.10)$$

Considering the cyclic rotation of the indices i, j and k we obtain the coordinates of the point m on the side b and side c as.

$$Z'_m = Z_j - eZ_{jk} - Z_G \text{ and } X'_m = X_j - eX_{jk} - X_G \quad \text{(side b)} \qquad \text{(B.11)}$$

$$Z'_m = Z_k - eZ_{ki} - Z_G \text{ and } X'_m = X_k - eX_{ki} - X_G \quad \text{(side c)} \qquad \text{(B.12)}$$

Consider Fig.B.3, where the point 1, 3 and 5 have $e = \frac{1}{3}$ and 4, 6 and 2 have $e = \frac{2}{3}$. Then the equations B.10, B.11, and B.12 give

$$\begin{aligned} Z'_1 &= -\tfrac{1}{3} Z_{ki} \text{ and } X'_1 = -\tfrac{1}{3} X_{ki} \\ Z'_2 &= \tfrac{1}{3} Z_{jk} \text{ and } X'_2 = \tfrac{1}{3} X_{jk} \\ Z'_3 &= -\tfrac{1}{3} Z_{ij} \text{ and } X'_3 = -\tfrac{1}{3} X_{ij} \\ Z'_4 &= \tfrac{1}{3} Z_{ki} \text{ and } X'_4 = \tfrac{1}{3} X_{ki} \\ Z'_5 &= -\tfrac{1}{3} Z_{jk} \text{ and } X'_5 = -\tfrac{1}{3} X_{jk} \\ Z'_6 &= \tfrac{1}{3} Z_{ij} \text{ and } X'_6 = \tfrac{1}{3} X_{ij} \end{aligned} \qquad \text{(B.13)}$$

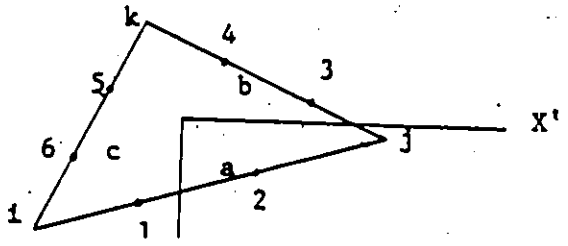

Fig. B.3 Coordinates of the point along side a, b, c

EQUATIONS OF EQUILIBRIUM

d) For each element as shown in Fig.B.4 we consider it to be subjected to external forces, external moments and the internal stresses.

External force - W, KW and P (Fig.B.4.a)

External moment - M_0 (Fig.B.4.a)

Internal stresses - σ_{rs} and τ_{rs}, where rs = ia, ja, jb, kb, kc and ic (Fig.B.4.c).

Resultant due to pore water pressure U_a, U_b and U_c (Fig.B.4:d)

For the external force P either its inclination is known or the components P_1 and P_2 are known, (Fig.B.4.a,b). The paramrters e_0, e_1,

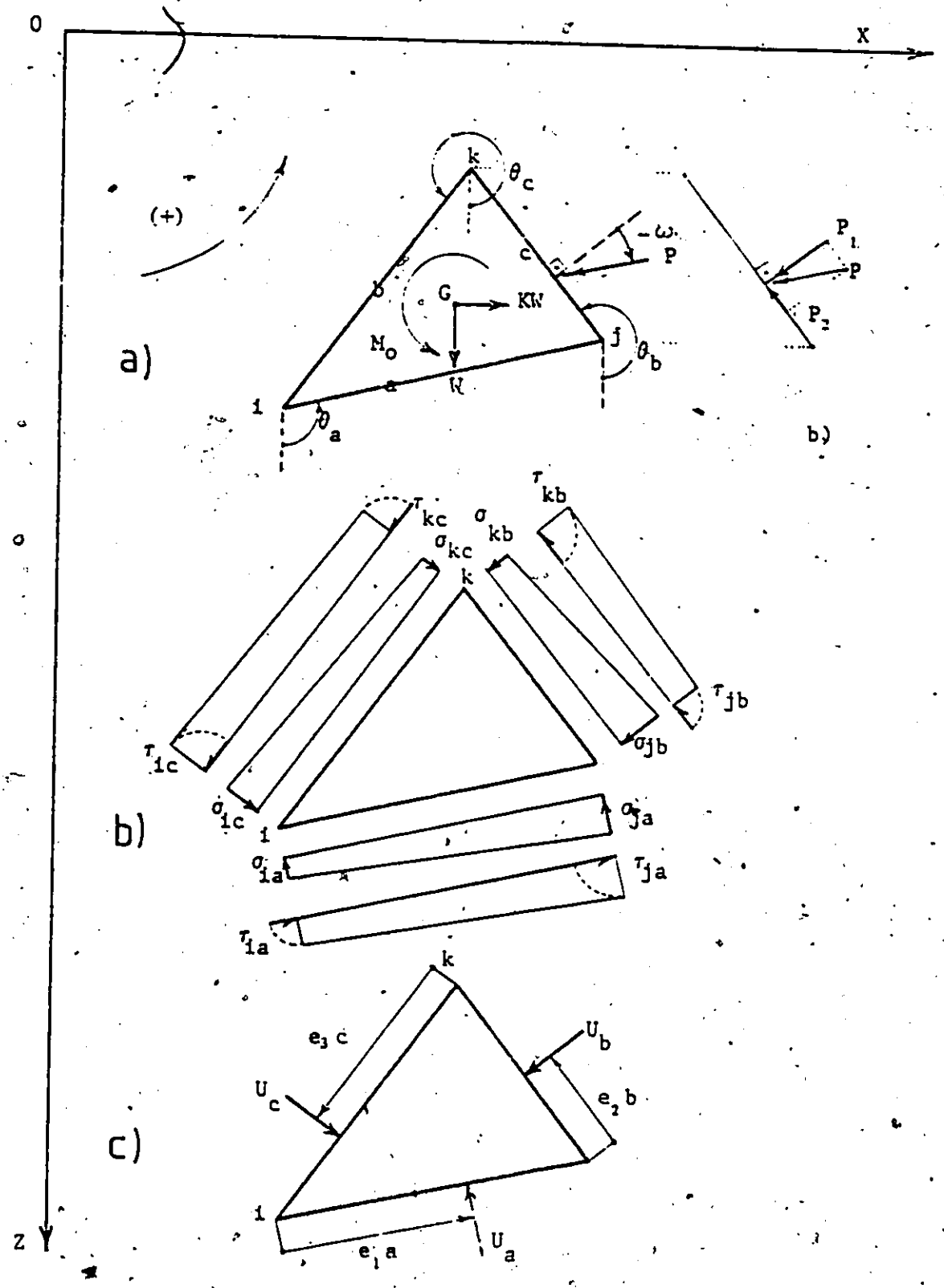

Fig. B.4 Moments and forces applied to the triangular element

e_2 and e_3 define the distance at which the forces P, U_a, U_b, and U_c act where $0 < e_0, e_1, e_2, e_3 < 1$. Fig.B.4 shows the point of application. The stresses σ_{rs} are perpendicular to the sides and τ_{rs} act along the sides of the triangle.

b) Forces and moments due to concentrated force P.

Let P_z and P_x be the components of the force P and M_p be the moment about the centroid G. It is assumed that P_1 is perpendicular to the side b and P_2 is parallel to the side b, where P_1 and P_2 are the components of the concentrated force P. Consider Fig.B.5.

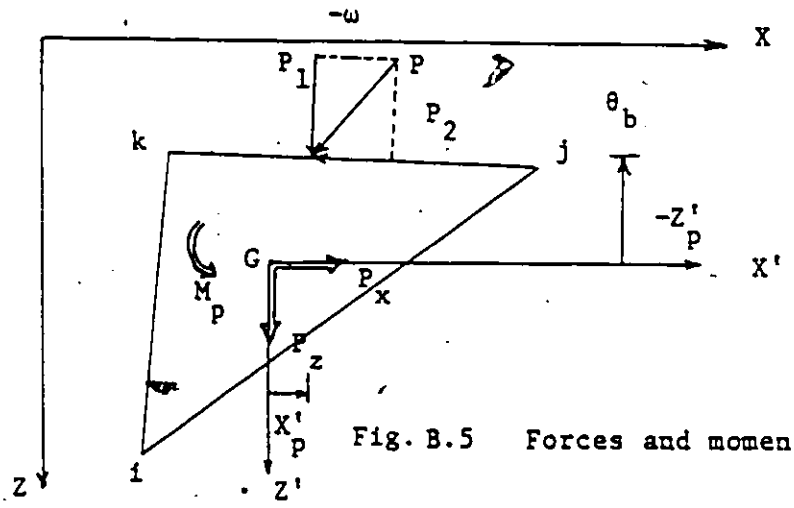

Fig. B.5 Forces and moments due to concentrated force

$$P_z = P_1 \mathrm{Sin}(\theta_b - 180) - P_2 \mathrm{Cos}(\theta_b - 180) = -P_1 \mathrm{Sin}\theta_b + P_2 \mathrm{Cos}\theta_b \qquad (B.14)$$

$$P_x = -P_1 \mathrm{Cos}(\theta_b - 180) - P_2 \mathrm{Sin}(\theta_b - 180) = P_1 \mathrm{Cos}\theta_b + P_2 \mathrm{Sin}\theta_b \qquad (B.15)$$

$$M_p = -P_z X'_p + P_x Z'_p = P_1(-\mathrm{Sin}\theta_b X'_p + \mathrm{Cos}\theta_b Z'_p) + P_2(\mathrm{Cos}\theta_b X'_p + \mathrm{Sin}\theta_b Z'_p)$$

$$= P_1 \eta_1 + P_2 \eta_2 \qquad (B.16)$$

where $\eta_1 = -\mathrm{Sin}\theta_b X'_p + \mathrm{Cos}\theta_b Z'_p \qquad (B.17)$

$$\eta_2 = \mathrm{Cos}\theta_b X'_p + \mathrm{Sin}\theta_b Z'_p \qquad (B.18)$$

From equation B.11 we obtain

$$Z'_p = Z_j - e_0 Z_{jk} - Z_G = (Z_{jk}(1 - 3e_0) - Z_{ij})/3 \qquad (B.19)$$

$$X'_p = X_j - e_0 X_{jk} - X_G = (X_{jk}(1 - 3e_0) - X_{ij})/3 \qquad (B.20)$$

If expressed in terms of the angle of inclination ω we obtain

$$P_1 = P\cos\omega \qquad P_2 = P\sin\omega \qquad \text{or} \qquad P_2 = -P_1 tg\omega \tag{B.21}$$

$$P_z = P_1(-\sin\theta_b - \cos\theta_b tg\omega) \text{ and } P_x = P_1(\cos\theta_b - \sin\theta_b tg\omega) \tag{B.22}$$

$$M_p = P_1(\eta_1 - \eta_2 tg\omega) \tag{B.23}$$

c) Forces and moments due to stresses.

Let S_{za} and S_{xa} be the components of the force due to the stresses acting on the side a as shown in Fig.B.6. M_1 is the moment at the centroid G.

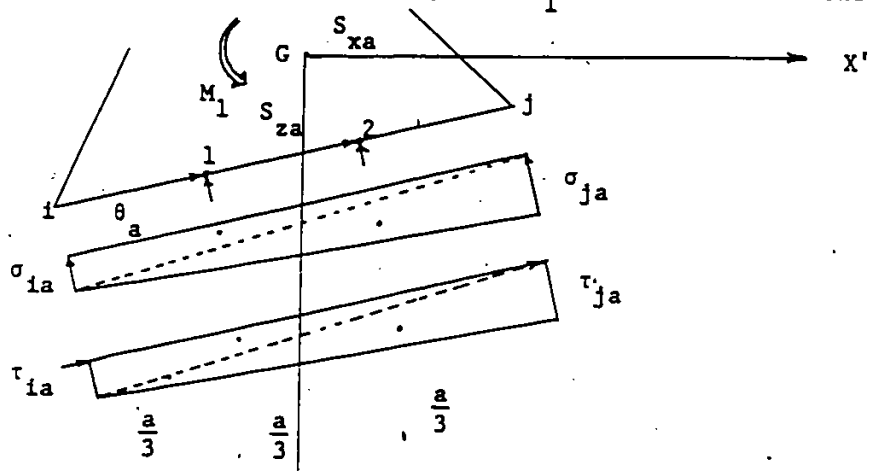

Fig. B.6 Forces and moments due to stresses acting on side a of the triangular element

$$S_{za} = -\frac{1}{2}a\sin\theta_a(\sigma_{ia} + \sigma_{ja}) + \frac{1}{2}a\cos\theta_a(\tau_{ia} + \tau_{ja})$$

Using equation B .2 and B .3 we obtain

$$S_{za} = \frac{1}{2}X_{ij}(\sigma_{ia} + \sigma_{ja}) - \frac{1}{2}Z_{ij}(\tau_{ia} + \tau_{ja}) \tag{B.24}$$

Similarly we obtain

$$S_{xa} = -\frac{1}{2}Z_{ij}(\sigma_{ia} + \sigma_{ja}) - \frac{1}{2}X_{ij}(\tau_{ia} + \tau_{ja}) \tag{B.25}$$

$$M_1 = -(\frac{1}{2}X_{ij}\sigma_{ia} - \frac{1}{2}Z_{ij}\tau_{ia})X'_1 - (\frac{1}{2}X_{ij}\sigma_{ja} - \frac{1}{2}Z_{ij}\tau_{ja})X'_2 + (-\frac{1}{2}Z_{ij}\sigma_{ia} - \frac{1}{2}X_{ij}\tau_{ia})Z'_1 + (-\frac{1}{2}Z_{ij}\sigma_{ja} - \frac{1}{2}X_{ij}\tau_{ja})Z'_2 \tag{B.26}$$

Introducing equation .13 we obtain

$$M_1 = \frac{1}{6}\sigma_{ia}(X_{ij}X_{ki} + Z_{ij}Z_{ki}) - \frac{1}{6}\sigma_{ja}(X_{ij}X_{jk} + Z_{ij}Z_{jk}) + \frac{1}{6}\tau_{ia}(-Z_{ij}X_{ki} + Z_{ki}X_{ij}) + \frac{1}{6}\tau_{ja}(Z_{ij}X_{jk} - Z_{jk}X_{ij}) \tag{B.27}$$

Using the results of equation B.6, B.7 and B.13 we obtain

$$M_1 = \frac{1}{6}(M_b\sigma_{ia} - M_c\sigma_{ja} + E\tau_{ia} + E\tau_{ja}) \qquad (B.28)$$

To obtain S_{zb}, S_{xb}, S_{zc}, S_{xc}, M_2 and M_3 we just have to rotate the indices a, b, c, i, j, k and 1, 2, 3 cyclically.

d) Forces and moments due to pore water pressure.

Let U_{za} and U_{xa} be the components of the force U_a acting on the side a and M_{ua} be the moment at the centroid G. From the geometry of Fig.B.7 we obtain the following relationships.

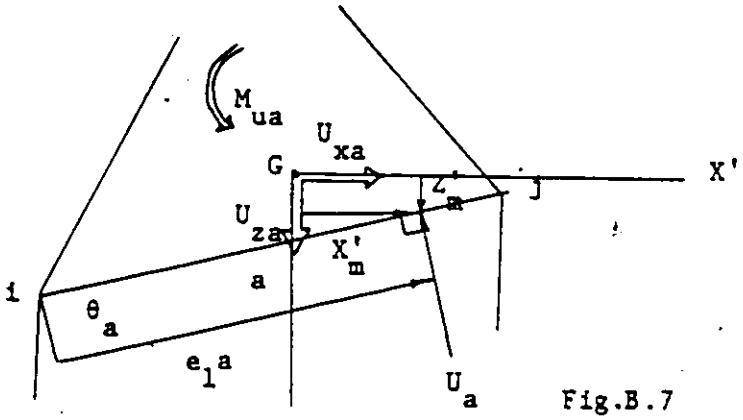

Fig.B.7

Fig. B.7 Forces and moments due to water pressure acting on the side a of the triangular element

$$U_{za} = -U_a\text{Cos}(\theta_a - 90) = -U_a\text{Sin}\,\theta_a \qquad (B.29)$$

$$U_{xa} = -U_a\text{Sin}(\theta_a - 90) = U_a\text{Cos}\,\theta_a \qquad (B.30)$$

$$M_{ua} = -U_{za}X'_m + U_{xa}Z'_m = U_a(\text{Sin}\,\theta_a X'_m + \text{Cos}\,\theta_a Z'_m) \qquad (B.31)$$

Using equation A.10 for the side a we obtain

$$Z'_m = Z_i - e_1 Z_{ij} - Z_G = \frac{1}{3}(Z_{ij}(1 - 3e_1) - Z_{ki}) \qquad (B.32)$$

$$X'_m = X_i - e_1 X_{ij} - X_G = \frac{1}{3}(X_{ij}(1 - 3e_1) - X_{ki}) \qquad (B.33)$$

Similarly for sides b and c we have to rotate a, b, c, i, j, k, and 1, 2, 3 cyclically.

R_1, R_2 and R_3 are the resultant forces and moment acting on the element.

$$R_1 = -(U_a\text{Sin}\theta_a + U_b\text{Sin}\theta_b + U_c\text{Sin}\theta_c) \qquad (B.34)$$

$$R_2 = U_a \cos\theta_a + U_b \cos\theta_b + U_c \cos\theta_c \qquad (B.35)$$

$$R_3 = U_a \eta_a + U_b \eta_b + U_c \eta_c \qquad (B.36)$$

$$\eta_a = (\sin\theta_a (X_{ij}(1 - 3e_1) - X_{ki}) + \cos\theta_a (Z_{ij}(1 - 3e_1) - Z_{ki})) \qquad (B.37)$$

$$\eta_b = (\sin\theta_b (X_{jk}(1 - 3e_2) - X_{ij}) + \cos\theta_b (Z_{jk}(1 - 3e_2) - Z_{ij})) \qquad (B.38)$$

$$\eta_c = (\sin\theta_c (X_{ki}(1 - 3e_3) - X_{jk}) + \cos\theta_c (Z_{ki}(1 - 3e_3) - Z_{jk})) \qquad (B.39)$$

e) Equations of equilibrium.

Considering the equilibrium of all the vertical forces acting on the triangular element, i.e. in the direction Z.

$$\frac{1}{2} X_{ij}(\sigma_{ia} + \sigma_{ja}) + \frac{1}{2} X_{jk}(\sigma_{jb} + \sigma_{kb}) + \frac{1}{2} X_{ki}(\sigma_{kc} + \sigma_{ic}) - \frac{1}{2} Z_{ij}(\tau_{ia} + \tau_{ja}) - \frac{1}{2} Z_{jk}(\tau_{jb} + \tau_{kb}) - \frac{1}{2} Z_{ki}(\tau_{kc} + \tau_{ic}) + W + P_z + R_1 = 0 \qquad (B.40)$$

Equilibrium of the horizontal forces, i.e. in the direction X.

$$-\frac{1}{2} Z_{ij}(\sigma_{ia} + \sigma_{ja}) - \frac{1}{2} Z_{jk}(\sigma_{jb} + \sigma_{kb}) - \frac{1}{2} Z_{ki}(\sigma_{kc} + \sigma_{ic}) - \frac{1}{2} X_{ij}(\tau_{ia} + \tau_{ja}) - \frac{1}{2} X_{jk}(\tau_{jb} + \tau_{kb}) - \frac{1}{2} X_{ki}(\tau_{kc} + \tau_{ic}) + KW + P_x + R_2 = 0 \qquad (B.41)$$

Considering the moment about the centroid G.

$$\frac{1}{6}(M_b \sigma_{ia} - M_c \sigma_{ja} + M_c \sigma_{jb} - M_a \sigma_{kb} + M_a \sigma_{kc} - M_b \sigma_{ic}) + \frac{E}{6}(\tau_{ia} + \tau_{ja} + \tau_{jb} + \tau_{kb} + \tau_{kc} + \tau_{ic}) + M_0 + M_p + R_3 = 0 \qquad (B.42)$$

Expressing the equilibrium equations in the matrix form.

$$[S][\sigma] + [T][\tau] = \gamma[W] + P_1[Q_1] + P_2[Q_2] + [R] + [M] \qquad (B.43)$$

where

$$[S] = \begin{bmatrix} -X_{ij} & -X_{ij} & -X_{jk} & -X_{jk} & -X_{ki} & -X_{ki} \\ Z_{ij} & Z_{ij} & Z_{jk} & Z_{jk} & Z_{ki} & Z_{ki} \\ M_b & -M_c & M_c & -M_a & M_a & M_b \end{bmatrix} \qquad (B.44)$$

$$[T] = \begin{bmatrix} Z_{ij} & Z_{ij} & Z_{jk} & Z_{jk} & Z_{ki} & Z_{ki} \\ X_{ij} & X_{ij} & X_{jk} & X_{jk} & X_{ki} & X_{ki} \\ E & E & E & E & E & E \end{bmatrix} \qquad (B.45)$$

$$[\sigma] = \begin{Bmatrix} \sigma_{ia} \\ \sigma_{ja} \\ \sigma_{jb} \\ \sigma_{kb} \\ \sigma_{kc} \\ \sigma_{ic} \end{Bmatrix} \qquad [\tau] = \begin{Bmatrix} \tau_{ia} \\ \tau_{ja} \\ \tau_{jb} \\ \tau_{kb} \\ \tau_{kc} \\ \tau_{ic} \end{Bmatrix} \qquad (B.46)$$

Since we are considering

$$\tau_a = \frac{1}{2}(\tau_{ia} + \tau_{ja}), \quad \tau_b = \frac{1}{2}(\tau_{jb} + \tau_{kb}) \quad \tau_c = \frac{1}{2}(\tau_{kc} + \tau_{ic})$$

We obtain

$$[T] = 2 \begin{bmatrix} Z_{ij} & Z_{jk} & Z_{ki} \\ X_{ij} & X_{jk} & X_{ki} \\ E & E & E \end{bmatrix} \qquad (B.47)$$

$$[\tau] = \begin{Bmatrix} \tau_a \\ \tau_b \\ \tau_c \end{Bmatrix} \qquad [W] = \begin{Bmatrix} E \\ KE \\ 0 \end{Bmatrix} \qquad [Q_2] = \begin{Bmatrix} 2\text{Cos}\theta_b \\ 2\text{Sin}\theta_b \\ -6\eta_1 \end{Bmatrix} \qquad (B.48)$$

$$[Q_1] = \begin{Bmatrix} -2\text{Sin}\theta_b \\ 2\text{Cos}\theta_b \\ -6\eta_2 \end{Bmatrix} \qquad [R] = \begin{Bmatrix} -2R_1 \\ 2R_2 \\ -6R_3 \end{Bmatrix} \qquad [M] = \begin{Bmatrix} 0 \\ 0 \\ -6M_0 \end{Bmatrix} \qquad (B.49)$$

Appendix C

MATRIX ASSEMBLY FOR GENERALISED LIMIT EQUILIBRIUM METHOD

Appendix C is taken from Papantonopoulos (1979).

Matrix [A] consists of six sub-matrices, i.e. $[A_1]$, $[A_2]$, [I], [0]. The identity and the null matrix pose no problem. The problem thus reduces down to the assembly of $[A_1]$ and $[A_2]$ matrix.

The matrix $[A_1]$ contains the coefficients a_{ij} corresponding to the equilibrium of each element, i.e. matrix [S']. The rows of the matrix $[A_1]$ correspond to the element numbers in an ascending order (see Fig. C.1). Each element has three equilibrium equations; thus there are three rows for each element.

The vector {X} is the vector of unknowns, i.e. σ_{rs}, τ_s and is defined in the following way:

$$\{X\} = \begin{Bmatrix} X_1 \\ \vdots \\ X_s \\ \vdots \\ X_n \end{Bmatrix} \qquad C.1$$

or $\{X_s\}$; s = 1, w

where w is the number of interfaces at which σ_{rs}, τ_s are unknown.

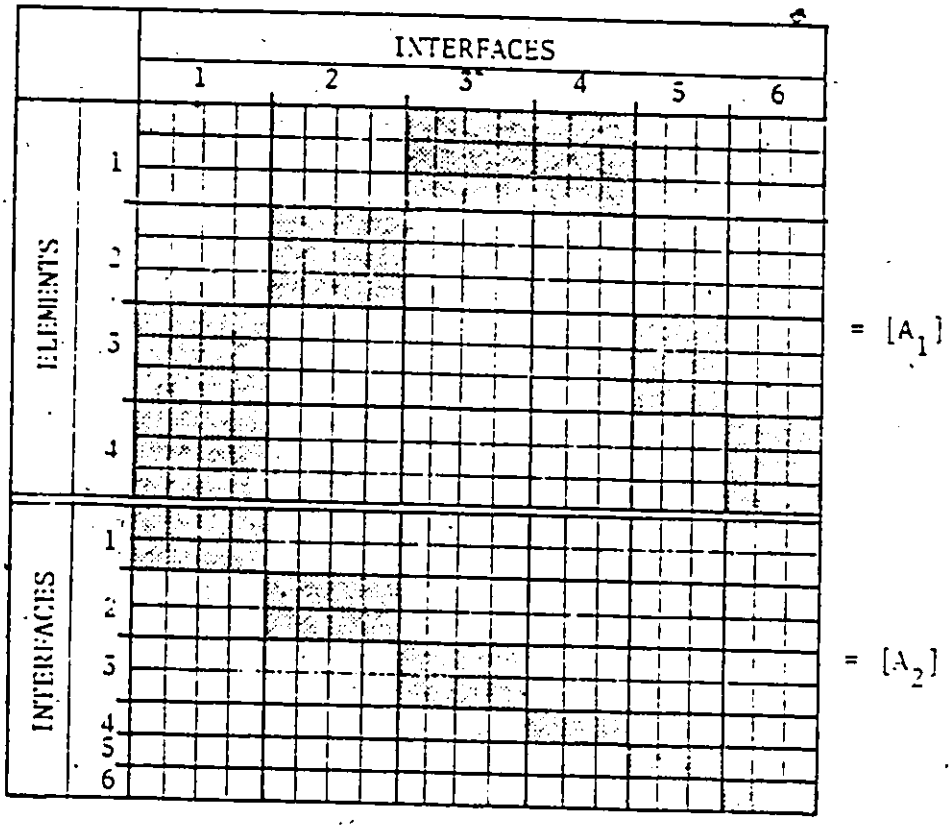

Fig. C.1 Assembly of the matrix [A]

$$\{X_s\}=\begin{Bmatrix}\sigma_{is}\\ \sigma_{js}\\ \tau_s\end{Bmatrix} \quad i<j \quad , \quad \{X_s\}=\begin{Bmatrix}\sigma_{js}\\ \sigma_{is}\\ \tau_s\end{Bmatrix} \quad i>j \qquad C.2$$

Where i and j are the numerical value of the node numbers.

The same vector of the unknown is also utilised for the assembly of matrix [A1]. To take into account the positive and negative values of τ_s the vector $\{X_s\}$ will take the following form :

$$\{X_s\} = \begin{Bmatrix}\sigma_{is}\\ \sigma_{js}\\ \tau_s\\ \tau_s\end{Bmatrix} \qquad C.3$$

this will correspond to both the matrix [A1] and [A2].

The matrix [A1] consists of the inequality matrix, the rows of the matrix correspond to the interface number. All the interfaces except those corresponding to the slip line will have two rows to take into account the signs of the tangential stress. For each slip line the direction of

sliding is known through kinematic conditions; thus the signs of the tangential stresses are known.

The assembly is best explained by an example problem in Fig. C.2.

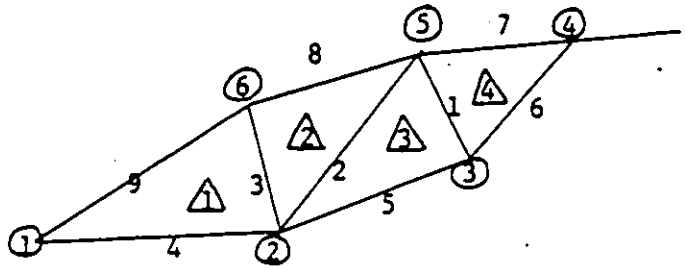

Fig. C.2 Indicial and interface numbering of the element for a given slope

Where the number of elements is 4, the number of slip lines is 3 and the number of interfaces is 6. The assembly is shown in Fig. C.1. The unshaded matrix elements have null values. The total number of unknowns is evaluated as follows. On each interface excluding the slip line there are four unknowns, i.e. two normal stresses corresponding to the nodes on the interface and two unknowns for the tangential stress as its direction is not known. Since there are 3 interfaces the number of unknowns is 12. On the slip line there are three unknowns as the direction of tangential stresses is known. Since there are three slip lines the number of unknowns is 9. Thus the total number of unknowns for the system is 21 and the assembled matrix will have 21 columns. These unknowns correspond to both matrix [A1] and [A2].

Considering the equality matrix [A1]. Each element has to satisfy three equations of equilibrium. The rows of the matrix [A1] correspond to the number of equations, since there are four elements, the number of equations is equal to twelve. Thus the number of rows of matrix [A1] is twelve.

Considering the inequality matrix [A2], each interface excluding the slip lines should have two rows to accommodate the failure criteria in which the tangential stresses could be positive or negative. Along the slip surface one row is sufficient, as the direction of the tangential stress is known, thus the number of rows for matrix [A2] is nine.

The entire assembled matrix has 21 columns and 21 rows. The assembly of the {B} vector is self explanatory, see Table 3.1.

Appendix D

DIFFERENTIATION OF THE [A!] MATRIX AND THE {B!} VECTOR WITH RESPECT TO θ AND T

1. Differentiation of the elements of [S'] matrix with respect to θ for evaluating the optimum angle of movement of the nodes by giving them a perturbation.

a) Let node i be given a perturbation in the direction θ_i by a distance equal to t. Fig. D.1

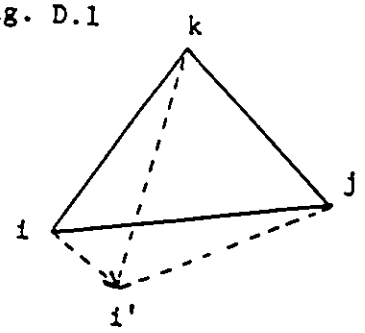

Fig. D.1 Node i given a perturbation

The other nodes are kept fixed. The new Coordinates of node i are as given below:

$$X_i' = X_i + t\text{Sin}\theta_i \quad \text{and} \quad Z_i' = Z_i + t\text{Cos}\theta_i \qquad (D.1)$$

where the prime denotes the new position and those without the prime are the original positions.

This convention will be followed throughout this Appendix.

Owing to the movement of node i only those elements in the [S'] matrix having the subscript i will be expressed as

functions of θ and t. Hence only their derivatives with respect to θ or t will exist. The others will be zero as the movement of node i does not affect them. The elements effected and their new values are as given below:

$$X'_{ij} = X'_i - X_j, \quad Z'_{ij} = Z'_i - Z_j, \quad X'_{ki} = X_k - X'_i, \quad Z'_{ki} = Z_k - Z'_i \tag{D.2}$$

$$M'_a = Z_{jk}Z'_{ki} + X_{jk}X'_{ki} = Z_{jk}(Z_k - Z_i) + X_{jk}(X_k - X'_i) \tag{D.3}$$

$$M'_b = Z'_{ki}Z'_{ij} + X'_{ki}X'_{ij} = (Z_k - Z'_i)(Z'_i - Z_j) + (X_k - X'_i)(X'_i - X_j) \tag{D.4}$$

$$M'_c = Z'_{ij}Z_{jk} + X'_{ij}X_{jk} = Z_{jk}(Z'_i - Z_j) + X_{jk}(X'_i - X_j) \tag{D.5}$$

$$E' = Z'_{ij}X_{jk} - X'_{ij}Z_{jk} = X_{jk}(Z'_i - Z_j) + Z_{jk}(X'_i - X_j) \tag{D.6}$$

Substituting equation D.1 in D.2, D.3, D.4, D.5 and D.6 and differentiating with respect to θ we obtain:

$$\frac{d}{d\theta}(X'_{ij}) = t\text{Cos}\theta_i; \quad \frac{d}{d\theta}(X'_{ki}) = -t\text{Cos}\theta_i$$

$$\frac{d}{d\theta}(Z'_{ij}) = -t\text{Sin}\theta_i; \quad \frac{d}{d\theta}(Z'_{ki}) = t\text{Sin}\theta_i \tag{D.7}$$

$$\frac{d}{d\theta}(M'_a) = t\text{Cos}\theta_i X_{kj} + t\text{Sin}\theta_i Z_{jk}$$

$$\frac{d}{d\theta}(M'_b) = + \text{Sin}\theta_i(Z_{ik} + Z_{ij}) + t\text{Cos}\theta_i(X_{ki} + X_{ji}) \tag{D.8}$$

$$\frac{d}{d\theta}(M'_c) = t\text{Sin}\theta_i Z_{kj} + t\text{Cos}\theta_i X_{jk}$$

$$\frac{d}{d\theta}(E') = t\text{Sin}\theta_i X_{kj} + t\text{Cos}\theta_i Z_{kj} \tag{D.9}$$

The differentiated [S'] matrix with respect to θ constitutes these elements and is shown in Table 4.1.

b) Let node j be given a perturbation in the direction θ_j by a distance equal to t. All other nodes are kept fixed. See Fig. D.2

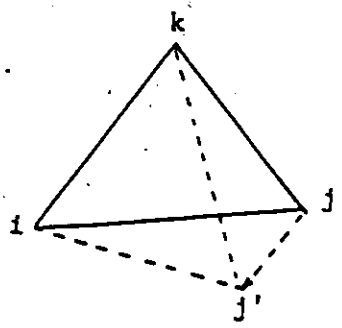

Fig. D.2 Node j given a perturbation

The new coordinates of node j are as given below:

$$X'_j = X_j + t\text{Sin}\theta_j \quad \text{and} \quad Z'_j = Z_j + t\text{Cos}\theta_j \tag{D.10}$$

The elements effected will have the subscript j in Table 3.3. Their new values are as given below:

$$X'_{ij} = X_i - X'_j;\ X'_{jk} = X'_j - X_k;\ Z'_{ij} = Z_i - Z'_j,\ Z'_{jk} = Z'_j - Z_k \tag{D.11}$$

$$M'_a = Z'_{jk}Z_{ki} + X'_{jk}X_{ki} = (Z'_j - Z_k)Z_{ki} + (X'_j - X_k)X_{ki} \tag{D.12}$$

$$M'_b = Z_{ki}Z'_{ij} + X_{ki}X'_{ij} = Z_{ki}(Z_i - Z'_j) + X_{ki}(X_i - X'_j) \tag{D.13}$$

$$M'_c = Z'_{ij}Z'_{jk} + X'_{ij}X'_{jk} = (Z_i - Z'_j)(Z'_j - Z_k) + (X_i - X'_j)(X'_j - X_k) \tag{D.14}$$

$$E' = Z'_{jk}X_{ki} - Z_{ki}X'_{jk} = X_{ki}(Z'_j - Z_k) - Z_{ki}(X'_j - X_k) \tag{D.15}$$

Substituting equation D.10 in equation D.11, D.12, D.13 D.14, D.15 and differentiating with respect to θ we obtain:

$$\frac{d}{d\theta}(X'_{ij}) = -t\text{Cos}\theta_j;\ \frac{d}{d\theta}(X'_{jk}) = t\text{Cos}\theta_j$$

$$\frac{d}{d\theta}(Z'_{ij}) = t\text{Sin}\theta_j;\ \frac{d}{d\theta}(Z'_{jk}) = -t\text{Sin}\theta_j \tag{D.16}$$

$$\frac{d}{d\theta}(M'_a) = t\text{Sin}\theta_j Z_{ik} + t\text{Cos}\theta_j X_{ki}$$

$$\frac{d}{d\theta}(M'_b) = t\text{Sin}\theta_j Z_{ki} + t\text{Cos}\theta_j X_{ik} \qquad \text{(D.17)}$$

$$\frac{d}{d\theta}(M'_c) = t\text{Sin}\theta_j (Z_{ji} + Z_{jk}) + t\text{Cos}\theta_j (X_{ij} + X_{kj})$$

$$\frac{d(E)}{d\theta} = t\text{Sin}\theta_j X_{ik} + t\text{Cos}\theta_j Z_{ik} \qquad \text{(D.18)}$$

The differentiated [S'] matrix with respect to θ constitutes these elements and is shown in Table 4.2.

c) Let node k be given a perturbation in the direction θ_k by a distance equal to t. The new Coordinates are as given below:

$$X'_k = X_k + t\text{Sin}\theta_k \quad \text{and} \quad Z'_k = Z_k + t\text{Cos}\theta_k \qquad \text{(D.19)}$$

The elements effected in the [S'] matrix will have the subscript k in Table 3.3, and their differentiation with respect to θ is as given below:

$$\frac{d}{d\theta}(X'_{jk}) = -t\text{Cos}\theta_k; \quad \frac{d}{d\theta}(X'_{ki}) = t\text{Cos}\theta_k$$

$$\frac{d}{d\theta}(Z'_{jk}) = t\text{Sin}\theta_i; \quad \frac{d}{d\theta}(Z'_{ki}) = -t\text{Sin}\theta_k \qquad \text{(D.20)}$$

$$\frac{d}{d\theta}(M'_a) = t\text{Sin}\theta_k (Z_{kj} + Z_{ki}) + t\text{Cos}\theta_k (X_{jk} + X_{ik})$$

$$\frac{d}{d\theta}(M'_b) = t\text{Sin}\theta_k Z_{ji} + t\text{Cos}\theta_k X_{ij} \qquad \text{(D.21)}$$

$$\frac{d}{d\theta}(M'_c) = t\text{Sin}\theta_k Z_{ij} + t\text{Cos}\theta_k X_{ji}$$

$$\frac{d}{d\theta}(E') = t\text{Sin}\theta_k X_{ji} + t\text{Cos}\theta_k Z_{ji} \qquad \text{(D.22)}$$

The differentiated [S'] matrix with respect to θ constitutes these elements and is shown in Table 4.3.

2. Differentiation of the {B} vector with respect to θ.

The perturbation of the nodes are assumed to effect only the weight of the element. See Table 3.3. Thus the only element in the {B} vector which is effected is E', whose differential with respect to θ by moving nodes i, j and k has already been obtained. Table 4.4 shows the differentiated {B} vector by moving nodes i, j and k respectively.

3. Differentiation of the [S'] matrix with respect to t to evaluate the Sensitivity Coefficients of the nodes by giving the nodes a perturbation.

a) The same perturbation as previous is given to node i and the equations are the same except that they have to be differentiated with respect to t. Differentiating with respect to t we obtain:

$$\frac{d}{dt}(X'_{ij}) = \text{Sin}\theta_i; \quad \frac{d}{dt}(X'_{ki}) = -\text{Sin}\theta_i$$
$$\frac{d}{dt}(Z'_{ij}) = \text{Cos}\theta_i; \quad \frac{d}{dt}(Z'_{ki}) = -\text{Cos}\theta_i \qquad \text{(D.23)}$$

$$\frac{d}{dt}(M'_a) = \text{Cos}\theta_i Z_{kj} + \text{Sin}\theta_i X_{kj}$$
$$\frac{d}{dt}(M'_b) = \text{Cos}\theta_i(Z_{ki} + Z_{ji}) + \text{Sin}\theta_i(X_{ki} + X_{ji}) - 2t \qquad \text{(D.24)}$$

$$\frac{d}{dt}(M'_c) = \text{Cos}\theta_i Z_{jk} + \text{Sin}\theta_i X_{jk}$$
$$\frac{d}{dt}(E') = \text{Cos}\theta_i X_{jk} + \text{Sin}\theta_i Z_{kj} \qquad \text{(D.25)}$$

The assembled differentiated matrix is shown in Table 4.5.

b) Similarly, when node j is given a perturbation the elements of the differentiated [S'] matrix with respect to t is as given below:

$$\frac{d}{dt}(X'_{ij}) = -\text{Sin}\theta_j; \quad \frac{d}{dt}(X'_{jk}) = \text{Sin}\theta_j$$

$$\frac{d}{dt}(Z'_{ij}) = -\text{Cos}\theta_j; \quad \frac{d}{dt}(Z'_{jk}) = \text{Cos}\theta_j \qquad \text{(D.26)}$$

$$\frac{d}{dt}(M'_a) = \text{Cos}\theta_j Z_{ki} + \text{Sin}\theta_j X_{ki}$$

$$\frac{d}{dt}(M'_b) = \text{Cos}\theta_j Z_{ik} + \text{Sin}\theta_j X_{ik} \qquad \text{(D.27)}$$

$$\frac{d}{dt}(M'_c) = \text{Cos}\theta_j(Z_{ij} + Z_{kj}) + \text{Sin}\theta_j(X_{ij} + X_{kj})$$

$$\frac{d(E)}{dt} = \text{Cos}\theta_j X_{ki} + \text{Sin}\theta_j Z_{ik} \qquad \text{(D.28)}$$

The assembled differentiated matrix [S'] with respect to t is shown in Table 4.6.

c) When node k is given the same perturbation, the elements of [S'] matrix when differentiated with respect to t are as given below:

$$\frac{d}{dt}(X'_{jk}) = -\text{Sin}\theta_k; \quad \frac{d}{dt}(X'_{ki}) = \text{Sin}\theta_k$$

$$\frac{d}{dt}(Z'_{jk}) = -\text{Cos}\theta_k; \quad \frac{d}{dt}(Z'_{ki}) = \text{Cos}\theta_k \qquad \text{(D.29)}$$

$$\frac{d}{dt}(M'_a) = \text{Cos}\theta_k(Z_{jk} + Z_{ik}) + \text{Sin}\theta_k(X_{jk} + X_{ik}) - 2t$$

$$\frac{d}{dt}(M'_b) = \text{Cos}\theta_k Z_{ij} + \text{Sin}\theta_k X_{ij} \qquad \text{(D.30)}$$

$$\frac{d}{dt}(M_c') = \text{Cos}\theta_k Z_{ji} + \text{Sin}\theta_k X_{ji}$$

$$\frac{d}{dt}(E') = \text{Cos}\theta_k X_{ij} + \text{Sin}\theta_k Z_{ji} \qquad \text{(D.31)}$$

The assembled differentiated [S'] matrix is shown in Table 4.7.

4. Differentiation of the {B} vector with respect to t.

This is similar to obtaining the {B} vector as done previously. The effected term is E'.whose differentiation with respect to t is already obtained. Table 4.8 shows the differentiated {B} vector by moving nodes i, j and k respectively.

Appendix E

DIFFERENTIATED [A1] MATRIX AND {B1} VECTOR ASSEMBLY

The procedure is best explained by an example. Consider the slope shown in Fig. C.2. The individual split up of the triangles with its nodal and interface numbering are shown in Fig. E.1. The nodes i, j and k are numbered in counterclockwise direction.

a) Assembly of the differentiated [A1] matrix

Let node 2 be given a perturbation to find the angle θ. Element numbers one, two and three will be affected. Thus all the terms below the line A-A in Fig. E.2 (b) will be zero. The terms corresponding to the interface numbers seven, eight and nine will also be zero as these are the external boundaries of the slope and the stresses are known to be zero.

Element Number 1: The movement of node 2 corresponds to the jth node of this element. See Fig.E.1 (a). Thus the differentiated matrix in Table 4.2 will be used. The interface numbering of this element is as shown in Fig. E.1(a). In this element interface number nine, i.e. side c is an external boundary, thus the terms corresponding to side c of Table 4.2 are not assembled as they are zero.

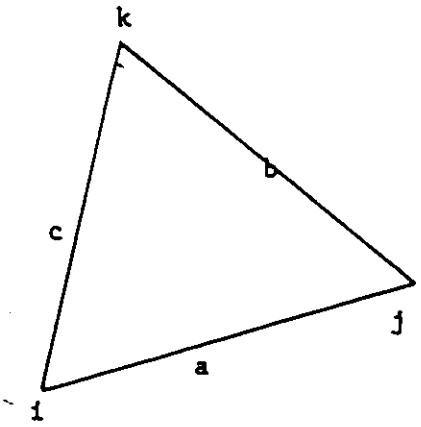

i=1 a = 4
j=2 b = 3
k=6 c = 9

a
Element 1

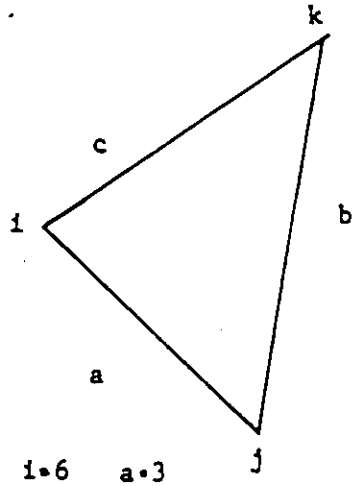

i=6 a=3
j=2 b=2
k=5 c=8

b
Element 2

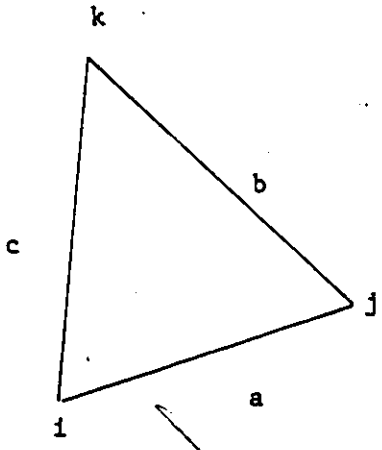

i = 2 a=5
j = 3 b=1
k = 5 c=2

c
Element 3

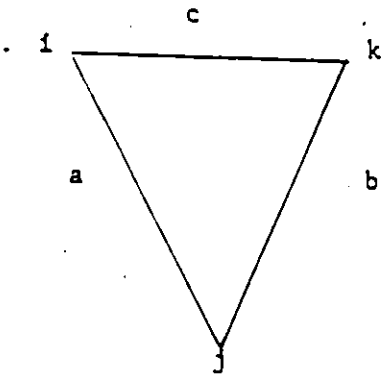

i = 5 a = 1
j = 3 b = 6
k = 4 c = 7

d
Element 4

Fig.E.1 Geometry of the triangular elements for a given slope

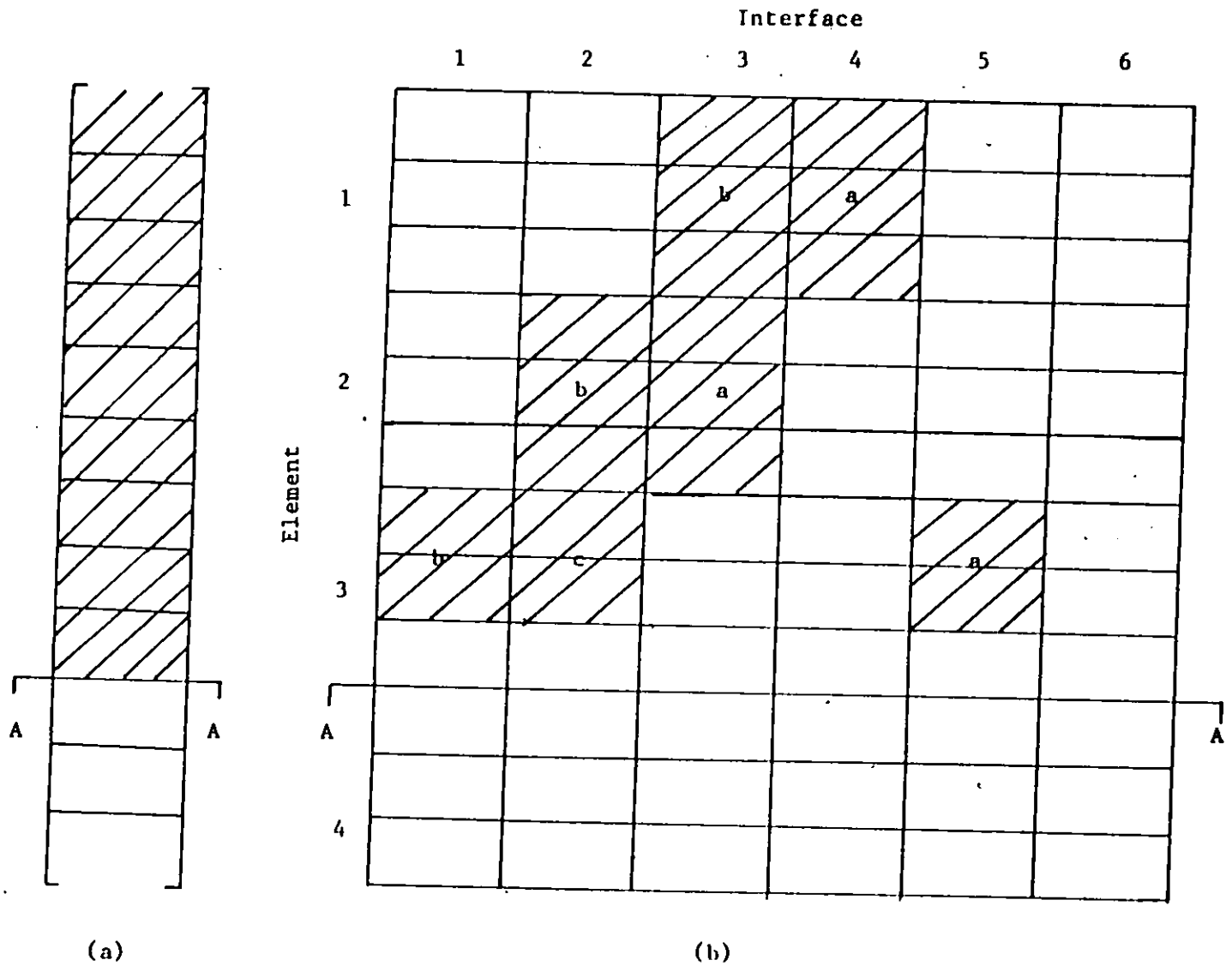

Fig.E.2 Assembly of the Differentiated matrix [A1] and vector {B1}

Only the terms corresponding to side a and b, i.e. 4 and 3 of Table 4.2 are put in the assembled differentiated matrix as shown in Fig. E.2 (b). These will occupy the first three rows corresponding to the element number one.

Element Number 2: The movement of node 2 corresponds to the jth node of this element. The differentiated matrix in Table 4.2 will be used. The terms corresponding to side a and b, i.e. 3 and 2 of Table 4.2 will be put in the assembled matrix as shown in Fig. E.2 (b). These will occupy the fourth, fifth and sixth rows, i.e. corresponding to element number two. Side c, i.e. 8 is an external boundary of the slope for this element and the stresses are known to be zero.

Element Number 3: The movement of node 2 corresponds to the ith node of this element. The matrix in Table 4.1 will be used. As there are no external surfaces all the terms of Table 4.1 are used and are put in the appropriate location as shown in Fig. E.2 (b).

b) Assembly of the Differentiated $\{B_1\}$ Vector

The {B} vector is assembled as shown in Chapter 3. It consists of two subvectors {B1} and {B2}, i.e.

$$\{B\} = \left\{\begin{array}{c} B1 \\ \hline B2 \end{array}\right\} \qquad \text{E.1}$$

The vector {B2} contains the cohesive terms and thus its derivative with respect to θ is zero. The vector {B1} is the vector of external forces. The application of the

external forces is not considered in the procedure for finding the critical slip surface. Hence the only term in the {B1} vector which varies with θ is the weight of each element, see Table 3.1 these derivatives thus exist. The derivative of the {B1} vector with respect to θ is shown in Table 4.4. The detailed analysis can be seen in the appendix D. The assembly of the differentiated {B1} vector is shown in Fig. E.2 (a). This corresponds to the movement of node 2 as in the problem considered in Fig. C.2. The movement of node 2 corresponds to the jth node of element number one. Thus the first three rows of the {B1} vector correspond to the terms of Table 4.4(b). For element number two the corresponding node is j. Thus the row number three to six, i.e. element 2, are occupied by the terms corresponding to Table 4.4(b). For element number three the movement of node 2 corresponds to the ith node. Thus the terms of Table 4.4(a) are placed corresponding to element number 3. Since the movement of node 2 in no way influences element number four, the corresponding terms are all zero.

Appendix F

PROCEDURE FOR EFFECTIVE STRESS ANALYSIS

The system of forces shown in Fig.F.1(a) acting on any one of the elements is exactly equivalent to those of Fig.F.1(b) plus Fig.F.1(c). Utilising the boundary pressure method, the forces acting on the element as shown in Fig.F.1(c) can be replaced by an equivalent seepage force as shown in Fig.F.1(d). Thus, if one knows the pore water distribution, one can obtain the seepage force in magnitude and direction.

The system of forces as shown in Fig.F.1(a) can be replaced by an equivalent system by considering the submerged unit weight of the element and the seepage force acting at the centroid of each element as in Fig.F.1(e).

Simulation of Seepage Forces :

Consider the element shown in Fig. F.1(e). The seepage force has components in the X and Z direction, i.e.

$$F_x = \gamma_w i_x A$$

$$F_z = \gamma_w i_z A \qquad \text{F.1}$$

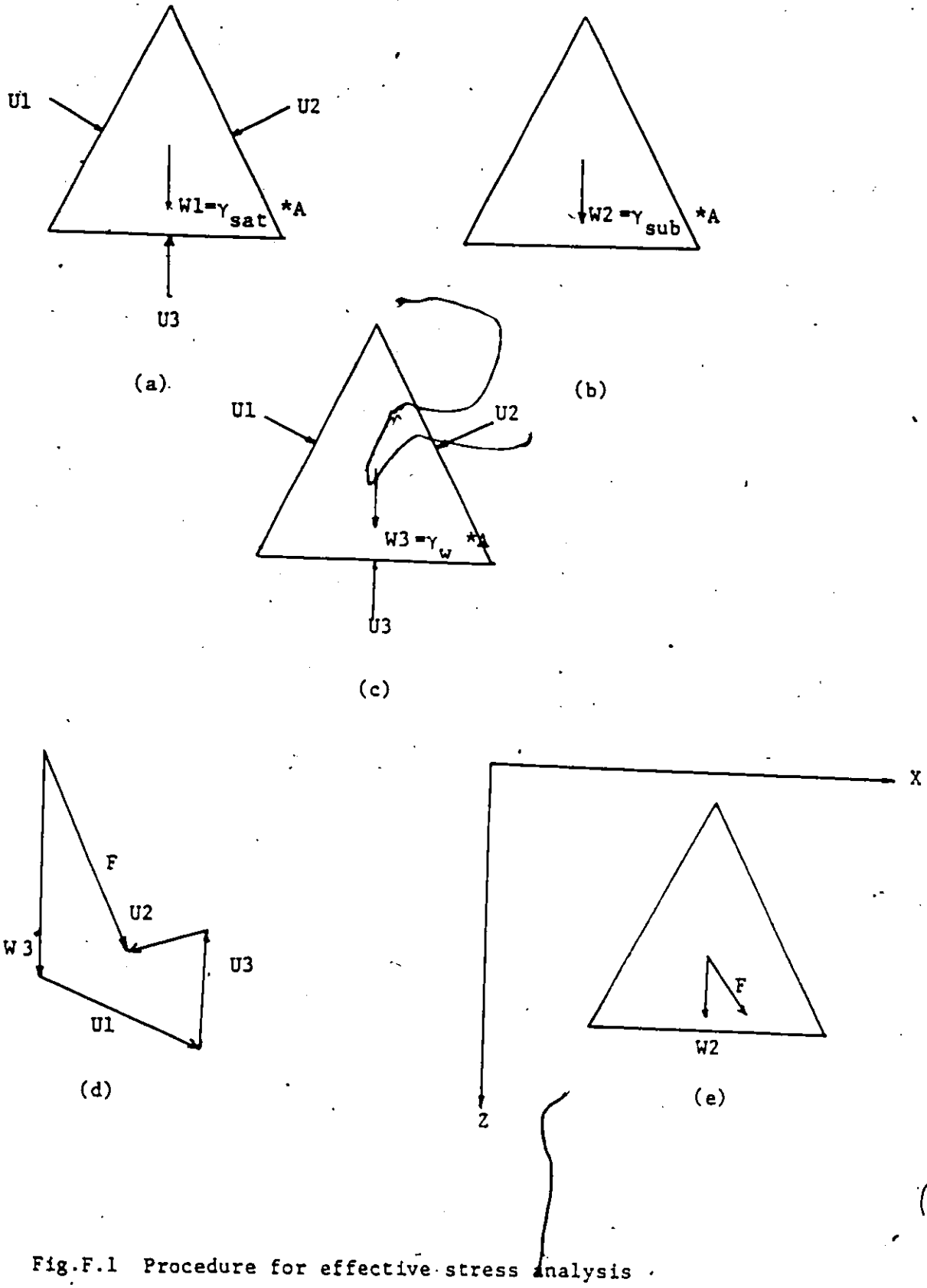

Fig.F.1 Procedure for effective stress analysis

i_x = Hydraulic gradient in the X direction

i_z = Hydraulic gradient in the Z direction

A = Area of the triangular element

To simulate the Fz component, one may increase the weight of the material by a suitable amount as shown below.

$$F_z = \gamma_w i_z A = \Delta\gamma A \ , \ \Delta\gamma = \gamma_w i_z \qquad \text{F.2}$$

the weight of the element will be

$$\gamma = \gamma_{sub} + \gamma_w i_z \qquad \text{F.3}$$

To simulate the Fx component, one may take advantage of the seismic force capability of the code and give a seismic force to the elements the magnitude of which is determined as follows.

$$F_x = \gamma_w i_x A = \gamma A K \qquad \text{F.4}$$

where K = seismic coefficient.

$$K = \gamma_w i_x A / \gamma A = \gamma_w i_x / (\gamma_{sub} + \gamma_w i_z) \quad F.5$$

The seepage forces can be easily simulated both γ and K are functions of the hydraulic gradients i_x and i_z. In the procedure the average seepage force acting on each of the element is calculated by knowing the pore water pressure distribution on each element. From the seepage forces the average hydraulic gradients i_x and i_z are evaluated. These gradients are assumed to remain the same for all subsequent iterations performed in the computer program as one does not expect a radical change in the location of these elements. From the gradients evaluated the values of γ and K for each element are calculated and these are input in the program.